UNIVERSITÀ DEGLI STUDI DI MILANO

CORSO DI DOTTORATO IN SCIENZE FARMACEUTICHE – CICLO XXXVIII

DIPARTIMENTO DI SCIENZE FARMACEUTICHE

PRINTING MUCOADHESIVE AND ORODISPERSIBLE FILMS FOR THE PERSONALIZATION OF THERAPY

SETTORE CHIM/09 - FARMACEUTICO TECNOLOGICO APPLICATIVO

Tesi redatta con il contributo finanziario dell'Unione europea - Next Generation EU e Pharmafilm s.r.l.

CUP n. G43C22002470004

Dott.ssa Chiara Meazzini

Matricola: R13930

ORCID n. 0009-0008-2064-1063

Tutor: Prof. Francesco Cilurzo

Co-Tutor: Prof. Umberto M. Musazzi

Coordinatore del dottorato: Prof. Giulio Vistoli

A.A. 2024/2025

TABLE OF CONTENTS

INTRODUCTION **1**

1. BACKGROUND AND RESEARCH AIM 1
2. REFERENCES 8

CHAPTER 1: 3D-PRINTED MUCOADHESIVE FILMS MANUFACTURED BY DIRECT POWDER EXTRUSION FOR PERSONALIZED CLOBETASOL PROPIONATE BASED PAEDIATRIC THERAPIES **12**

1. INTRODUCTION 12
2. MATERIALS AND METHODS 15
   - 2.1 Materials 15
   - 2.2 Quantitative analysis of CBS by HPLC-UV 16
   - 2.3 Phase solubility studies 16
   - 2.4 Inclusion complex stoichiometry determination (Job's plot method) 17
   - 2.5 Preparation of the powder blends 17
   - 2.6 Direct Powder Extrusion 3D printing 18
   - 2.7 Extruded filaments characterization 18
   - 2.8 Solid state characterization of the powder blends 19
   - 2.9 Characterization of the mucoadhesive films 20
   - 2.10 Solid state characterization of the mucoadhesive films 20
   - 2.11 Mucoadhesive properties 20
   - 2.12 Tensile properties 21
   - 2.13 *In vitro* permeation study 22
   - 2.14 *In vitro* retention study 23
   - 2.15 *Ex-vivo* mucoadhesion and dissolution test 23
   - 2.16 Stability studies 24
   - 2.17 Statistical analysis 24
3. RESULTS AND DISCUSSION 24
   - 3.1 CBS phase solubility studies 25
   - 3.2 Job's plot method 26
   - 3.3 Extruded filaments characterization 27
   - 3.4 Direct Powder Extrusion 3D printing 29
   - 3.5 Characterization of mucoadhesive films 30

3.6 Solid state characterization of the printed mucoadhesive films....31
3.7 Mucoadhesive properties....33
3.8 Tensile properties....35
3.9 *In vitro* permeation and retention studies....35
3.10 *Ex vivo* mucoadhesive and dissolution studies....36
3.11 Stability studies....36
4. CONCLUSIONS....37
5. REFERENCES....38

CHAPTER 2: 3D-PRINTED S-PROTECTED MUCOADHESIVE LIDOCAINE-BASED FILMS FOR IMMEDIATE AND SUSTAINED RELEASE OF THE DRUG IN PAEDIATRIC THERAPIES....42

1. INTRODUCTION....42
2. MATERIALS AND METHODS....45
2.1 Materials....45
2.2 Synthesis of thiolated (CS-SH) and S-protected chitosan (CS-MNA)....46
2.3 Preparation of the powder blends....46
2.4 Direct Powder Extrusion 3D printing....47
2.5 Quantitative analysis of LID by HPLC-UV....48
2.6 Characterization of the extruded filaments and films....48
2.7 Mucoadhesive properties....52
2.8 *Ex-vivo* mucoadhesion and dissolution test....53
2.9 *In Vitro* Permeation Study....53
2.10 *In vitro* retention study....54
2.11 Stability studies....55
2.12 Statistical analysis....55
3. RESULTS AND DISCUSSION....55
3.1 Preparation of the powder blends....56
3.2 Characterization of the extruded filaments....57
3.3 Characterization of mucoadhesive films....59
3.4 Mucoadhesive properties....67
3.5 *Ex-vivo* mucoadhesion and dissolution test....68
3.6 *In vitro* permeation and retention studies....70
3.7 Stability studies....71
4. CONCLUSIONS....72
5. REFERENCES....74

CHAPTER 3: β-GALACTOSIDASE ORODISPERSIBLE DOSAGE FORMS FOR THE TREATMENT OF LACTOSE INTOLERANCE 78

1. INTRODUCTION 78
2. MATERIALS AND METHODS 80
   - 2.1 Materials 80
   - 2.2 Orodispersible films (ODF) preparation by solvent casting 81
   - 2.3 Orodispersible films (ODF) preparation by hot-melt ram-extrusion 3D printing 81
   - 2.4 Oral lyophilizate (OL) preparation 82
   - 2.5 Disintegration time 83
   - 2.6 β-gal content 83
   - 2.7 Enzymatic activity assay 83
   - 2.8 *In vitro* lactose hydrolysis 84
   - 2.9 Stability assay 85
3. RESULTS AND DISCUSSION 86
   - 3.1 Orodispersible films (ODF) preparation 86
   - 3.3 Oral lyophilizates (OL) preparation 87
   - 3.4 Hydrolysis of lactose contained in a medicinal product in water 88
   - 3.5 *In vitro* lactose hydrolysis to simulate the digestion of milk 89
4. CONCLUSIONS 92
5. REFERENCES 93

CHAPTER 4: DESIGN AND CONSTRUCTION OF A SEMI-SOLID EXTRUSION 3D PRINTER FOR THE EXTEMPORANEOUS PREPARATION OF HIGHLY CUSTOMIZABLE ORODISPERSIBLE FILMS 95

1. INTRODUCTION 95
2. MATERIALS 97
3. DESIGN AND CONSTRUCTION 97
   - 3.1 Outer structure 97
   - 3.2 XY axes 98
   - 3.3 Z axis 98
   - 3.4 Syringe pump extruder (E0 axis) 99
   - 3.5 Drying oven (E1 axis) 100
   - 3.6 Control system 100
4. DESCRIPTION OF A TYPICAL PRINT RUN AND PRELIMINARY STEPS 102
   - 4.1 Generating a 3D model 102

4.2 Generating the gcode file ... 102
4.3 Setting up the printer ... 103
4.4 Execution of a print job ... 103
5. TESTING THE VERSATILITY OF THE PRINTER FOR THE PREPARATION OF ODF ... 104
Case study 1: β-galactosidase ODF ... 105
Case study 2: CBD oil ODF ... 106
Case study 3: diclofenac-loaded solid lipid microparticles ODF ... 108
6. CONCLUSIONS ... 112
7. REFERENCES ... 114

CHAPTER 5: CUSTOMIZABLE EXTENDED-RELEASE ORODISPERSIBLE FILMS CONTAINING TRIHEXYPHENIDYL ... 115
1. INTRODUCTION ... 115
2. MATERIALS AND METHODS ... 117
2.1 Materials ... 117
2.2 Preparation of the drug/clay hybrid ... 117
2.3 Solid state characterization ... 117
2.4 Preparation and characterization of the ODF by semi-solid extrusion 3D printing ... 118
2.5 Dissolution studies ... 120
3. RESULTS ... 120
3.1 Solid state characterization ... 121
3.2 Dissolution studies on the THP/clay hybrids ... 126
3.3 Characterization of the THP-loaded ODF ... 127
4. CONCLUSIONS ... 127
5. REFERENCES ... 129

FINAL REMARKS ... 130

INTRODUCTION

1. BACKGROUND AND RESEARCH AIM

Orodispersible Films (ODF) and Mucoadhesive Films (MAF) are single- or multilayer sheets of suitable materials intended for administration to the oral cavity, where one or more active pharmaceutical ingredients (API) are released for local or systemic action. According to the European Pharmacopoeia (Supplement 11.8), upon contact with saliva ODF should disperse rapidly, resulting in a solution or suspension of the API which can then be swallowed for adsorption in the gastrointestinal tract, whereas MAF adhere to the oral mucosa, allowing for the release of the API over an extended period of time [1], [2].

Compared with conventional oral dosage forms, ODF and MAF present several advantages. Since their administration does not involve swallowing the intact dosage form, as opposed to the more conventional tablets and capsules, they are particularly suitable for patients with special needs who have difficulties swallowing solid objects, such as children, elders and dysphagics, as well as the mentally ill, the bedridden, patients that are on reduced liquid intake plans, and workers or travellers with limited access to water [3], [4], and even among the general population they are associated with higher patient acceptability compared to conventional solid oral dosage forms [5]. Additionally, especially in the case of MAF due to their higher residence time in the buccal cavity, absorption via the oral mucosa can result in a fast onset of action as well as improve the bioavailability of the drug by bypassing hepatic first-pass metabolism and preventing degradation in the GI tract [6]. Finally, both ODF and MAF are characterized by excellent dosing flexibility, as changing the drug strength is as simple as changing the size of the film. For all these reasons, they are widely studied for personalized treatment [7], [8], which can be defined as the tailoring of treatments according to the individual characteristics, needs, and preferences of patients [9]. In particular, the possibility of easily obtaining different drug strengths from the same starting material makes these dosage forms good candidates for point-of-care manufacturing, and efforts are

being made to develop technologies that are suitable for the on-demand extemporaneous production of these films in the compounding laboratories of community or hospital pharmacies [10], [11], [12].

As regards formulation, the main components of both ODF and MAF are the film-forming polymers that constitute the matrix within which the API is dispersed. Film-forming polymers with different chemical properties and molecular weights may be used to achieve the desired stickiness, disintegration time, drug loading, mechanical strength and ease of handling [13].

Several hydrophilic polymers have been investigated and proposed as excipients for ODF, such as cellulose ethers [14], polyvinyl alcohol [15], polyethylene oxide [16], pullulan [17], maltodextrins [18], [19], and modified starches [20], [21]. In the case of MAF, the choice of the polymers should also be based on their mucoadhesive properties, i.e. their ability to interact with mucin, as one of their main functions is to ensure that the film remain attached to the mucosa without shifting, swelling or detaching prematurely. The factors that have the biggest influence on mucoadhesiveness are the polymer's charge, with polyanions and polycations performing better than neutral polymers; its molecular weight, with high molecular weight improving the mucoadhesiveness of linear polymers; chain flexibility, which is necessary for polymer/mucin interpenetration; the presence of hydrogen-bonding groups, which contribute to the polymer's interaction with mucin [22], [23], [24]. For example, chitosan, one of the most commonly used polymers in mucoadhesive preparations, is characterized by the presence of hydroxyl and amine groups along its backbone [25]. These are responsible for the formation of hydrogen bonds with mucin, and under acidic conditions the protonated amine groups can form electrostatic interactions with the negatively charged components of mucus. To further enhance the mucoadhesive performance of chitosan, synthetic derivatives have also been studied, such as chitosans that are permanently cationic to promote electrostatic interactions, or thiolated chitosans, whose thiols can form disulfide bonds with the cysteine residues in mucins [25].

Besides the polymeric excipients, which usually make up the bulk of the film, additional components may be added to achieve the desired mechanical properties,

mouthfeel, or dissolution profile. Plasticizers, such as glycerol or sorbitol, can be used to lower the glass transition temperature of polymers, improving the flexibility of the film. Surfactants can improve the wettability of the film and therefore reduce its disintegration time, or they may be added for reasons related to the manufacturing process. Saliva-stimulating agents, such as citric acid, can help reduce disintegration time, especially in individuals suffering from dry mouth. Sweetening and flavoring agents can be added to mask the taste of unpalatable drugs [10], [26].

As for manufacturing, the main techniques reported in the literature for producing ODF or MAF are solvent casting, hot melt extrusion, and printing technologies [10], [27], [28].

Solvent casting is the most widely used method to produce films on an industrial scale [26]. In this process, a slurry containing the constituents of the formulation is cast onto a release liner using a doctor blade and then dried. The resulting laminate is cut into single films with the desired size, determining the drug strength of the dosage units. The versatility of this technique, which is an important aspect to consider in view of its potential adoption in compounding pharmacies, is well established. Indeed, chemically-diverse API can be successfully loaded into ODF or MAF with only minor formulation adjustments [7].

Hot melt extrusion is a solvent-free technology in which a mixture of the film-forming polymer, other excipients, and the API is processed above the polymer's glass transition temperature and the API's melting point to form a solid dispersion, which is then extruded through a die. Its use in the production of films is limited by the high operating temperatures, which are incompatible with heat-sensitive drugs and excipients. In some cases, this obstacle can be overcome by preliminary amorphization of the API or by promoting the formation of lower-melting co-crystals to reduce its melting point, allowing the process to be conducted at lower temperatures [29], [30], or by selecting excipients that can interact with the API to reduce its melting point and stabilize it [31].

Neither solvent casting nor hot melt extrusion are suitable for the production of very small batches as required by the compounding process in a pharmacy setting [10].

In the case of solvent casting, the processing steps (casting the slurry, cutting the laminate, packaging) cannot be automated in a small laboratory apparatus and, therefore, the quality of the final dosage unit can be limited by human operations, even if some authors proposed the use of petri dishes and an oven [32], [33]. An alternative method based on the same principle consisting in the use of unit-dose plates that can be filled with the slurry has been proposed [34]. The hot melt extrusion process, as stated above, requires the study of ad hoc strategies for each new molecule and/or the addition of more steps to the process, making this technique impractical for compounding laboratories, where the possibility of preparing on-demand dosage forms requires simple and versatile processes and formulations that can be used for a wide range of API with minimal modifications.

Printing techniques, conversely, make it possible to automate the production of correctly dosed films, improving dosing accuracy. The most studied 2D-printing technology to date is inkjet printing, in which a solution or dispersion of the drug in a liquid medium is used as an ink and deposited onto a preformed placebo film. This prevents the drug from negatively impacting the mechanical properties of the film, as can be the case with technologies where the drug is mixed with the excipients before the film is formed. The printers used for inkjet printing are – or are adapted from – commercial inkjet printers, and can be controlled using any word processor [35]. The main drawback of this technique is the limited flexibility of the ink, whose formulation has to be modified to counterweigh the impact of the loaded drug on the critical surface tension of the dispersion [10]. Another is the need for pre-formed placebo films to print on, which can be either produced using another technique, thereby doubling the amount of equipment required for the process, or externally sourced, possibly increasing the overall cost of the process.

3D printing has also emerged as a cost- and time-effective possibility for pharmacy and small laboratory compounding of on-demand personalized products [36]. Fused deposition modelling (FDM) is a 3D printing technique by which a polymeric filament loaded with the API is fused and deposited layer-by-layer onto a print bed, following a pattern determined by the user. Despite being the most studied 3D printing technique in the field of pharmaceutical manufacturing [37], it has two main

drawbacks that limit its suitability for personalized therapy: first, since the filaments have to be fused, the same limitations outlined for hot melt extrusion apply; second, API-loaded filaments with suitable properties have to be prepared preliminarily, usually by hot melt extrusion or by impregnating placebo filaments with the API, which makes the technology impractical for on-demand extemporaneous compounding.

To overcome this limitation, novel approaches have emerged based on the direct extrusion of a mixture of API and excipients through a nozzle. Depending on whether the mixture is in the form of a powder blend, a paste, or a viscous liquid, the technique is termed direct powder extrusion (DPE) 3D printing, hot melt ram-extrusion (HMRE) 3D printing, or semisolid extrusion (SSE) 3D printing, respectively. In all cases, the process can be divided into three steps: (1) a mixture containing the film-forming polymer, the API, and any additional excipients is prepared; (2) the mixture is transferred into the printer's extrusion chamber; (3) the mixture is extruded through a nozzle onto the print bed.

In the case of DPE, which shares the same mechanism as hot melt extrusion, high-temperature heating is required to melt the powder blend and obtain an extrudable paste prior to printing. Despite its potential incompatibility with heat-sensitive API, promising results have been reported using this technique [38], [39], and this limitation appears to be largely outweighed by the simplicity and practicality of the process, as evidenced by the fact that DPE printers for the extemporaneous preparation of pharmaceutical dosage forms are becoming available [40], [41]. However, while this technique has been used extensively in the production of conventional solid dosage forms such as tablets [42], data on the feasibility of obtaining ODF or MAF is lacking. Indeed, only two works have been published so far describing the preparation of ODF by DPE 3D printing, in one case loaded with olanzapine [38] and in the other with aripiprazole [43].

In HMRE, a paste is heated and then extruded. The paste is obtained by wetting the API and the dry excipients with a liquid plasticizer. The process can therefore be conducted at lower temperatures, which makes it compatible with a wider range of API compared to DPE. The adequacy of this technique for the extemporaneous

preparation of small batches of ODF with a custom-made printer has already been demonstrated using paracetamol [19] and diclofenac [44].

Finally, in the case of SSE, since the starting mixture is already fluid, the extrusion can generally be conducted at room temperature, making this technique compatible with an even wider range of API and excipients. A final drying stage is however necessary to obtain the finished film from the deposited slurry, but this can usually be achieved at relatively low temperatures, ranging from room temperature to about 60 °C. This technique was successfully used to prepare ODF loaded with a wide variety of API, including warfarin [45] and phenytoin [46], two API that would benefit greatly from personalized dosing due to their narrow therapeutic index, caffeine [47], [48], levocetirizine [49], montelukast [50], benzydamine hydrochloride, in which case the films were printed on a heated bed for in-process drying [51], and, more recently, even a vaccine [52]. However, to our knowledge, a machine custom-built specifically for SSE printing and drying of pharmaceutical dosage forms is not currently available, forcing researchers to use expensive machines designed for bioprinting [53].

The aim of this PhD project was to demonstrate the suitability of 3D printing technologies for the preparation of MAF (via DPE 3D printing) and ODF (via SSE 3D printing), with the ultimate goal of developing robust printing processes suitable for the on-demand extemporaneous compounding of personalized films in a pharmacy setting.

First, the feasibility of obtaining MAF by DPE was assessed using clobetasol propionate and lidocaine as model drugs and chitosan or its derivatives as mucoadhesive materials (Chapter 1 and Chapter 2). A new DPE 3D printer specifically designed for the production of pharmaceutical dosage forms was used (3DForMe® [41]).

Secondly, HMRE 3D printing was tested as a milder alternative to DPE in the preparation of ODF containing heat-sensitive molecules, and compared with the traditional method of solvent casting used in industrial manufacturing. In particular, the enzyme β-galactosidase was either incorporated in a maltodextrin-based

mixture and printed using a custom-made HMRE printer, or dispersed in a maltodextrin-based slurry, spread onto a release liner and dried in the case of solvent casting (Chapter 3). Since the former resulted in the thermal degradation of the enzyme while the latter yielded promising results, the attention was directed toward scaling down the solvent casting process and making it suitable for compounding. Thus, the activities were focused on the prototyping of a 3D printer that could print slurries similar to those used for solvent casting, i.e. a SSE 3D printer (Chapter 4). The versatility of the designed SSE printer was tested by printing β-galactosidase ODF (Case study 1, Chapter 4), CBD oil ODF (Case study 2, Chapter 4), and ODF loaded with diclofenac-loaded lipid microparticles (Case study 3, Chapter 4). Finally, the feasibility of applying SSE 3D printing to the preparation of ODF containing a trihexyphenidyl/clay hybrid to obtain a prolonged release orodispersible dosage form was studied (Chapter 5).

2. REFERENCES

[1] "Orodispersible Films, monograph 3195. Ph. Eur. Suppl. 11.8. Strasbourg, France: Council of Europe; 2025."

[2] "Oromucosal Preparations, monograph 1807. Ph. Eur. Suppl. 11.8. Strasbourg, France: Council of Europe; 2025."

[3] A. R. Patel, D. S. Prajapati, and J. A. Raval, "Fast dissolving films (FDFs) as a newer venture in fast dissolving dosage forms," *International Journal of Drug Development and Research*, vol. 2, no. 2, pp. 232–246, Apr. 2010.

[4] H. Seager, "Drug-delivery Products and the Zydis Fast-dissolving Dosage Form," *Journal of Pharmacy and Pharmacology*, vol. 50, no. 4, pp. 375–382, Apr. 2011, doi: 10.1111/J.2042-7158.1998.TB06876.X.

[5] Y. Tian *et al.*, "Oromucosal films: from patient centricity to production by printing techniques," *Expert opinion on drug delivery*, vol. 16, no. 9, pp. 981–993, Sept. 2019, doi: 10.1080/17425247.2019.1652595.

[6] R. P. Dixit and S. P. Puthli, "Oral strip technology: Overview and future potential," *Journal of Controlled Release*, vol. 139, no. 2, pp. 94–107, June 2009, doi: 10.1016/J.JCONREL.2009.06.014.

[7] J. C. Visser *et al.*, "Orodispersible films in individualized pharmacotherapy: The development of a formulation for pharmacy preparations," *International Journal of Pharmaceutics*, vol. 478, no. 1, pp. 155–163, Jan. 2015, doi: 10.1016/J.IJPHARM.2014.11.013.

[8] R. Krampe, J. C. Visser, H. W. Frijlink, J. Breitkreutz, H. J. Woerdenbag, and M. Preis, "Oromucosal film preparations: points to consider for patient centricity and manufacturing processes," *Expert Opinion on Drug Delivery*, vol. 13, no. 4, pp. 493–506, Nov. 2015, doi: 10.1517/17425247.2016.1118048.

[9] L. Zema, A. Melocchi, A. Maroni, and A. Gazzaniga, "Three-Dimensional Printing of Medicinal Products and the Challenge of Personalized Therapy," *Journal of Pharmaceutical Sciences*, vol. 106, no. 7, pp. 1697–1705, July 2017, doi: 10.1016/j.xphs.2017.03.021.

[10] U. M. Musazzi, G. M. Khalid, F. Selmin, P. Minghetti, and F. Cilurzo, "Trends in the production methods of orodispersible films," *International Journal of Pharmaceutics*, vol. 576, p. 118963, Feb. 2020, doi: 10.1016/J.IJPHARM.2019.118963.

[11] H. Öblom, E. Sjöholm, M. Rautamo, and N. Sandler, "Towards Printed Pediatric Medicines in Hospital Pharmacies: Comparison of 2D and 3D-Printed Orodispersible Warfarin Films with Conventional Oral Powders in Unit Dose Sachets," *Pharmaceutics*, vol. 11, no. 7, p. 334, July 2019, doi: 10.3390/pharmaceutics11070334.

[12] M. B. Bernhardt, F. Shokraneh, L. Hrizanovska, J. Lahtinen, C. A. Brasher, and N. Sandler, "Automated 3D Printing-Based Non-Sterile Compounding Technology for Pediatric Corticosteroid Dosage Forms in a Health System Pharmacy Setting," *Pharmaceutics*, vol. 17, no. 6, p. 762, June 2025, doi: 10.3390/pharmaceutics17060762.

[13] A. F. Borges, C. Silva, J. F. J. Coelho, and S. Simões, "Oral films: Current status and future perspectives: I-Galenical development and quality attributes," *Journal of Controlled Release*, vol. 206, pp. 1–19, Mar. 2015, doi: 10.1016/J.JCONREL.2015.03.006.

[14] A. Y. F. Al-Oran and E. Yenilmez, "Hydroxypropyl Methylcellulose Orodispersible Film Containing Desloratadine for Geriatric Use: Formulation and Evaluation," *Antiinflamm Antiallergy Agents Med Chem*, vol. 22, no. 2, pp. 79–91, 2023, doi: 10.2174/1871523022666230816090942.

[15] C. Wei, N. G. Solanki, J. M. Vasoya, A. V. Shah, and A. T. M. Serajuddin, "Development of 3D Printed Tablets by Fused Deposition Modeling Using Polyvinyl Alcohol as Polymeric Matrix for Rapid Drug Release," *Journal of Pharmaceutical Sciences*, vol. 109, no. 4, pp. 1558–1572, Apr. 2020, doi: 10.1016/j.xphs.2020.01.015.

[16] I. d'Angelo, A. Fraix, F. Ungaro, F. Quaglia, and A. Miro, "Poly(ethylene oxide)/hydroxypropyl-β-cyclodextrin films for oromucosal delivery of hydrophilic drugs," *International Journal of Pharmaceutics*, vol. 531, no. 2, pp. 606–613, Oct. 2017, doi: 10.1016/j.ijpharm.2017.06.029.

[17] M. S. Gupta *et al.*, "Development and Characterization of Pullulan-Based Orodispersible Films of Iron," *Pharmaceutics*, vol. 15, no. 3, p. 1027, Mar. 2023, doi: 10.3390/pharmaceutics15031027.

[18] V. Pechová, J. Gajdziok, J. Muselík, and D. Vetchý, "Development of Orodispersible Films Containing Benzydamine Hydrochloride Using a Modified Solvent Casting Method," *AAPS PharmSciTech*, vol. 19, no. 6, pp. 2509–2518, Aug. 2018, doi: 10.1208/s12249-018-1088-y.

[19] U. M. Musazzi *et al.*, "Personalized orodispersible films by hot melt ram extrusion 3D printing," *International Journal of Pharmaceutics*, vol. 551, no. 1–2, pp. 52–59, Nov. 2018, doi: 10.1016/J.IJPHARM.2018.09.013.

[20] E. Limpongsa and N. Jaipakdee, "Physical modification of Thai rice starch and its application as orodispersible film former," *Carbohydrate Polymers*, vol. 239, p. 116206, July 2020, doi: 10.1016/j.carbpol.2020.116206.

[21] A. Alayoubi, L. Haynes, H. Patil, B. Daihom, R. Helms, and H. Almoazen, "Development of a fast dissolving film of epinephrine hydrochloride as a potential anaphylactic treatment for pediatrics," *Pharm Dev Technol*, vol. 22, no. 8, pp. 1012–1016, Dec. 2017, doi: 10.3109/10837450.2015.1131715.

[22] K. Park, J. R. Robinson, and J. R. Robinson, "Bioadhesive polymers as platforms for oral-controlled drug delivery: method to study bioadhesion," *International Journal of Pharmaceutics*, vol. 19, pp. 107–127, Nov. 1983.

[23] N. A. Peppas and P. A. Buri, "Surface, interfacial and molecular aspects of polymer bioadhesion on soft tissues," *Journal of Controlled Release*, vol. 2, pp. 257–275, Nov. 1985, doi: 10.1016/0168-3659(85)90050-1.

[24] P. Subramanian, "Mucoadhesive Delivery System: A Smart Way to Improve Bioavailability of Nutraceuticals," *Foods*, vol. 10, no. 6, p. 1362, June 2021, doi: 10.3390/foods10061362.

[25] T. M. M. Ways, W. M. Lau, and V. V. Khutoryanskiy, "Chitosan and Its Derivatives for Application in Mucoadhesive Drug Delivery Systems," *Polymers (Basel)*, vol. 10, no. 3, p. 267, Mar. 2018, doi: 10.3390/polym10030267.

[26] S. Jacob, S. H. S. Boddu, R. Bhandare, S. S. Ahmad, and A. B. Nair, "Orodispersible Films: Current Innovations and Emerging Trends," *Pharmaceutics*, vol. 15, no. 12, p. 2753, Dec. 2023, doi: 10.3390/pharmaceutics15122753.

[27] M. Preis, J. Breitkreutz, and N. Sandler, "Perspective: Concepts of printing technologies for oral film formulations," *International Journal of Pharmaceutics*, vol. 494, no. 2, pp. 578–584, Feb. 2015, doi: 10.1016/J.IJPHARM.2015.02.032.

[28] B. M. A. Silva, A. F. Borges, C. Silva, J. F. J. Coelho, and S. Simões, "Mucoadhesive oral films: The potential for unmet needs," *International journal of pharmaceutics*, vol. 494, no. 1, pp. 537–551, Oct. 2015, doi: 10.1016/J.IJPHARM.2015.08.038.

[29] D. Huang *et al.*, "Hot melt extrusion of heat-sensitive and high melting point drug: Inhibit the recrystallization of the prepared amorphous drug during extrusion to improve the bioavailability," *International Journal of Pharmaceutics*, vol. 565, pp. 316–324, June 2019, doi: 10.1016/j.ijpharm.2019.04.064.

[30] X. Liu, M. Lu, Z. Guo, L. Huang, X. Feng, and C. Wu, "Improving the Chemical Stability of Amorphous Solid Dispersion with Cocrystal Technique by Hot Melt Extrusion," *Pharm Res*, vol. 29, no. 3, pp. 806–817, Mar. 2012, doi: 10.1007/s11095-011-0605-4.

[31] A. Haser, S. Huang, T. Listro, D. White, and F. Zhang, "An approach for chemical stability during melt extrusion of a drug substance with a high melting point," *International Journal of Pharmaceutics*, vol. 524, no. 1, pp. 55–64, May 2017, doi: 10.1016/j.ijpharm.2017.03.070.

[32] V. Y. Londhe and K. B. Umalkar, "Formulation Development and Evaluation of Fast Dissolving Film of Telmisartan," *Indian J Pharm Sci*, vol. 74, no. 2, pp. 122–126, 2012, doi: 10.4103/0250-474X.10384.

[33] R. M. Zaki *et al.*, "Fabrication and characterization of orodispersible films loaded with solid dispersion to enhance Rosuvastatin calcium bioavailability," *Saudi Pharmaceutical Journal*, vol. 31, no. 1, pp. 135–146, Jan. 2023, doi: 10.1016/j.jsps.2022.11.012.

[34] W. C. Foo, Y. M. Khong, R. Gokhale, and S. Y. Chan, "A novel unit-dose approach for the pharmaceutical compounding of an orodispersible film," *International Journal of Pharmaceutics*, vol. 539, no. 1–2, pp. 165–174, Mar. 2018, doi: 10.1016/J.IJPHARM.2018.01.047.

[35] N. Genina, E. M. Janßen, A. Breitenbach, J. Breitkreutz, and N. Sandler, "Evaluation of different substrates for inkjet printing of rasagiline mesylate," *European Journal of Pharmaceutics and Biopharmaceutics*, vol. 85, no. 3, pp. 1075–1083, Nov. 2013, doi: 10.1016/J.EJPB.2013.03.017.

[36] J. Norman, R. D. Madurawe, C. M. V. Moore, M. A. Khan, and A. Khairuzzaman, "A new chapter in pharmaceutical manufacturing: 3D-printed drug products," *Advanced Drug Delivery Reviews*, vol. 108, pp. 39–50, Jan. 2017, doi: 10.1016/J.ADDR.2016.03.001.

[37] S. Cailleaux, N. M. Sanchez-Ballester, Y. A. Gueche, B. Bataille, and I. Soulairol, "Fused Deposition Modeling (FDM), the new asset for the production of tailored medicines," *Journal of Controlled Release*, vol. 330, pp. 821–841, Feb. 2021, doi: 10.1016/j.jconrel.2020.10.056.

[38] H.-W. Cho, S.-H. Baek, B.-J. Lee, and H.-E. Jin, "Orodispersible Polymer Films with the Poorly Water-Soluble Drug, Olanzapine: Hot-Melt Pneumatic Extrusion for Single-Process 3D Printing," *Pharmaceutics*, vol. 12, no. 8, p. 692, July 2020, doi: 10.3390/pharmaceutics12080692.

[39] M. Rosch *et al.*, "Development of an immediate release excipient composition for 3D printing via direct powder extrusion in a hospital," *International Journal of Pharmaceutics*, vol. 643, p. 123218, Aug. 2023, doi: 10.1016/j.ijpharm.2023.123218.

[40] "Pharmaceutical 3D Printing | FABRX Ltd. - Personalized Medicine." [Online]. Available: https://fabrx.co.uk/

[41] "STAMPANTE 3DFORME | Farmalabor." 2022. [Online]. Available: https://www.farmalabor.it/stampante-3dforme.html

[42] Á. Aguilar-de-Leyva, M. Casas, C. Ferrero, V. Linares, and I. Caraballo, "3D Printing Direct Powder Extrusion in the Production of Drug Delivery Systems: State of the Art and Future Perspectives," *Pharmaceutics*, vol. 16, no. 4, p. 437, Apr. 2024, doi: 10.3390/pharmaceutics16040437.

[43] B.-C. Oh, G. Jin, C. Park, J.-B. Park, and B.-J. Lee, "Preparation and evaluation of identifiable quick response (QR)-coded orodispersible films using 3D printer with directly feeding nozzle," *International Journal of Pharmaceutics*, vol. 584, p. 119405, June 2020, doi: 10.1016/j.ijpharm.2020.119405.

[44] G. M. Khalid, U. M. Musazzi, F. Selmin, S. Franzè, P. Minghetti, and F. Cilurzo, "Extemporaneous printing of diclofenac orodispersible films for pediatrics," *Drug Development and Industrial Pharmacy*, vol. 47, no. 4, pp. 636–644, Apr. 2021, doi: 10.1080/03639045.2021.1908335.

[45] E. Sjöholm and N. Sandler, "Additive manufacturing of personalized orodispersible warfarin films," *International Journal of Pharmaceutics*, vol. 564, pp. 117–123, June 2019, doi: 10.1016/j.ijpharm.2019.04.018.

[46] P. Panraksa, S. Udomsom, P. Rachtanapun, C. Chittasupho, W. Ruksiriwanich, and P. Jantrawut, "Hydroxypropyl Methylcellulose E15: A Hydrophilic Polymer for Fabrication of Orodispersible Film Using Syringe Extrusion 3D Printer," *Polymers (Basel)*, vol. 12, no. 11, p. E2666, Nov. 2020, doi: 10.3390/polym12112666.

[47] M. Elbadawi, D. Nikjoo, T. Gustafsson, S. Gaisford, and A. W. Basit, "Pressure-assisted microsyringe 3D printing of oral films based on pullulan and hydroxypropyl methylcellulose," *International Journal of Pharmaceutics*, vol. 595, p. 120197, Feb. 2021, doi: 10.1016/j.ijpharm.2021.120197.

[48] A. Roche, N. M. Sanchez-Ballester, A. Aubert, J.-C. Rossi, S. Begu, and I. Soulairol, "Preliminary Study on the Development of Caffeine Oral Solid Form 3D Printed by Semi-Solid Extrusion for Application in Neonates," *AAPS PharmSciTech*, vol. 24, no. 5, p. 122, May 2023, doi: 10.1208/s12249-023-02582-z.

[49] T.-T. Yan *et al.*, "Semi-solid extrusion 3D printing ODFs: an individual drug delivery system for small scale pharmacy," *Drug Dev Ind Pharm*, vol. 46, no. 4, pp. 531–538, Apr. 2020, doi: 10.1080/03639045.2020.1734018.

[50] E. Özcan-Bülbül, Y. Kalender, A. Bal-Öztürk, and N. Üstündağ-Okur, "Preparation and In Vitro Evaluation of Montelukast Sodium-Loaded 3D Printed Orodispersible Films for the Treatment of Asthma," *AAPS PharmSciTech*, vol. 25, no. 7, p. 218, Sept. 2024, doi: 10.1208/s12249-024-02938-z.

[51] J. Elbl, J. Gajdziok, and J. Kolarczyk, "3D printing of multilayered orodispersible films with in-process drying," *International Journal of Pharmaceutics*, vol. 575, p. 118883, Feb. 2020, doi: 10.1016/J.IJPHARM.2019.118883.

[52] S. Shah *et al.*, "Buccal Administration of a Zika Virus Vaccine Utilizing 3D-Printed Oral Dissolving Films in a Mouse Model," *Vaccines (Basel)*, vol. 12, no. 7, p. 720, June 2024, doi: 10.3390/vaccines12070720.

[53] E. Sjöholm *et al.*, "3D-Printed Veterinary Dosage Forms—A Comparative Study of Three Semi-Solid Extrusion 3D Printers," *Pharmaceutics*, vol. 12, no. 12, p. 1239, Dec. 2020, doi: 10.3390/pharmaceutics12121239.

CHAPTER 1: 3D-PRINTED MUCOADHESIVE FILMS MANUFACTURED BY DIRECT POWDER EXTRUSION FOR PERSONALIZED CLOBETASOL PROPIONATE BASED PAEDIATRIC THERAPIES

1. INTRODUCTION

Oral Lichen Planus (OLP) is a chronic mucocutaneous disorder of the stratified squamous epithelium affecting the oral mucous membranes [1]. The disease occurs as a T-cell-mediated autoimmune condition, in which self-cytotoxic CD8+ T cells trigger apoptosis of basal cells of the oral epithelium [2]. Although its incidence is often reported in middle-aged patients, an important occurrence in the paediatric population is also observed [3], [4].

The use of corticosteroids is to date the most indicated therapy for reducing the symptoms and local effects of autoimmune diseases of the oral mucosae [5]. Topical corticosteroids, in fact, efficiently reduce inflammation-related symptoms [6] by reducing leukocyte exudation and the formation of inflammatory mediators and preserving the integrity of cell membrane [7]. Clobetasol propionate (CBS) is a corticosteroid with strong anti-inflammatory, antipyretic, and vasoconstrictive properties [8] that is commonly used for the topical treatment of OLP [9]. Topical application of CBS is promoted in clinical practice because it provides high benefits while maintaining minimal the possibility of side effects occurrence [10]. However, CBS is characterized by low aqueous solubility, which significantly limits its therapeutic efficacy [11].

The administration of CBS in the buccal cavity occurs by using off-label semisolid preparations, even if a few works report the possibility to develop mucoadhesive dosage forms such as tablets [12] or oral lyophilizates containing mucoadhesive interpolymeric complexes [13]. However, neither approach can be considered suitable when this pathology affects the paediatric population, since tablets and

semisolid formulations are poorly tolerated and mucoadhesive nanoparticles can be swallowed if the patient does not maintain the saliva in the buccal cavity for a sufficient period of time to ensure the adhesion of the formulation to the mucosa [14]. Moreover, an off-label use of semisolid preparations in the buccal cavity of paediatric patients could adversely affect drug bioavailability and therapy outcomes [15]. Hence, an unmet medical need in the paediatric population is evident, which could be addressed with the development of personalized oral formulations characterised by accurate and flexible dosages, sizes, and shapes suitable for children [16].

The aim of this study was to obtain mucoadhesive oral films (MAF) containing approximately 125 μg/dose of CBS, a dose deemed therapeutically appropriate and functional for OLP treatment [12], in order to enhance paediatric patients' compliance toward therapy [17]. In order to produce mucoadhesive oral films that accurately meet the personal needs of the individual patient, the 3D printing technique was used [18]. In fact, among all techniques available to date for obtaining oromucosal films, 3D printing ensures a better uniformity of active compounds and reduced operational units, allowing a continuous production process [19]. Therefore, the 3D printing technique can be used to produce polymer matrices with greater precision for the incorporation of the active compound [20]. The concentration of active ingredients can be fully customized by changing the print settings and geometry, producing a final pharmaceutical form on demand according to individual patient needs [21], [22].

To date, several natural and synthetic hydrophilic polymers, such as hydroxypropylmethylcellulose (HPMC) [23], maltodextrin [24], polyvinyl alcohol (PVA) [25], polyethylene oxide (PEO) [26], polylactic acid (PLA) [27], and polyvinylpyrrolidone (PVP) [28] have been investigated for the manufacture of 3D-printed pharmaceutical forms for personalized therapy [29]. Among them, PEO and HPMC have been already studied for the design of mucoadhesive oral films [30], [31], [32].

Indeed, efficient oromucosal administration requires a prolonged contact time of the drug with the mucosal surface, preventing saliva elution and thus allowing the

continuous treatment of local conditions [33]. Therefore, the dosage form must possess mucoadhesive properties that increase the exposure time of the drug to the mucosae, improving its therapeutic efficacy and minimizing its toxicity [34]. Even if HPMC and PEO exhibit quite good mucoadhesive properties, they are often used in combination with other polymeric materials that can enhance their interactions with mucins [32], [35], [36].

Chitosan (CS) is a linear polysaccharide copolymer with mucoadhesive properties provided by –OH and –NH2 groups, leading to the formation of hydrogen and covalent bonds with the cysteine groups of the mucosal layers [37]. This polymer is widely used in the pharmaceutical field not only because of its strong mucoadhesive properties, but also because its biocompatibility and toxicity characteristics make it safe to use [38].

In addition, to improve the aqueous solubility of CBS, hydroxypropyl-β-cyclodextrin (HP-β-CD) was included in the formulation. HP-β-CD has been widely used in pharmaceutical formulations with the purpose of increasing the aqueous solubility of poorly soluble drugs through the formation of inclusion complexes [39]. CDs are a class of cyclic oligosaccharides consisting of six, seven or eight glucose units linked by α-(1,4)-glycosidic bonds. The spatial arrangement of the molecules gives CDs a hydrophilic shell and a hydrophobic core. It takes the shape of a truncated cone, which can be used as a host molecule to encapsulate insoluble compounds of appropriate size [40]. In addition, the formation of multicomponent complexes (drug, CD, and polymer) in which the polymer can improve the stability of the drug-CD complex has been demonstrated in the past by the formation of ternary complexes that can greatly increase the aqueous solubility of the drug [41]. In this case, HP-β-CD is also responsible for masking the taste of the drug in the final formulation by hindering its interaction with taste receptors [42].

In order to make the resulting pharmaceutical forms fully customizable, the mucoadhesive films were produced through an innovative 3D printing technique, Direct Powder Extrusion (DPE) [43], [44]. With this technique, the final pharmaceutical form can be obtained directly from medicated powder pellets or blends, bypassing the intermediate step of thermoplastic filament formation

required by other printing techniques currently in use and thus preserving the active from the possibility of degradation [41], [45]. An additional advantage of this technique is the possibility of obtaining different drug strengths either by changing the concentration of the drug or by changing the size of the films, allowing complete customization of the final pharmaceutical form, making it adherent to the individual patient's needs [46].

Therefore, in this work, CBS-loaded mucoadhesive films were produced by the DPE 3D printing technique starting from different powder mixtures. Subsequently, the obtained films were fully characterised in terms of chemical and physical characteristics in order to evaluate their differences and identify the best formulations. Finally, an evaluation of mucoadhesive and tensile properties and in vitro permeation and retention characteristics was performed in order to validate the obtained mucoadhesive films as possible drug delivery systems in paediatric OLP therapy.

2. MATERIALS AND METHODS

2.1 Materials

CBS and HP-β-CD (Cavasol W7, HP-β-CD with MW = 1540, molar substitution degree SD = 7) were purchased from Farmalabor Srl (Italy). AFFINISOL™ HPMC HME 15 LV (hydroxypropyl methylcellulose) was gifted by Pharma Solutions – Nutrition & Biosciences (Italy). PEO (Polyox WSR N10, MW = 100.000) was purchased from DuPont (Italy). Chitosan (low molecular weight) and Crude (Type II) mucin from porcine stomach were purchased from Sigma-Aldrich (Merck, Germany). Potassium Phosphate Dibasic was purchased from Honeywell Fluka (Italy). For the analysis, distilled and purified water (resistivity of 18.2 MΩ.cm at 23 °C) was obtained by the purification system Milli-Q (Purelab DI, MK2) (Elga, UK). Acetonitrile and methanol were purchased from VWR S.r.l. (Italy). All solvents were of analytical grade, unless otherwise specified.

2.2 Quantitative analysis of CBS by HPLC-UV

The concentration of CBS was determined by HPLC-UV (HP 1100, ChemStation, Agilent Technologies, USA), modifying the analytical method proposed by Kamberi et al. [47]. Compound separation was carried out using a reverse-phase column (Inertclone 5 µm, ODS(3), 100 Å, 150 × 4.6 mm, Phenomenex Inc., USA) and HPLC-grade water/acetonitrile as mobile phase. The gradient applied during the analysis was: 0 min, B: 52%; 2.5 min, B: 65%; 2.6 min, 68%; 4.9 min, B: 68%; 10 min, B: 52%. The flow rate was 1.0 mL/min, and the injection volume was 20 µL. The retention time of CBS was around 6.3 min. The drug concentration was determined at 240 nm from calibration curves in the range of 0.05–1 µg/mL (R^2 = 1.000).

2.3 Phase solubility studies

The phase solubility study of CBS with HP-β-CD was performed according to the Higuchi-Connors method [48]. Briefly, 2 mL samples were prepared with solutions of different concentrations of HP-β-CD covering a concentration range from 0.0064 to 0.19 M. An excess amount of the drug was added to each solution and the resulting suspensions were sonicated at 37 °C for 2 min. They were then allowed to settle for 48 h in a thermostatic bath at 37 °C with constant oscillation. After reaching equilibrium, the samples were centrifuged at 10,000 rpm for 15 min, and the supernatant was filtered through 0.45-µm cellulose acetate membrane filters (CA) and analysed. The concentration of CBS was determined by HPLC according to the method described above. A solubility diagram was obtained by plotting the molar concentration of the drug against the HP-β-CD molar concentration. The complexation constant ($Kc_{1:1}$) was calculated using the Higuchi-Connors method (Equation 1):

$$Kc_{1:1} = \frac{P}{S_0\,(1-P)} \qquad \textit{Equation 1}$$

where:

S_0 = Intrinsic solubility of CBS in water.

P = Slope of the phase solubility diagram.

Moreover, a solubility study was carried out in the presence of 3% (w/w) HP-β-CD, 15% (w/w) CS, 81.45% (w/w) PEO, and 0.35 % (w/w) HPMC to see if the formation of a multiple polymer system could further increase the solubility of the drug. The same procedure was carried out as previously described.

2.4 Inclusion complex stoichiometry determination (Job's plot method)

The HP-β-CD/CBS inclusion complex in aqueous solution was analysed using the continuous variation method to verify stoichiometry [48]. The difference between the absorbance intensity with and without CD (ΔA) at 260 nm was determined using mixtures of CBS:CD with different molar ratios (from 0 to 1) while keeping the total molar concentration of the species constant. The mixtures were prepared using equimolar (1.0×10^{-4} M) acetonitrile/H2O (50/50 v/v) solutions of CBS and HP-β-CD. The ΔA × [CBS] was plotted against r, where r was defined by the following equation (Equation 2):

$$r = \frac{[\mathrm{CBS}]}{[\mathrm{CBS}]+[\mathrm{CD}]} \qquad \textit{Equation 2}$$

2.5 Preparation of the powder blends

Four samples consisting of polymer powder blends with different concentrations of CS and PEO and a constant drug concentration (CBS 0.20 % w/w) were prepared. In each mixture, HP-β-CD and HPMC were employed to improve drug solubility. The compositions of the mixtures are reported in Table 1.

Table 1 - Composition of the powder mixtures.

Blend ID	CBS	PEO	HPMC	CS	HP-β-CD
			(% w/w)		
Blend 1	0.20	86.45	0.35	10.00	3.00
Blend 2	0.20	81.45	0.35	15.00	3.00
Blend 3	0.20	71.45	0.35	25.00	3.00
Blend 4	0.20	66.45	0.35	30.00	3.00

Each component was sieved three times through a 355 μm mesh sieve to ensure better dimensional uniformity and mixing of the powder. The powders were then

mechanically stirred at 67 rpm for approximately one hour using a Turbula Willy A. Bachofen GmbH (Germany). The resulting powder mixtures were dried overnight in an oven at 40 °C.

2.6 Direct Powder Extrusion 3D printing

The films were printed using a 3DForMe® 3D printer (Farmalabor, Italy) specifically designed for pharmaceutical manufacturing. The 3D model of the film was created using Fusion360 software from Autodesk, which allowed the creation of stereolithography (.stl) files that were then exported to the 3D printer software (Ultimaker Cura). The stereolithography file describes the geometry of the object, while all other parameters are set directly in the Ultimaker Cura software. A cylindrical geometry was chosen to obtain a circular 3D printed film with dimensions of 20 mm (diameter) × 0.3 mm (height). This size made it possible to obtain films with the required weight of 62.5 mg. A parallelepiped geometry was used to obtain rectangular 3D printed films with dimensions of 50 mm (length) × 20 mm (width) × 0.3/0.6 mm (height) for the characterization of the films' mechanical properties. The parameters set in the software for printing were: infill 40% with infill pattern concentric, high resolution with brim, without raft, travel speed 5 mm/s, print speed 5 mm/s, number of shells 2, layer height 0.125 mm, floor temperature 40 °C and extrusion temperature170 °C. The prepared powder mixture was placed in the extruder hopper of the 3D printer, which was specially designed with a direct single-screw powder extruder and a nozzle diameter of 0.8 mm. The extruder design was based on single-screw hot-melt extrusion (HME), and the rotation speed was controlled by the 3D printer's software. In addition, the extruder nozzle moves in three dimensions to create objects with a layered texture. At the end of each print, the extruder was disassembled, removed from the screw, and cleaned to avoid contamination between the blends.

2.7 Extruded filaments characterization

Prior to the printing phase, preliminary studies were conducted to evaluate the behaviour of the four blends during extrusion and the properties of the extruded filament. In the present study, a 3DForMe® 3D printer was used, consisting of a feed

hopper, a single-screw extruder and temperature measurement and control systems. 2 g of each blend were placed in the hopper, and the extrusion temperature was set to 170 °C. At the end of each extrusion process, the filaments were weighed to calculate the yield of the process and visually inspected to assess their suitability for use in obtaining the final pharmaceutical form. From each blend, five pieces of 2 cm length were cut, weighed, and studied to demonstrate the homogeneity of the filament printed. Visual inspection and the amount of CBS were considered. The pieces were dissolved in 4 mL of acetonitrile and stirred overnight. After appropriate dilution, the solutions were analysed by HPLC to calculate the amount of CBS in each piece.

2.8 Solid state characterization of the powder blends

The medicated powder blends were characterized in the solid state, together with the pure drug and the physical blend consisting only of the excipients. They were analysed by Fourier transform infrared spectroscopy (FT-IR), differential scanning calorimetry (DSC) and powder X-ray diffraction (PXRD). For the FT-IR analysis, KBr pellets (2% of the sample) were analysed using a FT-IR 1600 Perkin Elmer spectrophotometer. Data were acquired between 4000 cm−1 and 400 cm−1. DSC was performed using a Mettler Toledo DSC822 instrument. About 5–10 mg of the sample was heated in an aluminium pan at a heating rate of 5 °C/min from 0 °C to 250 °C under N2 flow. The analysis was conducted by presenting a first phase of heating from 0 °C to 250 °C, a second phase of cooling from 250 °C to 0 °C, and a third phase of heating from 0 °C to 250 °C, in order to check the possible degradation of the polymers and the drug during the printing steps. An empty pan was used as reference. The X-ray powder diffraction patterns were collected using a Rigaku Rint2500 rotating Cu anode working at 50 kV and 200 mA in Debye–Scherrer geometry. The diffractometer was equipped with an asymmetric Johansson Ge (1 1 1) crystal to select monochromatic CuKα1 radiation (λ = 1.54056 Å) and a Rigaku D/teX Ultra silicon strip detector. The range from 5 to 70° (2ϑ) was collected with a 0.02° (2ϑ) step size and counting time of 6 s/step. Each powder sample was introduced into a glass capillary (diameter, 0.5 mm) and mounted on the axis of the goniometer. The capillary was rotated during the measurement to improve the

randomization of the orientations of the individual crystallites and reduce the effect of the preferred orientation.

2.9 Characterization of the mucoadhesive films

The physical dimensions of the printed films were assessed using a digital slide gauge (Hitech Diamond). The morphology of the film obtained during the printing stage was evaluated using an electrical scanning microscope (SEM) operating at 20 kV (Hitachi TM 3000 Tabletop SEM). Furthermore, a Chemical Microanalysis test was conducted on the samples to confirm the presence of F and Cl, which are elements present only in the CBS structure, and thus investigate the dispersion of the drug within them. The surface of each printed film was analysed using a Swift ED3000 Oxford Instrument with AZtecOne software. Finally, 10 mucoadhesive oral films were dissolved in acetonitrile to evaluate the actual CBS loading, in order to verify the presence of a therapeutic amount of CBS (125 μg). Each film was placed in 10 mL acetonitrile and stirred overnight at room temperature. Finally, after appropriate dilution, the drug concentration was assessed by HPLC, as previously reported.

2.10 Solid state characterization of the mucoadhesive films

The printed films were characterized by FT-IR, DSC, and PXRD following the same procedures previously described for the solid-state characterization of the blends. Before analysis, the printed formulations were fragmented, ground, and sieved.

2.11 Mucoadhesive properties

Characterization of film mucoadhesive properties were performed by using an Instron 5965 texture analyser (Instron, UK), equipped with a 50 N load cell. The samples of each (reported in Table 2) were attached to the mobile steel punch with cyanoacrylate glue. Mucin compacts, weighing 130 mg, were attached with cyanoacrylate glue to a steel plate fixed at the bottom of the tensile apparatus and hydrated with 80 μL water for 5 min, in order to obtain a jelly superficial mucin stratum. The compacts were preliminarily obtained applying a compression force 11 tons for 60 s, by using a hydraulic press (Glenrothes, UK) equipped with flat faced punches and having a die diameter of 11.28 mm. At the experiment start, upon

making contact between the sample and the hydrated mucin, a constant force of 1.3 N was imposed for 120 s. The mucoadhesive performance of the tested materials was determined by measuring the detachment force (DF) required to separate the sample from the mucin compact (maximum detachment force; DF_{max}) upon an elongation of 10.0 mm at the constant rate of 0.1 mm/s. The area under the curve (AUC) of the detachment force versus the elongation was also determined to represent the work or energy required for the detachment of the sample from the mucin.

Table 2 - Composition and dimensions of the films used for the test.

Form. ID	Blend ID	Dimension length x width x height (mm)
MAF-1	2	50 x 20 x 0.3
MAF-2	2	50 x 20 x 0.6
MAF-3	3	50 x 20 x 0.6

2.12 Tensile properties

Tests were conducted according to ASTM International Test Method for Thin Plastic Sheeting (D 882-02) using an Instron 5965 texture analyser (Instron, UK), equipped with a 50 N load cell. The samples were 50 × 20 mm strips.

Each test strip was longitudinally placed in the tensile grips of the texture analyser. Initial grip separation and the crosshead speed were 20 mm and 12.5 mm/min, respectively. The test was considered concluded at the film break. Tensile strength (TS) was calculated by dividing the maximum load by the original cross-sectional area of the specimen. Percent elongation at break (E%) was calculated according to the following equation (Equation 3):

$$E\% = \frac{L - L_0}{L_0} \times 100 \qquad \textit{Equation 3}$$

where L_0 is the initial gage length of the specimen and L is the length at the rupture.

Elastic modulus or Young's modulus (Y) was calculated as the slope of the linear portion of the stress–strain curve. Tensile energy to break (TBE) was defined by the area under the stress–strain curve. The results were expressed in MPa.

2.13 *In vitro* permeation study

Franz diffusion cells were used to investigate the kinetics of drug release rate in vitro. This cell comprises two compartments, one containing the active component (donor vehicle) and the other containing a receptor solution, separated by a slice of porcine oesophageal epidermis. The vertical cells used in the actual set of experiments had a wider column than the original Franz-type diffusion cell, and the bowl shape was removed. They had a diffusion area of 0.636 cm^2 and a 3.0 mL (approx.) receptor compartment. The receptor compartment of each cell was equipped with a magnetic stirrer and individually calibrated.

The permeation studies were performed using fresh porcine oesophageal tissue obtained by a local slaughterhouse. The mucosa was separated from the rest of the oesophageal tissue using a scalpel and stored at 2-8 °C until use for no more than 24 hours [49]. Before the experiments, the mucosae were thawed at room temperature and cut into squares of about 4.5 cm^2, and their integrity was visually checked.

A 2.0 cm^2 circular sample, obtained from each film by using a precision die cutter, was gently applied to the oesophageal epithelium specimen, preliminarily hydrated with 80 µL of HPLC-grade water to facilitate contact with the film. Then, the assembly was mounted on the receiver compartment of the Franz diffusion cell, whose receptor compartment was filled with sterile 0.9% sodium chloride aqueous solution (Eurospital S.p.A., Italy). Special care was taken to avoid air bubbles between the solution and the epidermis in the receptor compartment. The upper and lower parts of the Franz cell were sealed with Parafilm® (Pechiney Plastic Packaging Company, USA) and fastened together by means of a clamp, with the epidermis acting as a seal between the donor and receptor compartments. The system was kept at 37 ± 1 °C with a circulating water bath throughout the experiment. At predetermined times (1, 3, 5, 7 h), 200 µL samples were withdrawn from the receiver compartment and replaced with fresh receiver medium. Samples

were analysed by HPLC according to the above-described method. The values were the average of parallel experiments performed in triplicate. The cumulative amount permeated through the oesophageal mucosa per unit area ($Q_{t,perm}$) was calculated from the drug concentration in the receiving medium and plotted as a function of time.

2.14 *In vitro* retention study

At the end of the permeation experiments, the concentration of CBS retained in the epidermis ($Q_{7h,ret}$) was quantified by the following procedure. The oesophageal epithelium was removed from the Franz diffusion cell and stripped (Transpore®, 3M, USA) to eliminate the unabsorbed formulation. Then, each side of the membrane was gently treated with 5 mL of MeOH to wash out the unabsorbed drug. Subsequently, the sample was thinly sliced and placed in 5 mL of fresh MeOH. The suspension was soaked in a probe-sonicator (UP200St, Hielscher, Germany) for 10 min and then maintained for 24 h at 2–8 °C. Finally, the supernatant was centrifuged at 7000 rpm, 25 °C for 5 min (Z326K, Hermle LaborTechnik GmbH, Germany) to eliminate suspended materials and then analysed by HPLC. $Q_{7h,ret}$ was expressed as micrograms of CBS per milligram of oesophageal epithelium.

2.15 *Ex-vivo* mucoadhesion and dissolution test

The wash-off method was used to measure the mucoadhesive and dissolution properties of MAF-2 and MAF-3. In detail, an appropriate sample with dimensions of 2 cm (diameter) x 0,3 mm was 3D printed starting from Blend 2 and Blend 3 to standardize the membrane surface area of contact. The obtained samples were placed on a 2 × 3 cm section of the animal mucosa and fixed on a 45° inclined surface. Animal mucosae, derived from porcine oesophagus, were obtained from a local slaughterhouse (Bari, Italy). The mucosae were separated from the rest of the oesophageal tissue using a scalpel, cleaned, and stored at 4 °C in phosphate buffer solution (pH 7.2) before use [49]. Then, 60 mL of the simulated salivary fluid solution was poured using a syringe connected to a pump onto the sample placed on the mucosa at a constant flow rate of 1 mL/min to simulate salivary flushing. At time intervals of 5 min for a total time of 60 min, 300 µl were withdrawn from the

washing solution and replaced with the same volume of simulated salivary fluid solution. The obtained samples, after appropriate dilutions, were analysed by the previously reported HPLC method in order to assess the concentration of CBS removed from the oesophageal mucosa over time. Determination of the percentage of CBS that remained in the mucosa was performed by an indirect method using the following equation (Equation 4):

$$Remaining\ CBS\ (\%) = \frac{CBS\ (Total\ Amount) - CBS\ (collected\ sample)}{CBS\ (Total\ Amount)} x\ 100 \qquad Equation\ 4$$

2.16 Stability studies

The samples were stored in a Climacell 222 – ECO line climatic chamber (MMM Group, Semmelweis Strasse, München, Germany) at 25 °C and 60% relative humidity (RH) for 3 months. The printed films were packaged in amber glass bottles and closed using plastic screw caps. They were monitored using DSC analysis and measuring CBS content over the storage period.

2.17 Statistical analysis

Experimental data are reported as mean ± standard deviation (St.Dev.). Statistical analysis was conducted using JMP® Pro 16 (Marlow, UK). Statistically significant differences in obtained results were determined by Tukey-Kramer post-hoc tests after One-way ANOVA analysis.

3. RESULTS AND DISCUSSION

This work employed the new 3DForMe® printer based on the DPE printing technique to obtain mucoadhesive films capable of oral delivery of CBS in OLP therapy. In order to achieve a rapid dissolution of the finished pharmaceutical form in the oral cavity, different hydrophilic polymers of certain effectiveness were used in the initial powder mixture. Moreover, a notoriously mucoadhesive polymer such as CS was added. Therefore, different powder mixtures composed of CBS, HPMC, HP-β-CD, PEO and CS at different concentrations were first characterized and then extruded through the DPE technique. A complete solid-state characterization of the

different blends and the printed films is described, along with an evaluation of the mucoadhesive and tensile properties of the printed films and the *in vitro* permeation and retention characteristics.

3.1 CBS phase solubility studies

Phase solubility studies of the drug were performed in the presence of HP-β-CD, which allowed evaluation of the stability constant and prediction of the stoichiometric ratio of the CBS/HP-β-CD complex. Pure CBS has an intrinsic solubility of 2 µg/ml in water. The phase solubility diagram showed a significant and linear increase in CBS solubility with increasing HP-β-CD concentration (Fig. 1). The drug showed a solubility of 566.46 µg/mL in the presence of HP-β-CD at a concentration of 0.194 M. The regression analysis (R^2 = 0.9974) describes an AL-type curve, according to the Higuchi-Connors classification, with a slope of less than 1, which could be associated with a 1:1 M ratio between CBS and HP-β-CD. Using the Higuchi-Connors equation, a stability constant of 1335.74 M^{-1} was calculated, indicating a good interaction between CBS and HP- β -CD. Indeed, stability constants between 50 and 2000 M^{-1} are considered advantageous [40].

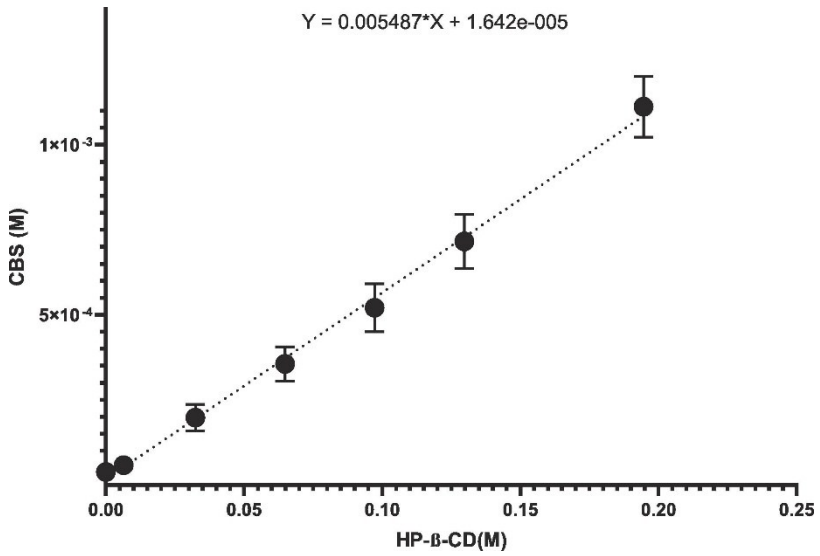

Fig. 1 - Phase solubility studies of CBS/HP-β-CD complex.

The addition of HPMC and PEO to the HP-β-CD solution significantly improved the aqueous solubility of CBS, confirming that the use of hydrophilic polymers increased the CD complexation efficiency for drugs [50]. In all samples containing the

cyclodextrin multicomponent complex (hydrophilic polymers/HP-β-CD/drug), a significant increase in aqueous solubility of CBS was observed in comparison to solutions containing HP-β-CD alone with CBS. Samples in which HPMC was also present showed higher drug solubility enhancement, resulting in a 25-fold increase compared with samples presenting the binary inclusion complex (Fig. 2). Based on these results, it could be stated that hydrophilic polymers and HP-β-CD showed a synergistic effect in enhancing CBS solubility.

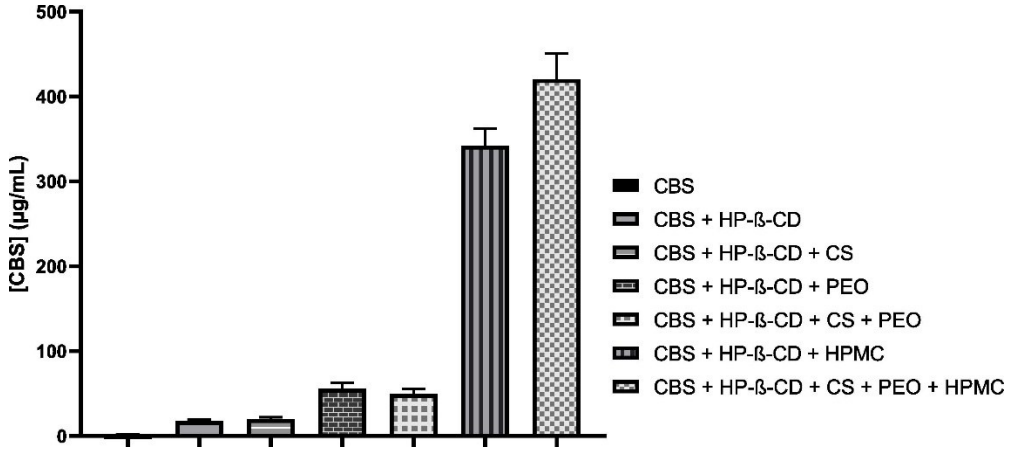

Fig. 2 - Aqueous solubility of CBS in the presence of binary (CD/Drug) and multicomponent complexes (hydrophilic polymers/CD/drug). The analysis was conducted in triplicate.

3.2 Job's plot method

Job's plot method was applied to determine the stoichiometry of the inclusion complexes. The maximum deviation value of ΔA indicated the stoichiometry of the CBS/HP-β-CD inclusion complex. The change in absorbance (ΔA) × [CBS] was calculated using equimolar (1.0×10^{-4} M) acetonitrile/H_2O solutions of CBS and CD solutions. As shown in Fig. 3, the maximum value at r = 0.5, with a symmetrical shape, demonstrated the presence of a 1:1 complex stoichiometry.

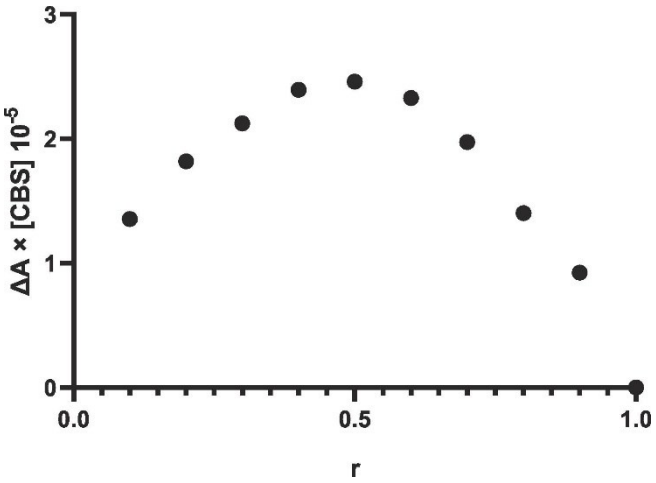

Fig. 3 - Job's plot diagram for stoichiometry determination of CBS/HP-β-CD inclusion complexes.

3.3 Extruded filaments characterization

A visual evaluation was carried out on the filaments obtained from the extrusion of four different powder blends. The blends differed in the percentage (w/w) of PEO and CS present in their formulation. Analysing the filament obtained from Blend 1, it was observed that a high percentage of PEO in the composition resulted in a filament with a structure that was too brittle to be used in 3D printing and presented difficulties in solidification by quenching (Fig. 4A), leading to the formation of a film with areas of under-extrusion (Fig. 4B). Conversely, as shown in Fig. 4A, the filaments obtained from the extrusion of Blend 2 and Blend 3 were defect-free, making them preferable for deployment in the next stage of 3D printing of films (Fig. 4B), which proved to be flexible but firm in consistency. DPE requires that the powders have a certain degree of fluidity and homogeneity to ensure that the flow through the extruder is uniform [51]. The filaments obtained from Blend 4, on the other hand, had a high percentage of CS, which proved to be too structurally rigid and not malleable (Fig. 4A), and thus unsuitable for the purpose of 3D printing, leading to the formation of films with irregular surfaces and varying thicknesses owing to the difficulty of handling the extrudate (Fig. 4B).

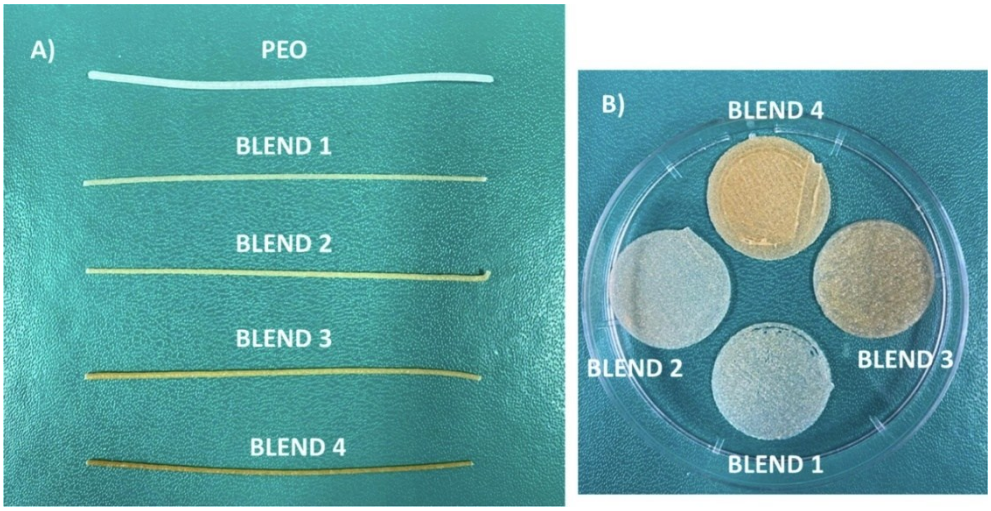

Fig. 4 - Filaments obtained from the four different blends used (A) and respective printed films (B).

Thereafter, further tests to assess the weight and homogeneity of CBS content were carried out for all blends. For all filament fragments (2 cm), the percentage of drug was in the range of 0.182–0.195 % w/w. However, the average of the values obtained was very close to the value of the theoretical concentration, thus demonstrating that the adopted process was not detrimental to the drug (Table 3) despite contact with the high temperatures of the extruder. The weight variations that characterize the filaments obtained from Blend 1 and Blend 4 could be the result of under-extrusion and over-extrusion, respectively.

Table 3 - Average CBS concentrations present within different filaments.

Filament ID	Weight* (g)	Theoretical CBS (% w/w)	Measured CBS* (% w/w)
Blend 1	0.014 ± 0.001	0.20	0.188 ± 0.005
Blend 2	0.016 ± 0.001	0.20	0.195 ± 0.002
Blend 3	0.017 ± 0.002	0.20	0.196 ± 0.008
Blend 4	0.021 ± 0.002	0.20	0.182 ± 0.011

*The value is the average of 5 fragments, ± is the standard deviation.

Evaluating the results obtained from characterization tests carried out on the extruded filaments, Blend 2 and Blend 3 were found to be the most suitable for printing by the DPE technique, owing to the ease of processing the extrudate and homogeneity in weight and CBS content.

3.4 Direct Powder Extrusion 3D printing

A single-screw extruder-printer model was used for DPE. The mixed powder was fed into the hopper, heated to a certain temperature, and used for direct printing of films. This innovative printing technique overcomes the limitations associated with conventional printing systems [52] and with established printing processes such as HME. By eliminating the preparatory HME step and subsequent FDM printing, the DPE printing process becomes simpler and faster. In fact, the overall process of printing a film takes about 3 min. In addition, by eliminating the intermediate steps, the amount of raw material waste has been greatly reduced. The design of the extruder, with a vertical orientation and an appropriate distance from the hopper, facilitates the flow of powder towards the screw. A functional amount of powder can be filled into the hopper to produce 1–15 films in a single cycle keeping the set dimensional values unchanged. This makes this 3D printing process suitable for formulating personalized mucoadhesive films for OLP therapy.

Blend 2 and Blend 3 were found to be suitable for DPE 3DP. The presence of cyclodextrin tends to moisten the powder, leading to an increased residence time in the printer creating vacuum zones along the screw, and blocking the extruder. The presence of a plasticizer and glidant agent as PEO assisted the printing process and promoted the flow of the powder along the screw. The resulting CBS-loaded printed films had cylindrical or rectangular shapes and good adhesion between the printed layers (Fig. 5). The obtained printed films showed two distinct faces, one rougher, given by the deposition and shaping of the extrudate during the printing stage, and one flatter, corresponding to the face lying on the print bed.

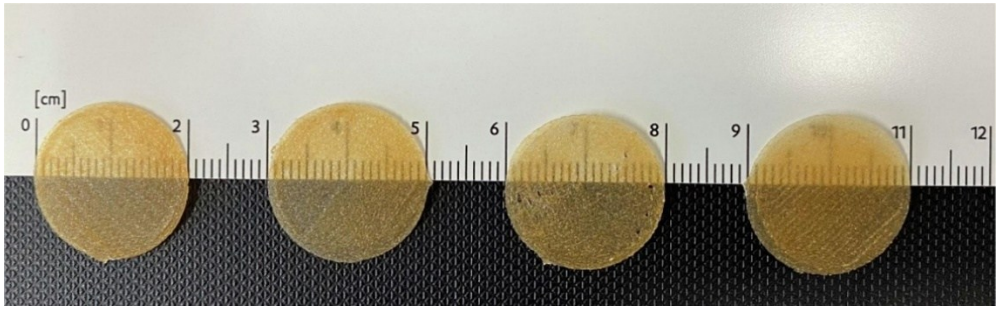

Fig. 5 – Size uniformity of mucoadhesive films derived from the extrusion of Blend 3.

3.5 Characterization of mucoadhesive films

The obtained mucoadhesive films exhibited good uniformity in physical dimensions, with the diameter and height values deviating only slightly from the values set in the digital model (20 mm × 0.3 mm). The mean diameter ranged from 19.88 mm to 20.50 mm, and the mean height ranged from 0.292 mm to 0.312 mm. The mean mass ranged from 62.32 to 62.67 mg. All mucoadhesive films had mechanical properties that were functional for packaging and handling. From the content uniformity test, the drug concentration present in 10 mucoadhesive films was obtained, confirming the closeness to the theoretical drug value (125 µg) and demonstrating no degradation of the drug during extrusion.

The SEM images show the surface and transverse planes of the two films (Fig. 6). In the cross-section, a three-dimensional layer-by-layer structure, which is characteristic of mucoadhesive films obtained by 3D printing, can be seen (Fig. 6C). Each layer has a thickness of 0.15 mm, as determined by the printing parameters. The surface plane shows the concentric geometry of the selected infill.

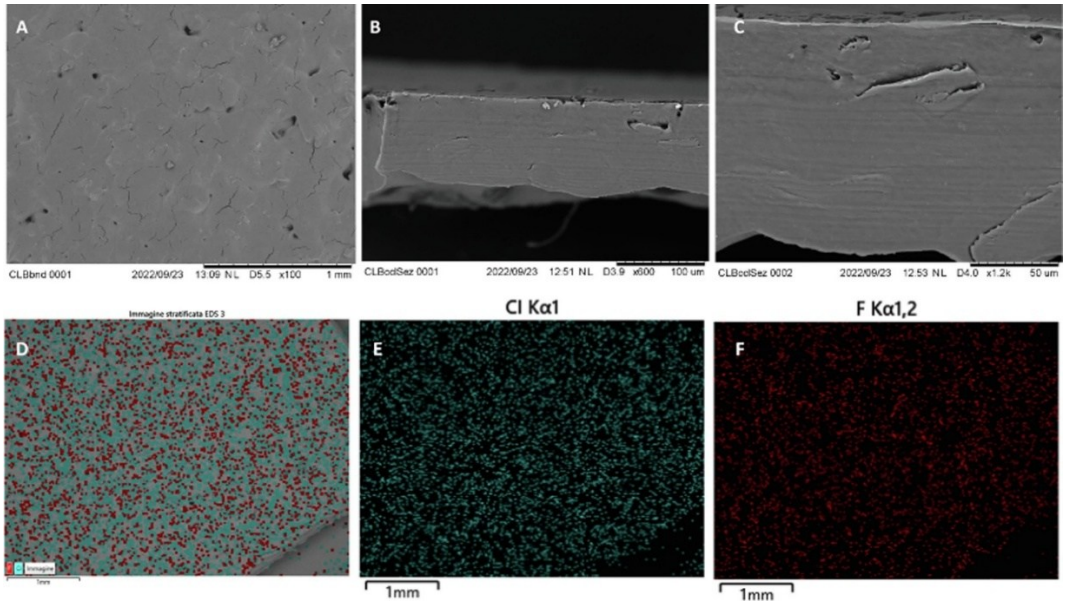

Fig. 6 - SEM images of the printed film surface (A) and film cross-section (B – C). Surface chemical microanalysis of the printed mucoadhesive films (D) with images related to the presence of the element Cl (E) and F (F).

The data obtained from the chemical microanalysis show a homogeneous presence of the elements Cl (green in Fig. 6E) and F (red in Fig. 6F), which, being atoms

exclusively present in the structure of the drug, indicate an equal distribution of CBS within the printed mucoadhesive films (Fig. 6D).

3.6 Solid state characterization of the printed mucoadhesive films

The possible amorphization of the drug during extrusion was verified by solid-state characterization studies of the printed mucoadhesive films. Using FT-IR, the characteristic peaks in the CBS spectrum were observed at 1063 (ether), 1606 (C = O), 1662 (C = C) and 1735 (Ester C = O) cm^{-1} (Fig. 7). The presence of these peaks was confirmed in the medicated blend spectra of each formulation. The peaks around 3300 cm^{-1} are characteristic of HP-β-CD, as observed in the complex, physical mixture, and extruded blend (Fig. 7). Analysing the spectrum in comparison with the printed mucoadhesive films prepared from the above blends, we can observe a relative broadening of the HP-β-CD peak in the range 3350–3100 cm^{-1}. This widening could be attributed to the interaction of HP-β-CD with HPMC and CBS during printing [53]. The same observation can be made for the CBS peaks between 1600 cm^{-1} and 1800 cm^{-1} and between 1250 cm^{-1} and 1100 cm^{-1}. The absence of important peaks characteristic of the stretching of the ester and carbonyl groups of the drug could indicate a possible amorphization of the drug inside the printed film and/or an interaction between the drug and HP-β-CD [54]. These results confirm the formation of intimate complexes of HP-β-CD, CBS, and HPMC.

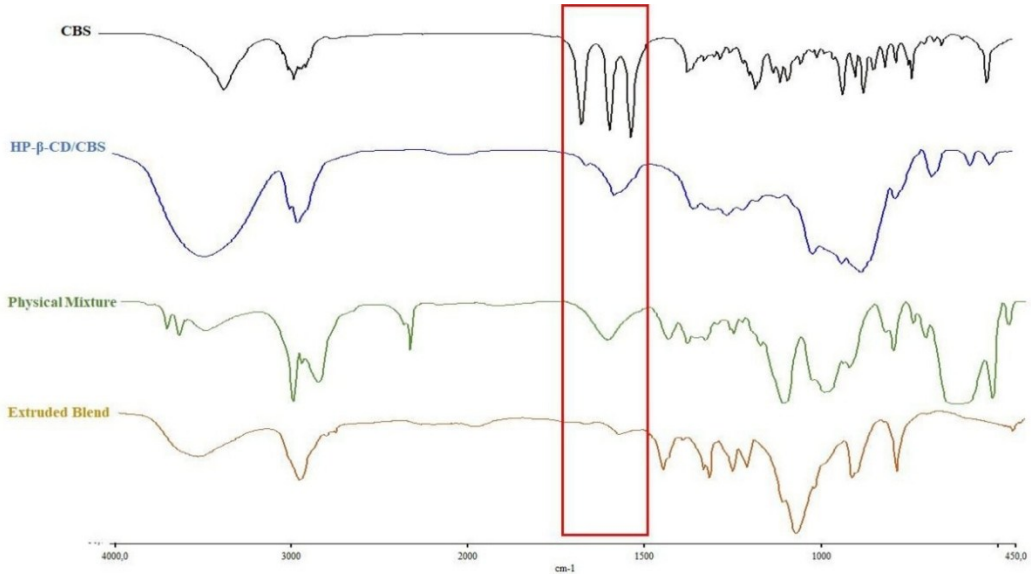

Fig. 7 - FT-IR spectra of the printed mucoadhesive films were compared with the spectra of the pure CBS, physical mixture, and HP-β-CD/CBS complex.

A second test to verify this condition was performed using DSC. CBS showed an endothermic peak at 220 °C, which is indicative of its crystalline nature (Fig. 8). In contrast, the peak at 220 °C was completely absent in the thermogram of the film, probably because of the amorphization of the drug during the printing phase and/or the formation of an inclusion complex between CBS and HP-β-CD.

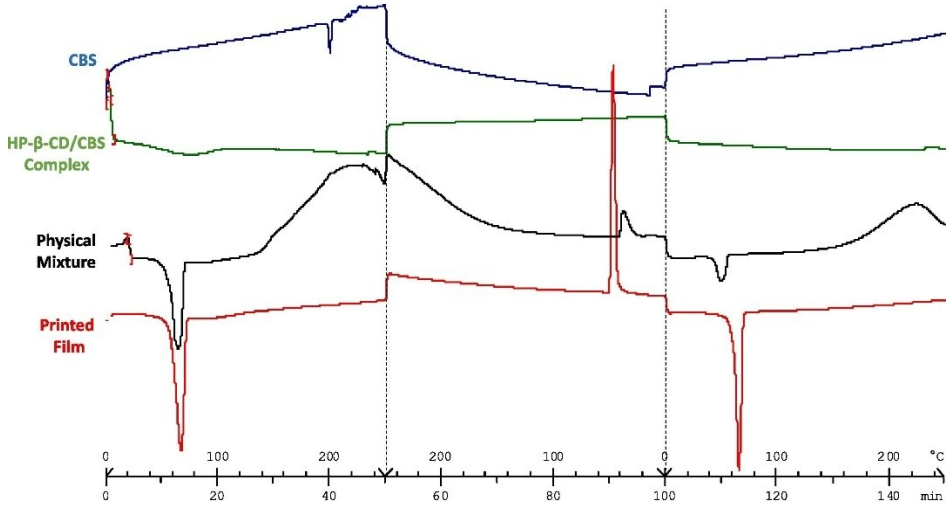

Fig. 8 - Thermograms of printed mucoadhesive films were compared with the thermograms of CBS, HP-β-CD/CBS complex, physical mixture, and printed film.

In Fig. 9, the powder diffraction patterns of CBS, medicated blend, and corresponding printed mucoadhesive films are reported. The sharp peaks present in the diffraction pattern of the pure CBS powder indicated its crystallinity. Drug-

related peaks were still observable in the diffractogram of the printed film, indicating the incomplete amorphization of the drug and the incomplete complexation with HP-β-CD.

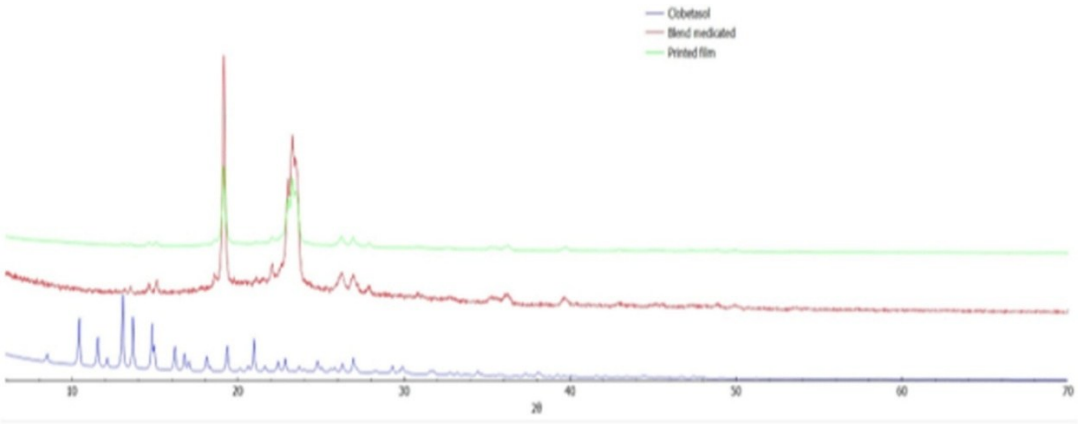

Fig. 9 - Diffractogram of a printed mucoadhesive film compared with the diffractogram of CBS and the corresponding medicated blend.

3.7 Mucoadhesive properties

The test was performed to provide a complementary characterization of the films' mucoadhesive properties. Indeed, while the wash-off method using porcine mucosae provided a prevision of the *in vivo* residence time, this test gave an idea of the initial bonding and provided a quantitative measure of the interaction between the film and a commercially available mucin. As shown in Table 4 and Fig. 10, significant differences in the mucoadhesive properties of the films were observable. During the early part of the profile, the DF increased in all formulations as a function of the elongation until a maximum value was reached. A plateau was observed in all formulations due to the gradual detachment of the film from the mucin compact, which resulted in a gradual decrease of the contact area between the two [55]. Finally, the DF rapidly dropped as a consequence of the complete detachment. As is evident from Fig. 10, the intensity of the plateau phase was influenced by the film composition. In particular, the higher the CS concentration, the longer the plateau phase. The peak detachment force (i.e., DF_{max}) of MAF-3, which had the highest CS concentration, was 1.2-time higher than MAF-1 and MAF-2 ($p < 0.01$). This evidence agreed with previously published results [56]. Such trend is also observable in terms

of detachment energy (i.e., AUC), although the significance of these results was weak ($p > 0.50$). On the contrary, other parameters, such as film thickness, seem not to impact on the mucoadhesive properties. Comparing MAF-1 and MAF-2, similar DF_{max} values were obtained ($p = 0.98$), suggesting that the number of deposed layers seems not to influence the mucoadhesive properties of the film (Table 4).

Table 4 - Results of mucoadhesive tests performed on mucoadhesive films, expressed as mean ± St.Dev. (n=3).

Form. ID	Contact surface	DF_{max} (N/mm²)	AUC (mJ)
MAF-1	Flat	60.67 ± 1.65	0.879 ± 0.231
MAF-2	Flat	59.79 ± 4.27	0.761 ± 0.388
MAF-3	Flat	74.14 ± 2.92	1.027 ± 0.687
MAF-3	Rough	63.32 ± 1.69	0.520 ± 0.055

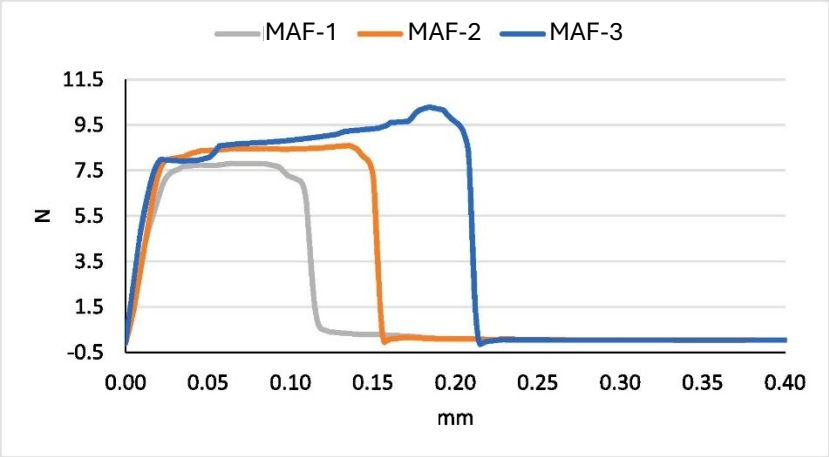

Fig. 10 - Representative detachment profiles of MAF-1, MAF-2, and MAF-3.

Finally, since the films' surfaces showed a different morphology due to the printing process, namely the surface in contact with the print bed turned out flatter and smoother than the other one, mucoadhesive tests on MAF-3 were also performed to determine the impact of surface morphology irregularities on the mucoadhesive properties. As reported in Table 4, a significant drop of both detachment force and detachment energy ($p = 0.02$) was observable in the case of the rougher surface due to a non-optimal contact between the mucin compact and the film.

3.8 Tensile properties

Table 5 reports the results of the tensile test on MAF-1. MAF-2 and MAF-3 were too tough to be analysed by the texture analyser. Indeed, for both formulations, the maximum load limit of dynamometer transducer (40 N) was reached after a few seconds from the experiment start. On the contrary, MAF-1 showed tensile properties measurable in instrumental range, and exhibited a higher toughness (TS) and a lower elasticity (Y) in comparison to published data obtained on films prepared using different casting and printing technologies [22], [24], [57].

Table 5 - Results of tensile tests performed on mucoadhesive films, expressed as mean ± St.Dev. (n=8).

Parameter	MAF-1
TS (MPa)	3.93 ± 1.32
E%	4.82 ± 1.98
Y (MPa)	291.85 ± 71.56
TBE (Mpa)	0.093 ± 0.038

3.9 *In vitro* permeation and retention studies

As reported in Table 6, for both tested formulations the drug permeated amounts turned out to be negligible at the end of the experiment. On the contrary, about 0.5–0.6 μg/cm^2 of CBS (corresponding to 0.3–0.5 μg/mg of epithelium) was retained in the oesophageal mucosa after 7 h. Such finding was in line with published results using different types of mucoadhesive films [58]. However, it's worth noting that, based on the results obtained, CS has a role in the penetration of CBS into the epithelium. In particular, the higher the CS concentration, the lower the $Q_{7h,ret}$ (p-value = 0.003, Student's T Test).

Table 6 - Penetration data (i.e., $Q_{7h,perm}$, $Q_{7h,ret}$) of CBS through oesophageal epithelium (mean ± St.Dev., n=3).

Form. ID	$Q_{7h,perm}$ (μg/cm^2)	$Q_{7h,ret}$ (μg/mg)
MAF-2	n.d.	0.518 ± 0.100
MAF-3	n.d.	0.376 ± 0.091

n.d.: not determined since drug concentration was lower than the LOD.

3.10 *Ex vivo* mucoadhesive and dissolution studies

Dissolution studies were performed on a film sample placed on the animal mucosa (porcine oesophagus) using the wash-off method. The dissolution of the samples was monitored by visual analysis at different time intervals (1, 5, 10, 15, 20, 25 and 30 min). The analysed samples produced from Blend 2 and Blend 3 showed gradual disintegration until complete dissolution 20 min and 30 min after the start of the test, respectively. At the same time, the residence time of CBS was assessed by calculating the amount of drug still present on the mucosae after washing with simulated salivary fluid. From the results shown in Fig. 11, it was noted that in both cases the medicated mucoadhesive films showed a gradual release of the drug over time and a significant increase in the amount of CBS present in the mucosae compared with the control consisting of a solution of the drug alone. This behaviour is due to the interaction of CS and PEO with the mucosal surface, which increases the drug's resistance to scavenging, resulting in a longer residence time of the drug at the site of action. The sample derived from Blend 3 showed greater resistance to scavenging and thus better mucoadhesive properties resulting from the higher presence of CS and, therefore, the higher number of bonds with the mucosal surface.

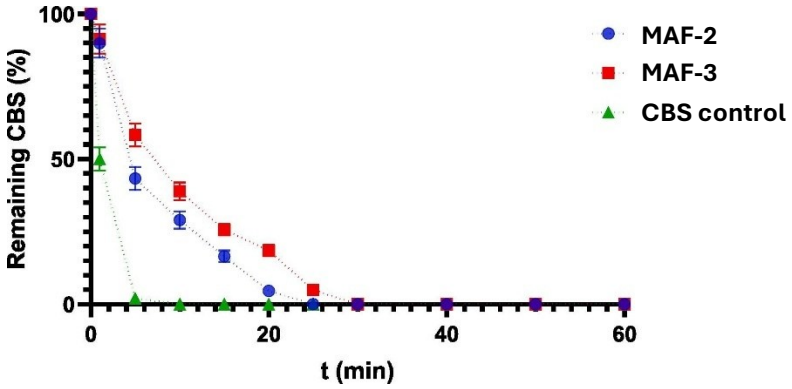

Fig. 11 - Residence time of CBS in oesophageal mucosa.

3.11 Stability studies

The amorphous condition of the drug, initially acquired by the printing process, was checked after 3 months under controlled storage parameters (25 °C, 60% RH). No

changes in the solid state of the compounds or the drug content were observed, thus indicating the 3-month stability of the obtained films.

4. CONCLUSIONS

The main objective of this work was to develop a novel mucoadhesive film obtained by DPE 3D printing capable of giving a sustained release of CBS for paediatric OLP therapy. In the obtained formulations, the physical characteristics of the drug were effectively improved due to its partial amorphization during the printing stage and owing to the formation of a multicomponent complex with HP-β-CD and HPMC. From the tests performed, the obtained mucoadhesive films exhibited good mucoadhesive properties, improving with increasing CS percentage, an elastic and tenacious structure, and marked retention of the drug inside the epithelium, thus avoiding systemic absorption of the drug. Therefore, mucoadhesive films could represent a suitable candidate in the paediatric therapy of OLP.

5. REFERENCES

[1] A. M. do Canto, H. Müller, R. R. de Freitas, and P. S. da S. Santos, "Oral lichen planus (OLP): clinical and complementary diagnosis," *An Bras Dermatol*, vol. 85, no. 5, pp. 669–675, 2010, doi: 10.1590/s0365-05962010000500010.

[2] L. R. Eversole, "Immunopathogenesis of oral lichen planus and recurrent aphthous stomatitis," *Semin Cutan Med Surg*, vol. 16, no. 4, pp. 284–294, Dec. 1997, doi: 10.1016/s1085-5629(97)80018-1.

[3] M. Boorghani, N. Gholizadeh, A. Taghavi Zenouz, M. Vatankhah, and M. Mehdipour, "Oral Lichen Planus: Clinical Features, Etiology, Treatment and Management; A Review of Literature," *J Dent Res Dent Clin Dent Prospects*, vol. 4, no. 1, pp. 3–9, 2010, doi: 10.5681/joddd.2010.002.

[4] R. Laeijendecker, T. Van Joost, B. Tank, A. P. Oranje, and H. A. M. Neumann, "Oral Lichen Planus in Childhood," *Pediatric Dermatology*, vol. 22, no. 4, pp. 299–304, July 2005, doi: 10.1111/j.1525-1470.2005.22403.x.

[5] M. M. Ferguson, "Treatment of erosive lichen planus of the oral mucosa with depot steroids," *Lancet*, vol. 2, no. 8041, pp. 771–772, Oct. 1977, doi: 10.1016/s0140-6736(77)90288-4.

[6] J. M. Plemons, T. D. Rees, and N. Y. Zachariah, "Absorption of a topical steroid and evaluation of adrenal suppression in patients with erosive lichen planus," *Oral Surgery, Oral Medicine, Oral Pathology*, vol. 69, no. 6, pp. 688–693, June 1990, doi: 10.1016/0030-4220(90)90349-W.

[7] J. Koch-Weser and R. L. Byyny, "Withdrawal from Glucocorticoid Therapy," *N Engl J Med*, vol. 295, no. 1, pp. 30–32, July 1976, doi: 10.1056/NEJM197607012950107.

[8] E. Oussedik, M. D. Saleem, and S. R. Feldman, "A Randomized, Double-Blind, Placebo-Controlled Study of the Vasoconstrictor Potency of Topical 0.25% Desoximetasone Spray: A High to Super High Range of Potency (Class I to Class II) Corticosteroid Formulation," *J Drugs Dermatol*, vol. 16, no. 10, pp. 972–975, Oct. 2017.

[9] M. Carbone *et al.*, "Topical clobetasol in the treatment of atrophic-erosive oral lichen planus: a randomized controlled trial to compare two preparations with different concentrations," *J Oral Pathology Medicine*, vol. 38, no. 2, pp. 227–233, Feb. 2009, doi: 10.1111/j.1600-0714.2008.00688.x.

[10] J. A. Carruthers, P. J. August, and R. C. Staughton, "Observations on the systemic effect of topical clobetasol propionate (Dermovate).," *BMJ*, vol. 4, no. 5990, pp. 203–204, Oct. 1975, doi: 10.1136/bmj.4.5990.203.

[11] M. Sarfaraz Alam *et al.*, "Enhancement of Anti-Dermatitis Potential of Clobetasol Propionate by DHA [Docosahexaenoic Acid] Rich Algal Oil Nanoemulsion Gel," *Iran J Pharm Res*, vol. 15, no. 1, pp. 35–52, 2016.

[12] F. Cilurzo *et al.*, "A new mucoadhesive dosage form for the management of oral lichen planus: Formulation study and clinical study," *European Journal of Pharmaceutics and Biopharmaceutics*, vol. 76, no. 3, pp. 437–442, Nov. 2010, doi: 10.1016/j.ejpb.2010.07.014.

[13] V. Garipova, C. Gennari, F. Selmin, F. Cilurzo, and R. Moustafine, "Mucoadhesive Interpolyelectrolyte Complexes for the Buccal Delivery of Clobetasol," *Polymers*, vol. 10, no. 1, p. 85, Jan. 2018, doi: 10.3390/polym10010085.

[14] B. Morath, S. Sauer, M. Zaradzki, and A. H. Wagner, "Orodispersible films – Recent developments and new applications in drug delivery and therapy," *Biochemical Pharmacology*, vol. 200, p. 115036, June 2022, doi: 10.1016/j.bcp.2022.115036.

[15] L. Cuzzolin, A. Zaccaron, and V. Fanos, “Unlicensed and off-label uses of drugs in paediatrics: a review of the literature,” *Fundamemntal Clinical Pharma*, vol. 17, no. 1, pp. 125–131, Feb. 2003, doi: 10.1046/j.1472-8206.2003.00123.x.

[16] I. Lafeber, E. J. Ruijgrok, H.-J. Guchelaar, and K. J. M. Schimmel, “3D Printing of Pediatric Medication: The End of Bad Tasting Oral Liquids?—A Scoping Review,” *Pharmaceutics*, vol. 14, no. 2, p. 416, Feb. 2022, doi: 10.3390/pharmaceutics14020416.

[17] M. Scarpa *et al.*, “Orodispersible films: Towards drug delivery in special populations,” *International Journal of Pharmaceutics*, vol. 523, no. 1, pp. 327–335, May 2017, doi: 10.1016/j.ijpharm.2017.03.018.

[18] L. Zema, A. Melocchi, A. Maroni, and A. Gazzaniga, “Three-Dimensional Printing of Medicinal Products and the Challenge of Personalized Therapy,” *Journal of Pharmaceutical Sciences*, vol. 106, no. 7, pp. 1697–1705, July 2017, doi: 10.1016/j.xphs.2017.03.021.

[19] S. C. Palezi, S. S. Fernandes, and V. G. Martins, “Oral disintegration films: applications and production methods,” *J Food Sci Technol*, vol. 60, no. 10, pp. 2539–2548, Oct. 2022, doi: 10.1007/s13197-022-05589-9.

[20] M. Preis, J. Breitkreutz, and N. Sandler, “Perspective: Concepts of printing technologies for oral film formulations,” *International Journal of Pharmaceutics*, vol. 494, no. 2, pp. 578–584, Feb. 2015, doi: 10.1016/J.IJPHARM.2015.02.032.

[21] J. Boniatti *et al.*, “Direct Powder Extrusion 3D Printing of Praziquantel to Overcome Neglected Disease Formulation Challenges in Paediatric Populations,” *Pharmaceutics*, vol. 13, no. 8, p. 1114, July 2021, doi: 10.3390/pharmaceutics13081114.

[22] G. M. Khalid, U. M. Musazzi, F. Selmin, S. Franzè, P. Minghetti, and F. Cilurzo, “Extemporaneous printing of diclofenac orodispersible films for pediatrics,” *Drug Development and Industrial Pharmacy*, vol. 47, no. 4, pp. 636–644, Apr. 2021, doi: 10.1080/03639045.2021.1908335.

[23] P. Polamaplly, Y. Cheng, X. Shi, K. Manikandan, G. E. Kremer, and H. Qin, “3D Printing and Characterization of Hydroxypropyl Methylcellulose and Methylcellulose for Biodegradable Support Structures,” *Procedia Manufacturing*, vol. 34, pp. 552–559, 2019, doi: 10.1016/j.promfg.2019.06.219.

[24] U. M. Musazzi *et al.*, “Personalized orodispersible films by hot melt ram extrusion 3D printing,” *International Journal of Pharmaceutics*, vol. 551, no. 1–2, pp. 52–59, Nov. 2018, doi: 10.1016/J.IJPHARM.2018.09.013.

[25] C. Wei, N. G. Solanki, J. M. Vasoya, A. V. Shah, and A. T. M. Serajuddin, “Development of 3D Printed Tablets by Fused Deposition Modeling Using Polyvinyl Alcohol as Polymeric Matrix for Rapid Drug Release,” *Journal of Pharmaceutical Sciences*, vol. 109, no. 4, pp. 1558–1572, Apr. 2020, doi: 10.1016/j.xphs.2020.01.015.

[26] S. Chung, P. Srinivasan, P. Zhang, S. Bandari, and M. A. Repka, “Development of ibuprofen tablet with polyethylene oxide using fused deposition modeling 3D-printing coupled with hot-melt extrusion,” *Journal of Drug Delivery Science and Technology*, vol. 76, p. 103716, Oct. 2022, doi: 10.1016/j.jddst.2022.103716.

[27] S. Liu, S. Qin, M. He, D. Zhou, Q. Qin, and H. Wang, “Current applications of poly(lactic acid) composites in tissue engineering and drug delivery,” *Composites Part B: Engineering*, vol. 199, p. 108238, Oct. 2020, doi: 10.1016/j.compositesb.2020.108238.

[28] F. Dores *et al.*, “Temperature and solvent facilitated extrusion based 3D printing for pharmaceuticals,” *European Journal of Pharmaceutical Sciences*, vol. 152, p. 105430, Sept. 2020, doi: 10.1016/j.ejps.2020.105430.

[29] M. A. Azad, D. Olawuni, G. Kimbell, A. Z. M. Badruddoza, Md. S. Hossain, and T. Sultana, “Polymers for Extrusion-Based 3D Printing of Pharmaceuticals: A Holistic Materials–Process

Perspective," *Pharmaceutics*, vol. 12, no. 2, p. 124, Feb. 2020, doi: 10.3390/pharmaceutics12020124.

[30] I. d'Angelo, A. Fraix, F. Ungaro, F. Quaglia, and A. Miro, "Poly(ethylene oxide)/hydroxypropyl-β-cyclodextrin films for oromucosal delivery of hydrophilic drugs," *International Journal of Pharmaceutics*, vol. 531, no. 2, pp. 606–613, Oct. 2017, doi: 10.1016/j.ijpharm.2017.06.029.

[31] E. Mašková *et al.*, "Hypromellose – A traditional pharmaceutical excipient with modern applications in oral and oromucosal drug delivery," *Journal of Controlled Release*, vol. 324, pp. 695–727, Aug. 2020, doi: 10.1016/j.jconrel.2020.05.045.

[32] E. Russo *et al.*, "A focus on mucoadhesive polymers and their application in buccal dosage forms," *Journal of Drug Delivery Science and Technology*, vol. 32, pp. 113–125, Apr. 2016, doi: 10.1016/j.jddst.2015.06.016.

[33] W.-Z. Jiang, Y. Cai, and H.-Y. Li, "Chitosan-based spray-dried mucoadhesive microspheres for sustained oromucosal drug delivery," *Powder Technology*, vol. 312, pp. 124–132, May 2017, doi: 10.1016/j.powtec.2017.02.021.

[34] A. B. Nair *et al.*, "Novel Dermal Delivery Cargos of Clobetasol Propionate: An Update," *Pharmaceutics*, vol. 14, no. 2, p. 383, Feb. 2022, doi: 10.3390/pharmaceutics14020383.

[35] A. Bernkopschnurch, "Thiomers: A new generation of mucoadhesive polymers," *Advanced Drug Delivery Reviews*, vol. 57, no. 11, pp. 1569–1582, Nov. 2005, doi: 10.1016/j.addr.2005.07.002.

[36] N. Salamatmiller, M. Chittchang, and T. Johnston, "The use of mucoadhesive polymers in buccal drug delivery," *Advanced Drug Delivery Reviews*, vol. 57, no. 11, pp. 1666–1691, Nov. 2005, doi: 10.1016/j.addr.2005.07.003.

[37] R. Cheung, T. Ng, J. Wong, and W. Chan, "Chitosan: An Update on Potential Biomedical and Pharmaceutical Applications," *Marine Drugs*, vol. 13, no. 8, pp. 5156–5186, Aug. 2015, doi: 10.3390/md13085156.

[38] G. Tejada *et al.*, "Development and Evaluation of Buccal Films Based on Chitosan for the Potential Treatment of Oral Candidiasis," *AAPS PharmSciTech*, vol. 18, no. 4, pp. 936–946, May 2017, doi: 10.1208/s12249-017-0720-6.

[39] G. F. Racaniello *et al.*, "Spray-dried mucoadhesive microparticles based on S-protected thiolated hydroxypropyl-β-cyclodextrin for budesonide nasal delivery," *International Journal of Pharmaceutics*, vol. 603, p. 120728, June 2021, doi: 10.1016/j.ijpharm.2021.120728.

[40] T. Loftsson, D. Hreinsdóttir, and M. Másson, "Evaluation of cyclodextrin solubilization of drugs," *International Journal of Pharmaceutics*, vol. 302, no. 1–2, pp. 18–28, Sept. 2005, doi: 10.1016/j.ijpharm.2005.05.042.

[41] M. Pistone *et al.*, "Direct cyclodextrin-based powder extrusion 3D printing for one-step production of the BCS class II model drug niclosamide," *Drug Delivery and Translational Research*, vol. 12, no. 8, pp. 1895–1910, Aug. 2022, doi: 10.1007/S13346-022-01124-7.

[42] J. Rincón-López, Y. C. Almanza-Arjona, A. P. Riascos, and Y. Rojas-Aguirre, "Technological evolution of cyclodextrins in the pharmaceutical field," *Journal of Drug Delivery Science and Technology*, vol. 61, p. 102156, Feb. 2021, doi: 10.1016/j.jddst.2020.102156.

[43] M. Fanous, S. Gold, S. Muller, S. Hirsch, J. Ogorka, and G. Imanidis, "Simplification of fused deposition modeling 3D-printing paradigm: Feasibility of 1-step direct powder printing for immediate release dosage form production," *International Journal of Pharmaceutics*, vol. 578, p. 119124, Mar. 2020, doi: 10.1016/j.ijpharm.2020.119124.

[44] J. J. Ong *et al.*, "3D printed opioid medicines with alcohol-resistant and abuse-deterrent properties," *International Journal of Pharmaceutics*, vol. 579, p. 119169, Apr. 2020, doi: 10.1016/j.ijpharm.2020.119169.

[45] A. Goyanes, N. Allahham, S. J. Trenfield, E. Stoyanov, S. Gaisford, and A. W. Basit, "Direct powder extrusion 3D printing: Fabrication of drug products using a novel single-step process," *International Journal of Pharmaceutics*, vol. 567, p. 118471, Aug. 2019, doi: 10.1016/j.ijpharm.2019.118471.

[46] M. Pistone *et al.*, "Direct cyclodextrin based powder extrusion 3D printing of budesonide loaded mini-tablets for the treatment of eosinophilic colitis in paediatric patients," *International Journal of Pharmaceutics*, vol. 632, p. 122592, Feb. 2023, doi: 10.1016/j.ijpharm.2023.122592.

[47] M. Kamberi, K. Fu, J. Lu, G. M. Chemaly, and D. Feder, "A Sensitive High-Throughput HPLC Assay for Simultaneous Determination of Everolimus and Clobetasol Propionate," *Journal of Chromatographic Science*, vol. 46, no. 1, pp. 23–29, Jan. 2008, doi: 10.1093/chromsci/46.1.23.

[48] A. Cutrignelli *et al.*, "A New Complex of Curcumin with Sulfobutylether-β-Cyclodextrin: Characterization Studies and In Vitro Evaluation of Cytotoxic and Antioxidant Activity on HepG-2 Cells," *Journal of Pharmaceutical Sciences*, vol. 103, no. 12, pp. 3932–3940, Dec. 2014, doi: 10.1002/jps.24200.

[49] A. Casiraghi, C. G. Gennari, U. M. Musazzi, M. A. Ortenzi, S. Bordignon, and P. Minghetti, "Mucoadhesive Budesonide Formulation for the Treatment of Eosinophilic Esophagitis," *Pharmaceutics*, vol. 12, no. 3, p. 211, Mar. 2020, doi: 10.3390/pharmaceutics12030211.

[50] D. Medarević, K. Kachrimanis, Z. Djurić, and S. Ibrić, "Influence of hydrophilic polymers on the complexation of carbamazepine with hydroxypropyl-β-cyclodextrin," *European Journal of Pharmaceutical Sciences*, vol. 78, pp. 273–285, Oct. 2015, doi: 10.1016/j.ejps.2015.08.001.

[51] S. Spath and H. Seitz, "Influence of grain size and grain-size distribution on workability of granules with 3D printing," *Int J Adv Manuf Technol*, vol. 70, no. 1–4, pp. 135–144, Jan. 2014, doi: 10.1007/s00170-013-5210-8.

[52] M. Pandey *et al.*, "3D printing for oral drug delivery: a new tool to customize drug delivery," *Drug Deliv. and Transl. Res.*, vol. 10, no. 4, pp. 986–1001, Aug. 2020, doi: 10.1007/s13346-020-00737-0.

[53] J. Thiry, F. Krier, S. Ratwatte, J.-M. Thomassin, C. Jerome, and B. Evrard, "Hot-melt extrusion as a continuous manufacturing process to form ternary cyclodextrin inclusion complexes," *European Journal of Pharmaceutical Sciences*, vol. 96, pp. 590–597, Jan. 2017, doi: 10.1016/j.ejps.2016.09.032.

[54] A. Lodagekar *et al.*, "Formulation and evaluation of cyclodextrin complexes for improved anticancer activity of repurposed drug: Niclosamide," *Carbohydrate Polymers*, vol. 212, pp. 252–259, May 2019, doi: 10.1016/j.carbpol.2019.02.041.

[55] F. Cilurzo, P. Minghetti, F. Selmin, A. Casiraghi, and L. Montanari, "Polymethacrylate salts as new low-swellable mucoadhesive materials," *Journal of Controlled Release*, vol. 88, no. 1, pp. 43–53, Feb. 2003, doi: 10.1016/S0168-3659(02)00459-5.

[56] J. O. Morales and J. T. McConville, "Manufacture and characterization of mucoadhesive buccal films," *European Journal of Pharmaceutics and Biopharmaceutics*, vol. 77, no. 2, pp. 187–199, Feb. 2011, doi: 10.1016/J.EJPB.2010.11.023.

[57] U. M. Musazzi *et al.*, "Poly(methyl methacrylate) salt as film forming material to design orodispersible films," *European Journal of Pharmaceutical Sciences*, vol. 115, pp. 37–42, Mar. 2018, doi: 10.1016/J.EJPS.2018.01.019.

[58] Z. Said, C. Murdoch, J. Hansen, L. Siim Madsen, and H. E. Colley, "Corticosteroid delivery using oral mucosa equivalents for the treatment of inflammatory mucosal diseases," *Eur J Oral Sci*, vol. 129, no. 2, p. e12761, Apr. 2021, doi: 10.1111/eos.12761.

CHAPTER 2: 3D-PRINTED S-PROTECTED MUCOADHESIVE LIDOCAINE-BASED FILMS FOR IMMEDIATE AND SUSTAINED RELEASE OF THE DRUG IN PAEDIATRIC THERAPIES

1. INTRODUCTION

Lidocaine (LID), an amino amide anaesthetic, has long been employed as a local anaesthetic due to its ability to block voltage-dependent sodium channels, thereby preventing impulse initiation and propagation along axons. Beyond topical use, intravenous LID has been applied in the treatment of postoperative and neuropathic pain, postherpetic neuralgia, diabetic neuropathy, hyperalgesia, visceral pain, centrally mediated pain, and cardiac dysrhythmias [1]. In paediatric settings, LID is administered at low doses (maximum 4.4 mg/kg) for procedures requiring short-term analgesia, such as oropharyngeal anaesthesia before intubation, dental extractions, or minor postoperative pain management [2]. While, in chronic conditions such as neuropathic pain or painful oral lesions (e.g., recurrent aphthous ulcers, oral lichen planus, chemotherapy-induced mucositis), sustained-release formulations (< 3 mg/kg/day) are beneficial to prolong therapeutic effect and reduce dosing frequency [3]. Moreover, LID is characterized by rapid onset and short duration of action, and conventional formulations often necessitate frequent re-application, which may not be feasible or well-tolerated, especially in paediatric patients. A mucoadhesive formulation capable of maintaining prolonged contact with the mucosa while gradually releasing LID can enhance therapeutic efficacy, reduce systemic exposure, and improve patient compliance. This rationale supports the exploration of sustained-release formulations as personalized, non-invasive delivery systems.

Currently available dosage forms (gels, sprays, rinses) exhibit limited mucosal residence time and present challenges in delivering precise doses to children,

potentially compromising therapeutic efficacy or safety [4], [5]. Furthermore, standard formulations are designed for adults, often necessitating manipulation to adapt doses for paediatric patients, with the associated risks of therapeutic inefficacy or toxicity [6], [7].

Mucoadhesive films (MAF) are flexible films designed to adhere to the oral mucosa. Their advantages include ease of administration, improved patient compliance, and the potential for rapid or targeted drug release [8]. In paediatric formulations, where accurate dosing and ease of administration are required, MAF provide a convenient alternative to traditional solid and liquid dosage forms, particularly for patients who have difficulty swallowing or are unable to take medication with water [9]. However, producing individualized MAF with precise dosages and tailored release profiles using conventional manufacturing remains a significant challenge [10], as adjusting dosages to match individual patient needs necessitates complex and time-consuming processes such as manual cutting or compounding, which can compromise accuracy and consistency.

Sustained-release MAF are particularly desirable for prolonging local therapeutic effects, but achieving their production requires advanced formulation strategies [11]. In fact, while conventional methods can be used to formulate MAF with either rapid or sustained drug release, achieving both tailored release profiles and mucoadhesive properties within a single, reproducible, and solvent-free manufacturing process remains challenging.

In recent years, additive manufacturing techniques such as 3D printing have revolutionized pharmaceutical production by enabling the fabrication of personalized dosage forms with unparalleled precision and customization [12]. Among these techniques, Direct Powder Extrusion (DPE) has emerged as a promising method to produce pharmaceutical films due to its ability to precisely control material deposition and layer thickness [13]. DPE involves the direct extrusion of powdered materials, typically using a single-screw extruder, to create solid dosage forms with precise control over composition and dosage. This technique enables the production of pharmaceutical products with tailored properties, including particle size, porosity, and drug release kinetics [14].

Furthermore, DPE allows for the incorporation of a wide range of active pharmaceutical ingredients (APIs) and excipients, facilitating the development of complex formulations with optimized drug delivery profiles [15].

This study aimed to exploit the potential of DPE 3D printing to fabricate LID-loaded ODF and MAF with either immediate or sustained release, by tailoring the formulation matrix. In order to modulate drug release profiles and optimize mucoadhesive performance, different polymeric systems were selected based on prior literature and the consolidated expertise of our research group. Kollidon VA 64 (Fig. 1A) was employed as the carrier in immediate-release formulations, owing to its documented hydrophilicity and rapid disintegration behaviour [16]. For sustained-release systems, combinations of polyethylene oxide (PEO) (Fig. 1B) and chitosan (CS) (Fig. 1C) were used, aligning with our previous work demonstrating their suitability for mucoadhesive delivery [17].

To further enhance the mucoadhesive properties of the films and achieve prolonged mucosal retention, we incorporated functionalized polymers, specifically thiolated chitosan (CS–SH) (Fig. 1D) and S-protected thiolated chitosan (CS–MNA) (Fig. 1E). Thiolated polymers (first generation thiomers) are obtained by introducing thiol (-SH) groups into polymer backbones, which can form covalent disulfide bonds with cysteine-rich subdomains of mucins, resulting in significantly improved mucoadhesive strength [18]. Furthermore, the subsequent introduction of protective groups, such as mercaptonicotinic acid (MNA), onto thiolated polymers enhances the stability of thiol functionalities by preventing premature oxidation and thermal degradation during processing. This strategy leads to the formation of so-called second-generation thiomers, characterized by improved handling and functional performance. In fact, this protective modification not only maintains the mucoadhesive properties of the polymer but also extends its functionality and shelf life [19].

Building upon our experience in the synthesis and pharmaceutical application of thiolated and S-protected polymers [20], [21], [22], we integrated these excipients directly into printable powder blends. This enabled, for the first time, a single-step DPE 3D printing process for the fabrication of MAF containing S-protected thiolated

chitosan, without requiring any post-printing chemical modifications. The resulting films were characterized in terms of disintegration, mechanical strength, mucoadhesion, and ex vivo permeation and retention, validating their potential as personalized, paediatric-friendly drug delivery systems for local analgesia.

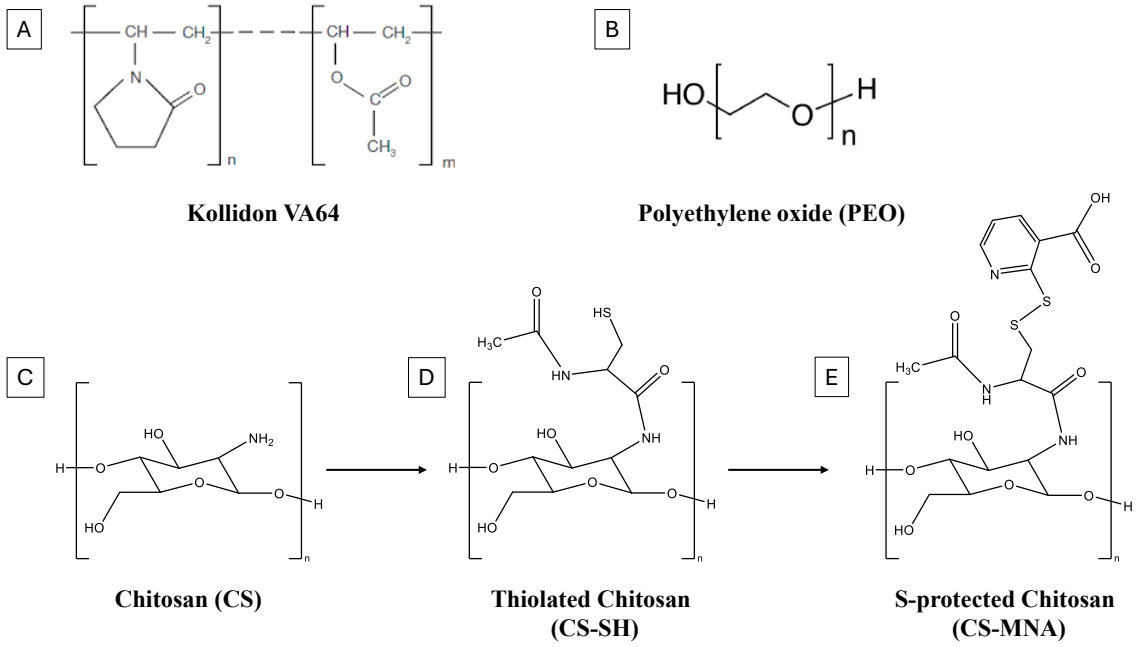

Fig. 1 - Chemical structure of Kollidon VA64 (A), PEO (B), CS (C), CS-SH (D) and CS-MNA (E).

2. MATERIALS AND METHODS

2.1 Materials

Lidocaine Hydrochloride (LID) was purchased from Farmalabor Srl (Italy). AFFINISOL™ HPMC HME 15 LV (hydroxypropyl methylcellulose) was gifted by Pharma Solutions – Nutrition & Biosciences (Italy). Polyethylene oxide (PEO) (Polyox WSR N10, MW=100.000) was purchased from DuPont (Italy). Chitosan (low molecular weight) (CS), N-acetylcysteine (NAC), 1-ethyl-3-(3-dimethylaminopropyl) carbodiimide hydrochloride (EDAC), 2,4,6-trinitrobenzenesulfonic acid (TNBS), 5,5-dithio-bis(2-nitrobenzoic acid) (Ellman's reagent), N-hydroxy succinimide (NHS), 2-mercaptonicotinic acid (2-MNA), 2-amino-2-(hydroxymethyl)-1,3-propanediol (TRIS), sodium borohydride (NaBH4), acetonitrile, methanol and Crude (Type II)

mucin from porcine stomach (Batch: SLCD8305) were purchased from Sigma-Aldrich (Merck, Germany). Kollidon® VA 64 was purchased from BASF (Germany). Potassium Phosphate Dibasic was purchased from Honeywell Fluka (Italy). For the analysis, distilled and purified water (resistivity of 18.2 MΩ.cm at 23 °C) was obtained by the purification system Milli-Q (Purelab DI, MK2) (Elga, UK). All solvents were of analytical grade, unless otherwise specified.

2.2 Synthesis of thiolated (CS-SH) and S-protected chitosan (CS-MNA)

The synthesis of CS–SH and its subsequent S-protection with 2-MNA was adapted from a previously published protocol on glycol chitosan thiolation and S-protection [23] with minor modifications. Briefly, CS–SH was obtained via carbodiimide-mediated coupling with N-acetylcysteine, followed by purification and lyophilization. The resulting thiolated polymer was then modified through disulfide exchange with pre-dimerized 2-MNA to obtain S-protected CS–MNA conjugates.

2.3 Preparation of the powder blends

To develop different formulations for both immediate and sustained release of LID, five distinct powder blends were prepared using various polymeric excipients. Depending on the intended release profile, Kollidon VA 64 or PEO was employed as the carrier polymer, while the drug concentration was kept constant at 3.0% w/w. Blends 3–5 incorporated mucoadhesive polymers, including both unmodified and functionalized chitosan derivatives (CS, CS–SH, and CS–MNA), as described above, to systematically evaluate the impact of thiolation and S-protection on the films' mucoadhesive performance. All powder blends contained mannitol, which was used as a plasticizer, while HPMC was included to facilitate interactions between the different polymers. The final compositions of the blends are summarized in Table 1.

Table 1 - Composition of the powder blends.

Blend ID	LID	PEO	HPMC	CS	CS-SH	CS-MNA	Kollidon	Mannitol
				(% w/w)				
Blend 1	3.0	40.0	-	-	-	-	47.0	10.0
Blend 2	3.0	91.5	0.5	-	-	-	-	5.0
Blend 3	3.0	81.5	0.5	10.0	-	-	-	5.0
Blend 4	3.0	81.5	0.5	-	10.0	-	-	5.0
Blend 5	3.0	81.5	0.5	-	-	10.0	-	5.0

Each component was sieved three times through a 355 μm mesh sieve to ensure better dimensional uniformity and mixing of the powder. The powders were then mechanically stirred at 67 rpm for approximately 20 minutes using a Turbula Willy A. Bachofen GmbH (Germany). The resulting powder mixtures were dried overnight in an oven at 40 °C.

2.4 Direct Powder Extrusion 3D printing

The films were fabricated using a 3DForMe® 3D printer specifically designed for pharmaceutical applications. The film design was created in Fusion 360 CAD software, generating stereolithography (.stl) files, which were subsequently imported into the 3D printing software (Ultimaker Cura). The .stl file defined the object's geometry, while all other printing parameters were configured directly within Ultimaker Cura.

Each powder blend (Blend 1 to Blend 5) was loaded into the printer and processed to obtain the corresponding 3D-printed film (ODF-1 and MAF-2 to MAF-5). A cylindrical geometry was selected for the MAF intended for disintegration, mucoadhesion, and in vitro permeation tests, with a diameter of 15 mm and a height of 0.7 mm, ensuring a target weight of 65 mg. For mechanical testing, a parallelepiped geometry was adopted, yielding rectangular films measuring 60 mm in length, 20 mm in width, and 0.7 mm in height.

The printing parameters were set as follows: 100% infill with a concentric pattern, high resolution with a brim (no raft), travel speed of 40 mm/s, print speed of 20 mm/s, two shell layers, a layer height of 0.125 mm, a platform temperature of 40 °C, and an extrusion temperature of 170 °C. The printer was equipped with a direct single-screw powder extruder and a nozzle diameter of 0.8 mm. The nozzle moved in three dimensions, enabling the precise deposition of the molten powder to form layered structures. All formulations were printed under identical conditions. After each print job, the extruder was disassembled and thoroughly cleaned to prevent cross-contamination between different formulations.

2.5 Quantitative analysis of LID by HPLC-UV

HPLC analysis was performed using a Shimadzu NexEra equipped with the following modules: CBM-40 system controller, LC-40D solvent delivery module (pump), SIL-40C Pharmaceutics 2024, 16, 277 6 of 20 autosampler, DGU-405 degassing unit, CTO-40C column oven, and SPD-M40 photodiode array detector. A specific HPLC method was used for the LID quantification [24] using a Zorbax Eclipse plus C18 250 × 45 mm column, pore size of 5 µm and a guard column, with Potassium dihydrogen phosphate (pH 5.5; 20 mM):acetonitrile in the ratio of 74:26 (v/v) as mobile phase, with a flow rate of 1.0 mL/min. The temperature of the column was set to 40 °C. The LID retention time was 7 min, and a 230 nm wavelength was adopted. Each sample was injected in triplicate using a volume of 20 µL. Linearity was evaluated in the range of 0.05–10 µg/mL, showing an excellent correlation coefficient (R^2 = 0.9996). The limit of detection (LOD) and limit of quantification (LOQ), calculated using the standard deviation of the response and the slope of the calibration curve, were 0.371 µg/mL and 1.124 µg/mL, respectively.

2.6 Characterization of the extruded filaments and films

2.6.1 Mass and content uniformity characterization

To evaluate the homogeneity of the powder blends and the reproducibility of the extrusion process, a preliminary characterization was carried out on filaments produced from each formulation prior to the printing phase. Specifically, each powder blend (10 g) was manually loaded into the hopper of the 3DForMe® printer

equipped with a single-screw extruder and set to operate at 170 °C. Once the temperature was reached and the system stabilized, extrusion was initiated by applying a constant feed of 100 mm at a speed of 5 mm/s. Under these conditions, each blend was extruded for 20 seconds, and the resulting filament segment was immediately collected and weighed. This procedure was repeated continuously over a 5-minute interval, yielding a total of 15 filament segments per blend. The weight of each segment was recorded to assess the consistency of mass over time and to evaluate the process efficiency in terms of extrusion stability.

Subsequently, five randomly selected 2 cm-long filament pieces from each blend were analysed to determine drug content uniformity. The segments were dissolved in 4 mL of distilled water: acetonitrile (1:1, v/v) and stirred overnight to ensure complete dissolution. After appropriate dilution, the solutions were analysed by HPLC as described in section 2.5 to quantify the amount of LID in each sample.

Finally, 10 MAF from each formulation were dissolved in acetonitrile to evaluate the actual LID loading, to verify the presence of a therapeutic amount of LID inside (2 mg). Each film was placed in 10 mL acetonitrile and stirred overnight at room temperature. Finally, after appropriate dilution, the drug concentration was assessed using HPLC, as previously reported.

2.6.2 Quantitative analysis of thiol and disulfide groups

The total amount of thiol and S-protected groups in Blend 4–5 and their corresponding extruded filaments was determined using Ellman's assay, as previously described [20], [22]. Briefly, 1 mg of each sample was dissolved in 0.5 mL of phosphate-buffered saline (PBS, 0.5 M, pH 8.0) and mixed with 0.5 mL of Ellman's reagent (3 mg DTNB in 10 mL PBS). After 90 minutes of incubation at room temperature in the dark, samples were centrifuged (9000 g, 2 min), and 100 µL of the supernatant was analyzed at 450 nm using a microplate reader (Tecan Infinite® M200, Tecan, Switzerland). Thiol content was calculated against a cysteine calibration curve (1 mg/mL stock).

To quantify oxidized thiol groups, 1 mg of each sample was reduced with 1 mL of freshly prepared $NaBH_4$ (4% w/v in Tris buffer, pH 8.0) at 37 °C for 1 hour. The

reaction was quenched with 250 µL of 5 M HCl, followed by the addition of PBS and Ellman's reagent. Absorbance was measured after 2 hours to determine total thiol content. All tests were performed in triplicate.

2.6.3 Solid state characterization of powder blends and printed films

Obtained printed filaments and final films were characterized in the solid state, together with the pure drug and the physical powder blend (excipients/drug). They were analyzed by differential scanning calorimetry (DSC), thermogravimetric analysis (TGA) and powder X-ray diffraction (PXRD). Differential scanning calorimetry (DSC) of the different samples was performed using a Perkin Elmer DSC 4000 equipment. Analyses were carried out on Blend 1 (ODF-1) and Blend 5 (MAF-5), selected as representative immediate-release and sustained-release MAF prototypes, respectively. About 5-10 mg of the sample was heated in an aluminium pan at a heating rate of 5 °C/min from 30 °C to 200 °C under N_2 flow. The analysis on LID was conducted by presenting a first phase of heating from 30 °C to 200 °C at 2 °C/min, a second phase of cooling from 200 °C to 30 °C at 5 °C/min, and a third phase of heating from 30 °C to 200 °C at 2 °C/min, to check the behavior of the drug during the printing steps. An empty pan was used as the reference.

The PerkinElmer Thermogravimetric Analyzer Pyris 1 TGA was employed to conduct TGA analysis on the pure drug. Each sample (~7 mg) was placed into platinum pans and heated at a rate of 10 °C/min to achieve a temperature of 600 °C. The thermal decomposition (or degradation) profile was examined using PyrisTM software version 11. During the trials, the nitrogen (N_2) gas flow rate was 20 mL/min.

The X-ray powder diffraction patterns were collected using a Rigaku Rint2500 rotating Cu anode working at 50 kV and 200 mA in Debye–Scherrer geometry. The diffractometer was equipped with an asymmetric Johansson Ge (111) crystal to select monochromatic CuKα_1 radiation (λ = 1.54056 Å) and a Rigaku D/teX Ultra silicon strip detector. The range from 5 to 70° (2ϑ) was collected with a 0.02° (2ϑ) step size and counting time of 6 s/step. Each powder sample was introduced into a glass capillary (diameter, 0.5 mm) and mounted on the axis of the goniometer. The

capillary was rotated during the measurement to improve the randomization of the orientations of the individual crystallites and reduce the effect of the preferred orientation.

2.6.4 Morphological and dimensional characterization

The physical dimensions of the printed films were assessed using a digital slide gauge (Hitech Diamond). The morphology of the film obtained during the printing stage was evaluated using an electrical scanning microscope (SEM) operating at 20 kV (Hitachi TM 3000 Tabletop SEM). Furthermore, a Chemical Microanalysis test was conducted on the samples to confirm the presence of N and Cl, which are elements present only in the LID structure, and thus investigate the dispersion of the drug within them. Chemical Microanalysis was also performed on samples MAF-4 and MAF-5 to detect the presence of S on the surface of the printed films. The surface of each printed film was analyzed using a Swift ED3000 Oxford Instrument with AZtecOne software.

2.6.5 Tensile properties

Tests were conducted according to ASTM International Test Method for Thin Plastic Sheeting (D 882-02) using an Instron 5965 texture analyser (Instron, UK), equipped with a 50 N load cell. The samples were 50×13mm film strips.

Each test strip was longitudinal by placed in the tensile grips on the texture analyser. Initial grip separation and the crosshead speed were 12.5 mm/min. The test was considered concluded at the film break. The following parameters were determined:

- Tensile strength (TS) was calculated by dividing the maximum load by the original cross-sectional area of the specimen.
- Percent elongation at break (E%) was calculated according to the following equation (Equation 1):

$$E\% = \frac{L - L_0}{L_0}\ x\ 100 \qquad \textit{Equation 1}$$

where L_0 is the initial gage length of the sample and L is the length at the rupture.

- Elastic modulus or Young's modulus (Y) was calculated as the slope of the linear portion of the stress–strain curve.

2.6.6 Disintegration and dissolution time evaluation

The disintegration properties of the MAF were assessed using a modified version of the Slide Frame and Ball (SFaB) test with simulated salivary fluid (SSF), as described in literature [25]. In this test, a 2 g steel cylinder was placed on top of the selected MAF to mimic the mechanical stress exerted by the tongue during oral administration. Simultaneously, SSF was pumped onto the film at a flow rate of 1 mL/min to replicate the salivary environment. The disintegration time was defined as the point at which the hydrated film broke apart, causing the weight to drop.

Following the disintegration assessment, a dissolution test was conducted using the Modified Petri Dish method [25]. Briefly, the MAF were placed in a Petri dish, which was then filled with 5 mL of preheated SSF (37 °C). The test was performed in a thermostatic shaking water bath set at 37 °C with an oscillation speed of 10 rpm. The dissolution time was recorded as the duration required for the film to completely dissolve, forming a homogeneous solution.

2.7 Mucoadhesive properties

Characterization of film mucoadhesive properties was performed by using an Instron 5965 texture analyser (Instron, UK), equipped with a 50 N load cell [17]. The tested films were attached to the mobile steel punch by cyanoacrylate glue. Mucin compacts, weighing 130 mg, were attached with cyanoacrylate glue to a steel plate fixed at the bottom of the tensile apparatus and hydrated with 80 µL water for 5 min, to obtain a jelly superficial mucin stratum. The compacts were preliminarily obtained by applying a compression force 11 tons for 60 s, by using a hydraulic press (Glenrothes, UK) equipped with flat faced punches and having a die diameter of 11.28 mm. As the experiment started, upon making contact between the sample and the hydrated mucin, a constant force of 1.3 N was imposed for 120 s. The mucoadhesive performance of the tested materials was determined by measuring the detachment force (DF) required to separate the film from the mucin compact (maximum detachment force; DF_{max}) upon an elongation of 10.0 mm at the constant

rate of 0.1 mm/s. The area under the curve (AUC) of the detachment force versus the elongation was also determined to represent the work or energy required for the detachment of the film from the mucin.

2.8 *Ex-vivo* mucoadhesion and dissolution test

The wash-off method was used to measure the mucoadhesive and dissolution properties of all the obtained MAF. In detail, an appropriate sample with dimensions of 2 cm (diameter) x 0,3 mm was 3D printed to standardize the membrane surface area of contact and validate the assay. The obtained samples were placed on a 2 × 3 cm section of the animal mucosae and fixed on a 45° inclined surface. Animal mucosae, derived from porcine oesophagus, was freshly obtained from a local slaughterhouse (Bari, Italy). The mucosae epithelium was separated by mucosal specimens using a scalpel, cleaned, and stored at 4 °C in phosphate buffer solution (pH 7.2) before use [26]. Then, 60 mL of the simulated salivary fluid solution was poured using a syringe connected to a pump onto the sample placed on the mucosae at a constant flow rate of 1 mL/min to simulate salivary flushing. At time intervals of 5 min for a total time of 60 min, 300 µl were withdrawn from the washing solution and replaced with the same volume of simulated salivary fluid solution. The samples obtained, after appropriate dilutions, were analysed by the previously reported HPLC method in order to assess the concentration of LID removed from oesophageal mucosa over time. Determination of the percentage of LID that remained in the mucosa was performed by an indirect method using the following equation (Equation 2):

$$Remaining\ LID\ (\%) = \frac{LID\ (Total\ Amount) - LID\ (collected\ sample)}{LID\ (Total\ Amount)}\ x\ 100 \qquad Equation\ 2$$

2.9 *In Vitro* Permeation Study

The permeation study was performed by using Franz diffusion cells (diffusion area: 0.636 cm^2; receptor volume: ≈ 3.0 mL) and porcine oesophageal tissues as membrane. Fresh porcine oesophageal tissue was obtained by a local slaughterhouse. The mucosae epithelium was separated by mucosal specimens using a scalpel and stored at 2-8 °C until use for not more than 24 hours [26]. Prior

to experiments, the mucosae epithelia were thawed at room temperature and cut into squares of about 4.5 cm^2. The integrity of oesophageal epithelia was visually checked before the experiments.

A 2.0 cm^2 circular sample, obtained from film by a precision die cutter, was gently applied to the oesophageal epithelium specimen, preliminary hydrated with 80 µL of HPLC-grade water to facilitate contact with the mucosae. Then, the assembly was mounted on the receiver compartment of the Franz diffusion cell whose receptor compartment was filled with sterile 0.9% sodium chloride aqueous solution (Eurospital S.p.A., Italy). Special care was given to avoid air bubbles between the solution and the mucosa in the receptor compartment. The upper and lower parts of the Franz cell were sealed with Parafilm® (Pechiney Plastic Packaging Company, USA) and fastened together by means of a clamp, with the oesophageal mucosa acting as a seal between the donor and receptor compartments. The system was kept at 37 °C with a circulating water bath throughout the experiment. At predetermined times (1, 3, 5, 8 h), 200 µL samples were withdrawn from the receiver compartment and replaced with fresh receiver medium. Samples were analysed by HPLC according to the method described above. The values were the average of parallel experiments performed in triplicate. The cumulative amount permeated through the oesophageal mucosae per unit area ($Q_{t,\ perm}$) was calculated from the drug concentration in the receiving medium and plotted as a function of time. MAF-2 was used as control.

2.10 *In vitro* retention study

At the end of the permeation experiments, the concentration of opioid retained into the epidermis ($Q_{8h,\ ret}$) was quantified by the following procedure. The oesophageal epithelium was removed from the Franz diffusion cell and stripped (Transpore®, 3M, USA) to eliminate the unabsorbed formulation. Then, each side of the membrane was gently treated with 5 mL of Acetonitrile to wash out the unabsorbed drug. Subsequently, the sample was thinly sliced and placed in 5 mL of fresh Acetonitrile The suspension was soaked for 10 min and then maintained for 24 h at 2-8 °C. Finally, the supernatant was centrifuged at 7000 rpm, 25 °C for 5 min (Z326K,

Hermle LaborTechnik GmbH, Germany) to eliminate suspended materials and then, analysed by HPLC. $Q_{8h,ret}$ was expressed as micrograms of LID per gram of oesophageal epithelium. The Q_{ret}/J ratio was used to underline the LID affinity for the mucosa and the influence of the formulation on such parameter [27]. In particular, the higher the Q_{ret}/J ratio ($Q_{ret}/J >> 1$), the higher the affinity of the LID to be retained. Otherwise, the formulation promotes drug permeation through the oesophageal mucosa ($Q_{ret}/J < 1$).

2.11 Stability studies

The stability of the printed MAF was assessed after 12 months of storage under controlled conditions in a Climacell 222 – ECO line climatic chamber (MMM Group, Semmelweis Strasse, München, Germany) set at 25 °C and 60% relative humidity (RH). The samples were stored in amber glass bottles sealed with plastic screw caps to prevent direct light exposure. After the storage period, the stability of LID in all MAF was evaluated by HPLC analysis to determine any variation in drug content. Additionally, Ellman's test was performed on selected formulations to assess the oxidation state of thiol groups and verify the integrity of the thiolated and S-protected functional groups under the applied storage conditions.

2.12 Statistical analysis

Statistically significant differences in obtained results were determined by Tukey-Kramer post-hoc tests after One-way ANOVA analysis ($p < 0.05$; JMP® Pro 16).

3. RESULTS AND DISCUSSION

The primary objective of this study was to develop MAF for immediate or sustained release of LID by employing, for the first time, thiolated and S-protected thiolated CS derivatives in a DPE 3D printing process. This approach enabled the solvent-free fabrication of mucoadhesive dosage forms in a single processing step, representing a significant advancement in the personalization and functionalization of oral drug delivery systems. By integrating advanced functional excipients into printable powder blends, we aimed to investigate how polymer composition could be

strategically modulated to tailor LID release kinetics and improve mucosal retention and local bioavailability.

To evaluate the performance of the printed MAF and validate this formulation strategy, a series of complementary analyses were conducted. Mechanical testing was performed to ensure adequate tensile strength and flexibility, essential for practical handling and patient administration. Disintegration and dissolution studies were used to distinguish between fast- and sustained-release profiles. Mucoadhesive properties were assessed to measure polymer–mucosa interactions, particularly relevant for prolonging drug retention at the site of action.

In addition, in vitro permeation and retention studies on porcine mucosa were carried out to investigate drug transport dynamics and to quantify the effect of thiolated polymers on tissue-level accumulation of LID. These experiments were designed to confirm the hypothesis that modifying polymer composition by incorporating hydrophilic carriers, mucoadhesive chitosan, and functionalized thiomers could enable tailored release kinetics and improve local bioavailability.

3.1 Preparation of the powder blends

The five powder blends (Table 1) were successfully formulated by a combination of sieving and mixing, yielding homogeneous mixtures with satisfactory flow characteristics. Processability of the blends was evaluated qualitatively during the DPE 3D printing process and deemed suitable, as no clogging of the extrusion nozzle or interruptions in the hopper feeding mechanism were observed throughout the production. Mannitol, included at 5–10 % w/w as a plasticizer and lubricant, markedly reduced interparticle friction and cohesion, thereby enhancing overall powder flow [28]. Concurrently, low-level addition of HPMC (0.5 % w/w) functioned as an effective binder, improving particle cohesion and granule strength without excessively compromising flowability [29]. Comparing the two carrier systems (Kollidon VA 64 and PEO), both blends exhibited similar powder densities and no visible segregation during handling, indicating that both the hydrophilic polymers were equally suitable for DPE of lidocaine MAF. Furthermore, despite the intrinsically higher cohesion of mucoadhesive polymers, incorporation of 10 % w/w

chitosan (CS-SH or CS-MNA) into Blends 3–5 did not adversely affect powder flow or mixing uniformity, as evidenced by the narrow content-uniformity Relative standard deviations (RSDs) (< 5 %) observed on the 2 cm filament samples (see Section 3.4). This improved processability may be attributed to the complementary physical roles of mannitol and HPMC, which appeared to reduce the stickiness and poor flow tendency qualitatively observed in blends containing CS-SH or CS-MNA. Importantly, the seamless processability of CS, CS-SH and CS-MNA containing blends confirms that direct powder extrusion can accommodate complex, multifunctional polymer systems without compromising feed consistency or print fidelity.

3.2 Characterization of the extruded filaments

A single-screw extruder-printer model was used for the DPE. The mixed powder was filled into the hopper, heated to a certain temperature, and used for direct printing of filaments. The single-screw DPE process produced continuous filaments with excellent material recovery (> 95 % yield for all blends), indicating efficient powder–to–filament conversion and minimal feedstock loss. Visual inspection revealed smooth, defect-free filaments with no signs of agglomeration or nozzle clogging, even when processing blends containing CS–SH or CS–MNA, demonstrating the compatibility of thiolated and S-protected chitosan derivatives with DPE conditions. Importantly, blends composed of different carrier polymers and incorporating 10 % mucoadhesive or thiolated polymers (Blends 3–5) all printed with equivalent quality and uniformity.

Additional weight and content-uniformity analyses were performed on all five blends to verify that extrusion at 170 °C did not compromise either the drug or excipients and to assess the efficacy of the powder-blend preparation [30]. Filament samples were collected at 20-second intervals over a continuous 300-second extrusion period and weighed. As shown in Fig. 2, the filament mass remained consistent across the entire extrusion run for each formulation, indicating uniform extrusion without zones of over- or under-extrusion. This mass stability is essential for minimizing the risk of dose variability and ensuring consistent drug delivery [31].

Blend 1 consistently produced higher filament mass per interval, which may be attributed to the lower effective viscosity and higher flowability of the Kollidon VA 64-based matrix at the set extrusion temperature. However, differences in the bulk density of the polymer blends and the extent of thermal softening during extrusion could also have contributed to the variations observed in extruded mass. In contrast, blends containing CS–SH or CS–MNA showed reduced extrusion efficiency under identical conditions, suggesting a higher effective viscosity and increased resistance to flow.

Notably, during the 3D printing process, slicing parameters encoded in the G-code, such as flow rate and layer height, were carefully optimized and maintained constant across all formulations. These parameters played a crucial role in regulating the volume of deposited material per layer and helped compensate for formulation-dependent flow differences, thereby ensuring uniform film geometry and drug loading.

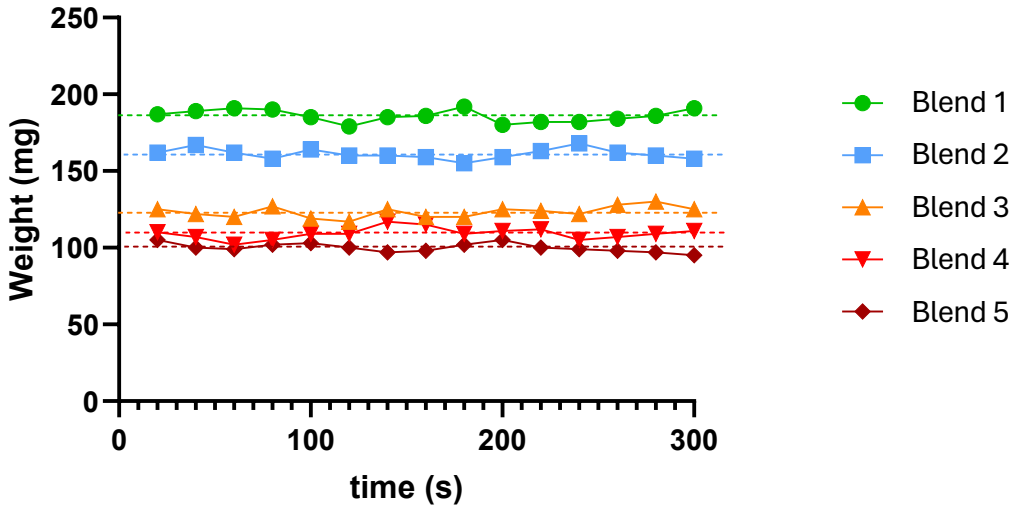

Fig. 2 - Weight of filaments from each of the five formulations, collected at 20 s intervals during a continuous 300 s extrusion run. The average weights are indicated by the dashed line for each sample.

Drug content analysis of the 2 cm filament segments revealed LID concentrations between 2.87 % and 2.96 % w/w, closely matching the theoretical 3.0 % loading (Table 2). This narrow assay range confirms that exposure to high extrusion

temperatures did not degrade the active compound or disrupt blend homogeneity [32].

Table 2 - Average LID concentrations (%) present within different HME filaments.

Filament ID	Weight (mg)*	Theoretical LID (% w/w)	Measured LID* (% w/w)
Blend 1	18 ± 0.10	3	2.88 ± 0.05
Blend 2	15 ± 0.09	3	2.95 ± 0.02
Blend 3	16 ± 0.05	3	2.96 ± 0.08
Blend 4	16 ± 0.12	3	2.87 ± 0.11
Blend 5	16 ± 0.15	3	2.92 ± 0.12

*The value is the average of 5 fragments, ± is the standard deviation.

3.3 Characterization of mucoadhesive films

3.3.1 Morphological and dimensional characterization

After confirming the printability of the selected powder blends and the filament-production performance of the 3DForMe system, the blends were used to fabricate LID-loaded MAF. Dimensional analysis of the 3D-printed MAF (15 mm diameter × 0.7 mm thickness) showed deviations within ± 5 % of their nominal values, confirming high geometric fidelity of both the extrusion and layer-by-layer deposition. All mucoadhesive films demonstrated adequate flexibility, hardness, and elasticity to ensure mechanical integrity during packaging and ease of handling prior to administration. The progressive colour shift shown in Fig. 3, from the pale yellow of MAF-3 to the deep brown of MAF-5, was partially evident already in the physical mixtures before printing, reflecting the intrinsic chromophoric nature of the thiolated and S-protected chitosan derivatives. Moreover, under aerobic DPE extrusion at 170 °C, surface thiol groups (–SH) may undergo spontaneous thermal oxidation to disulfides (–S–S–), contributing to the observed browning [33], [34]. To exclude any degradation of the active ingredient and ensure accurate dosing despite the observed colour change, content uniformity was assessed on five MAF per formulation. According to Pharmacopoeia guidelines, each unit must contain between ± 5 % of the label claim to comply with uniformity of content requirements.

HPLC analysis of the five films yielded LID contents within ± 5 % of the theoretical 3.0 % w/w loading (2.91 %–2.99 % w/w), confirming that the extrusion process did not induce any loss or degradation of the API [35]. These results validate both the stability of LID under the selected DPE conditions and the robustness of the powder blend preparation in delivering uniform drug content across all formulations

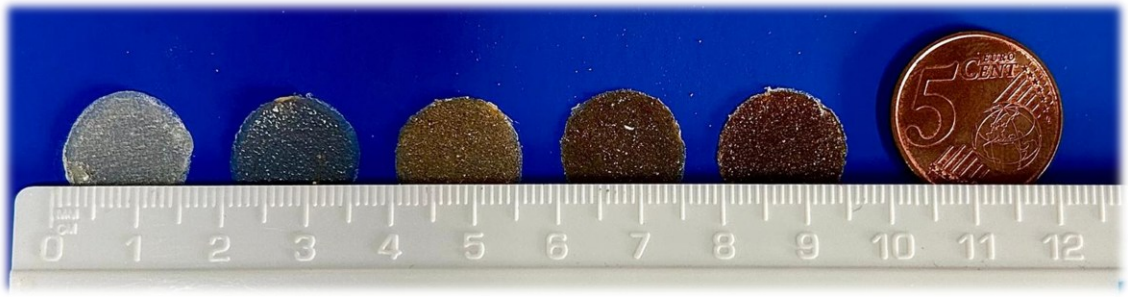

Fig. 3 - Final dimensions of the printed films for ODF-1 and MAF2–5 (left to right), shown alongside a 5 cent euro coin for scale.

Characterization studies were carried out on ODF-1 and MAF-5, which were preliminarily selected as candidate prototypes for immediate and sustained release profiles, respectively, based on their polymer composition. SEM micrographs of ODF-1 and MAF-5 revealed uniformly smooth surfaces across the entire film area, with no evidence of under- or over-extrusion (e.g., voids, ridges, or bulges) that could compromise dosing accuracy or lead to local overconcentration of drug (Fig. 4A,D). Such homogeneity indicates that all constituents are evenly distributed and that the direct powder extrusion parameters yielded continuous, well-fused layers without microcracks or fractures that might compromise film handling or dosing accuracy [36]. Notably, the same defect-free morphology was observed in all other formulations, confirming process consistency across different blend compositions.

Surface elemental mapping was then conducted to verify the spatial distribution of key chemical species. As shown in Fig. 4B, elemental maps of N and Cl, markers of LID, in ODF-1, confirmed uniform API incorporation across the film surface. Similarly, in MAF-5, strong signals for N and S were observed, attributable respectively to the combined presence of nitrogen-containing species in LID and MNA, and to the sulfur atoms from the S-protected thiol groups of 2-MNA (Fig. 4E);

This demonstrates that both drug and thiol-protection chemistry survive extrusion intact and remain evenly distributed.

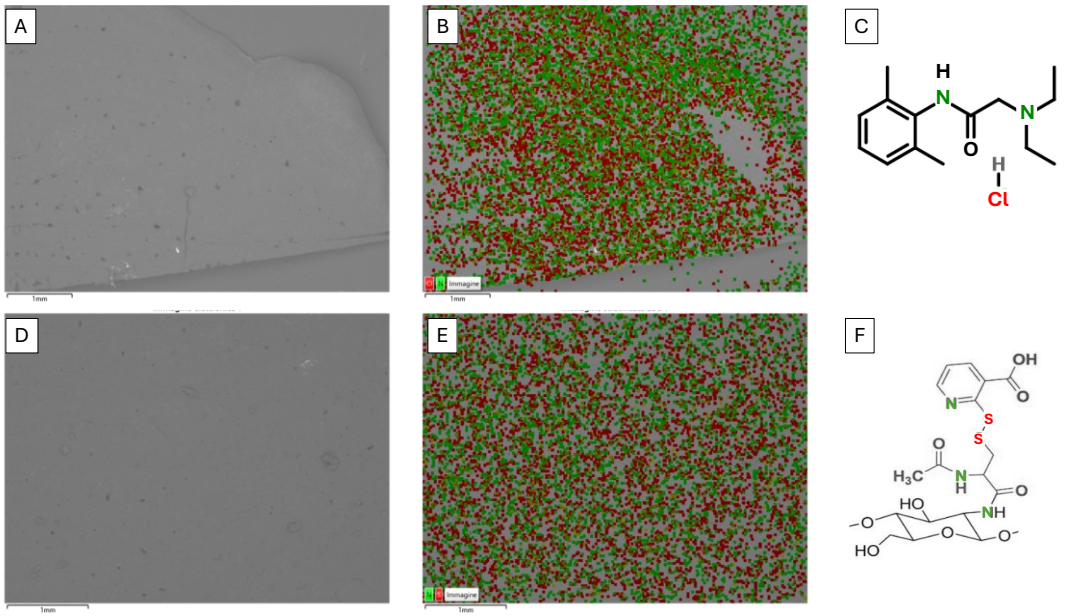

Fig. 4 - SEM images of the printed film surface of ODF-1 (A) and MAF-5 (D). Surface chemical microanalysis of the printed mucoadhesive film ODF-1 (B) with images related to the presence of the elements Cl and N, characteristics of the LID structure (C). Surface chemical microanalysis of the printed mucoadhesive film MAF-5 (E), with images related to the presence of the elements N and S, characteristics of the CS-MNA structure (F).

3.3.2 Quantitative analysis of thiol and disulfide groups

Ellman's assay was used to track free thiol (–SH), disulfide (–S–S–), and total thiol (Σ–SH) content from the thiolated polymers and powder blends through blending and extrusion (Table 3). Specifically, the CS–SH–based formulations showed a noticeable increase in disulfide content post-extrusion, reflecting partial surface oxidation of free thiols under 170 °C DPE conditions. In contrast, formulations based on CS–MNA retained a higher amount of free thiol groups after printing compared to unprotected CS–SH, indicating that the 2-MNA moiety acts as a reversible protecting group. Through transient disulfide bond formation, 2-MNA limits irreversible thiol oxidation during thermal processing, preserving the reactivity and mucoadhesive potential of the polymer [37]. This stabilizing effect is consistent with the behavior of preactivated S-protected thiomers, which exhibit enhanced resistance to oxidative degradation compared to first-generation thiomers. Overall, despite the inherently oxidative environment of high-temperature extrusion,

incorporation of the aromatic MNA chromophore preserves the bioactive thiol functionalities crucial for mucoadhesion, ensuring that downstream MAF performance is not compromised by loss of –SH groups [38].

Table 3 - The amount of immobilized thiol groups in reduced and oxidized form for raw materials, physical mixtures and extruded samples. –SH represents the total amount of reduced thiol groups per gram of sample, –S–S– represents the total amount of oxidized thiol groups per gram of sample, Σ–SH indicates the total thiol content per gram of sample, and Σ–SH on MAF refers to the total thiol content on the final MAF.

Sample ID	-SH	-S-S-	Σ-SH	Σ–SH on MAF
		(mmol/g)		nmol
CS-SH	5.98 ± 0.08	0.80 ± 0.04	6.78 ± 0.11	-
CS-MNA	1.00 ± 0.05	4.41 ± 0.07	5.41 ± 0.12	-
Blend 4	0.34 ± 0.03	0.19 ± 0.03	0.53 ± 0.05	-
MAF-4	0.16 ± 0.03	0.31 ± 0.03	0.47 ± 0.05	2.820
Blend 5	0.06 ± 0.01	0.39 ± 0.04	0.45 ± 0.04	-
MAF-5	0.04 ± 0.01	0.37 ± 0.04	0.41 ± 0.05	2.460

3.3.3 Solid state characterization of mucoadhesive films

Thermal analysis of lidocaine and formulations was conducted using TGA and DSC. The DSC thermogram of pure LID (Fig. 5A) showed a sharp endothermic peak at ~80 °C, corresponding to the melting point of its crystalline salt form [39]. To simulate thermal stress during 3D printing, a heating–cooling–heating cycle was applied. The absence of a recrystallization exotherm upon cooling, along with the disappearance of the melting peak in the second heating scan, indicated that LID underwent an irreversible transition to an amorphous state.

This behaviour is consistent with a Class III amorphous system, as defined in pharmaceutical classifications: compounds that form a stable glassy state upon melting and do not recrystallize under conventional DSC cooling conditions [40], [41]. Such irreversible amorphization implies that, during DPE processing at 170 °C, LID becomes molecularly dispersed and remains in a non-crystalline form within the film matrix, a state associated with improved dissolution properties [42].

To further explore drug–polymer interactions, DSC was performed on the physical mixtures (Blends 1 and 5) and their corresponding 3D-printed films (ODF-1 and MAF-5) across the 30–200 °C range (Fig. 5B). In the physical mixtures, the LID melting peak was still evident, albeit slightly shifted and broadened, likely due to partial solubilization in the polymer during heating and reduced lattice energy caused by specific interactions [43].

By contrast, the extruded films showed either a significant reduction or complete disappearance of the LID melting peak (Fig. 5B). This absence is a hallmark of successful amorphization via hot-melt extrusion, indicating that LID was transformed into a stable amorphous form within the polymer matrix [44]. The lack of recrystallization signals further confirmed the irreversible nature of this transition.

Overall, these data confirm that while simple blending preserves LID's crystalline structure, DPE processing at 170 °C leads to its complete amorphization within the MAF, potentially enhancing dissolution and therapeutic performance.

TGA analysis (Fig. 5C) of pure LID revealed that mass loss remains below approximately 5 % up to 170 °C, attributable to desorption of adsorbed moisture and partial volatilization of the salt, while the onset of pronounced thermal decomposition is only observed above 200 °C, where a steep weight-loss slope marks API degradation [42], [45]. Identical TGA profiles were obtained for both the physical powder mixtures (Blend 1 and Blend 5) and their corresponding extruded films (ODF-1 and MAF-5), with minimal weight reduction (< 5 %) at the DPE printing temperature of 170 °C, thus confirming that neither LID nor the polymeric excipients (PEO, HPMC, Kollidon VA 64, chitosan derivatives) undergo appreciable breakdown during processing. Major mass loss in all samples only commenced above 200 °C, reflecting the thermal decomposition of Kollidon VA64 (which begins around 250 °C) and chitosan backbones (onset at 200–220 °C) as well as the LID itself [46]. Together, these data validate 170 °C as a safe extrusion temperature, producing only minor volatile loss while fully preserving the chemical integrity of both API and excipients.

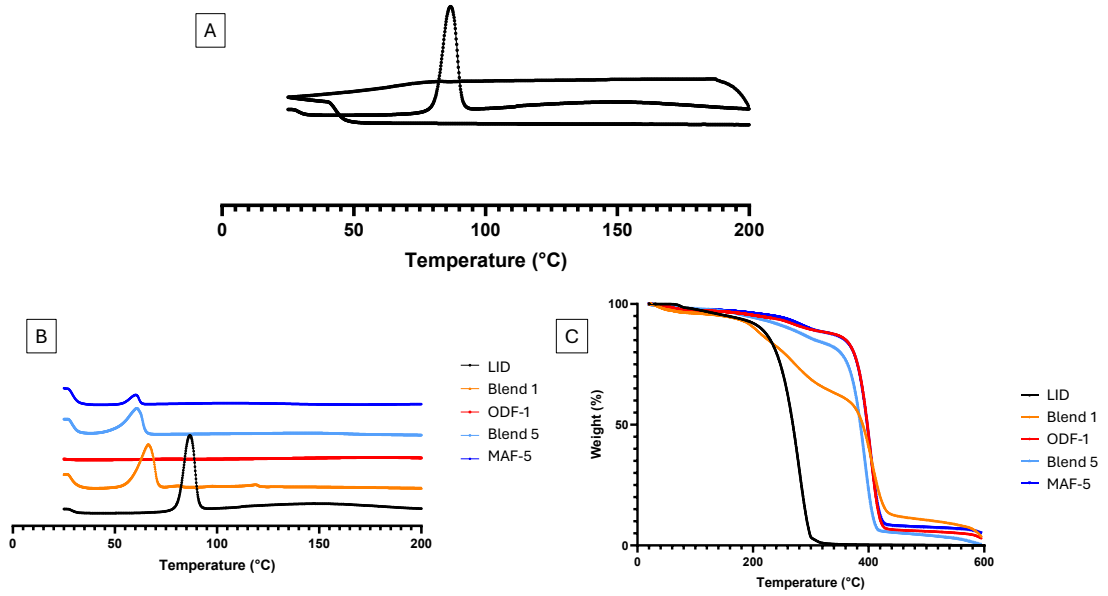

Fig. 5 - DSC thermogram of LID using multiple heating and cooling cycles (A). DSC thermograms of printed mucoadhesive films ODF-1 and MAF-5 compared with the thermograms of LID and physical mixtures (B). TGA curves of printed mucoadhesive films ODF-1 and MAF-5 compared with the thermograms of LID and physical mixtures (C).

PXRD analysis of both immediate-release ODF-1 and sustained-release MAF-5 systems confirms the solid-state transformations inferred from DSC and TGA. In the corresponding physical mixtures (Blend 1 and Blend 5), the diffractograms exhibit the sharp, characteristic reflections of crystalline LID alongside those of the polymeric excipients (Kollidon VA 64/HPMC/PEO, mannitol), indicating that the API remains fully crystalline within these blends. After the extrusion phase, however, both ODF-1 (Fig. 6A) and MAF-5 (Fig. 6B) lost all discernible LID diffraction peaks, while the broader, lower-intensity reflections of the polymers persist. This disappearance of API's crystalline signals demonstrates its conversion to an amorphous form during the 170 °C extrusion process, consistent with the irreversible amorphization observed by DSC and the minimal mass loss seen in TGA, while the retention of polymer peaks confirms structural integrity of the excipient matrix.

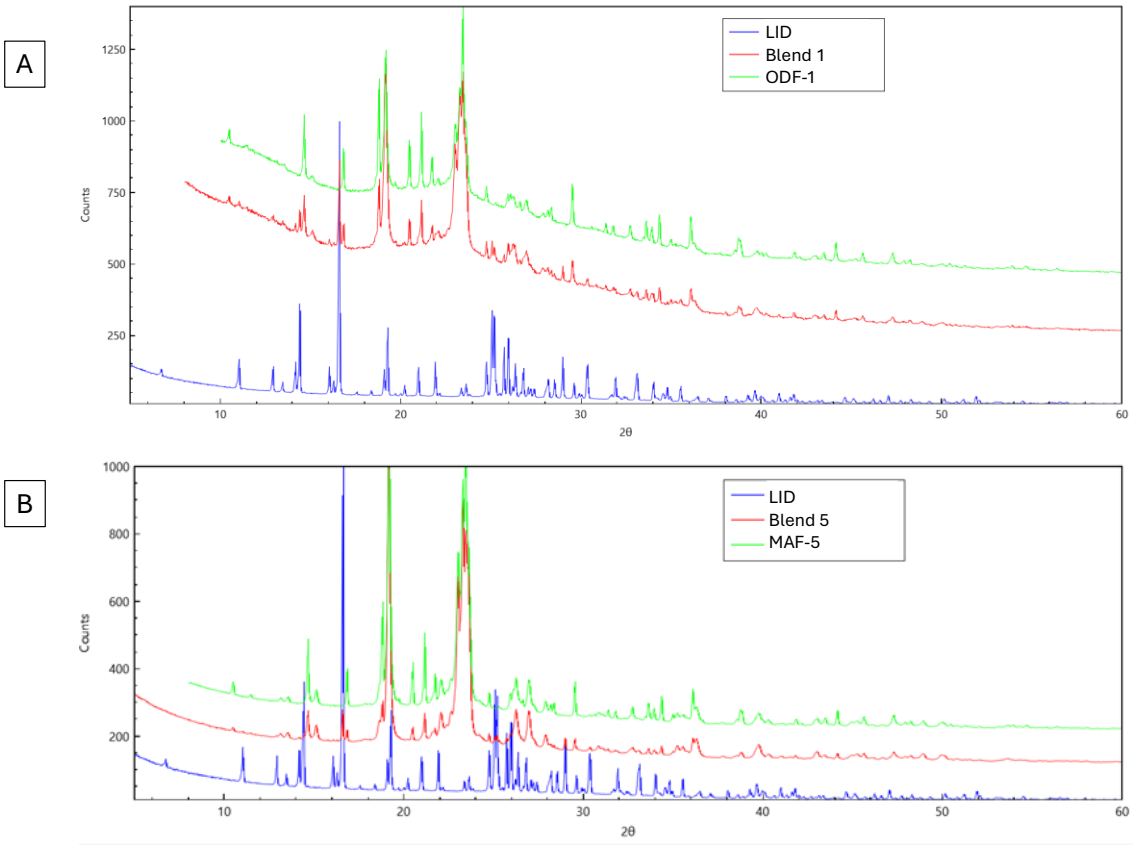

Fig. 6 - Diffractograms of the printed mucoadhesive films for ODF-1 (A) and MAF-5 (B), each compared with the diffractograms of LID and the respective medicated blend.

3.3.4 Tensile properties

Table 4 reports the results of tensile test on mucoadhesive films. The results demonstrated that tensile properties of all formulations are comparable to published data obtained with CS-based films prepared using different printing and casting technologies [17], [47], despite a lower elasticity (Y) and plasticity (E%). Among formulations, composition changes seem not significantly impact on their tensile properties ($p > 0.05$).

Table 4 - Results of tensile tests performed on mucoadhesive films, expressed as mean ± S.D. (n=4).

Form. ID	TS (MPa)	E%	Y (MPa)
ODF-1	5.94 ± 3.80	1.79 ± 0.67	969 ± 354
MAF-2	4.75 ± 1.20	3.49 ± 0.84	381 ± 52
MAF-3	3.91 ± 0.38	5.07 ±0.69	216 ± 19
MAF-4	6.75 ± 0.72	2.45 ± 0.13	532 ± 64
MAF-5	6.74 ± 1.10	2.66 ± 0.09	556 ± 93

3.4.5 Disintegration and dissolution time evaluation

To assess buccal performance, all the printed MAF were evaluated by disintegration and dissolution testing under simulated salivary conditions. Disintegration times were determined using a modified Slide Frame and Ball (SFaB) method, which combines continuous salivary flow with mechanical stress replicating tongue contact. As shown in Fig. 7A, ODF-1 disintegrated almost instantaneously, a behaviour that can be ascribed to the rapid hydration of Kollidon VA 64, which promotes swift water uptake and matrix collapse [13]. In contrast, MAF-2, composed by PEO and HPMC, exhibited a moderate delay, reflecting the more gradual swelling and gel formation typical of these hydrophilic polymers [48]. Notably, MAF-3–5, containing unmodified CS, CS–SH, and CS–MNA, respectively, showed progressively longer disintegration times. This gradual increase was statistically significant across all formulations (one-way ANOVA, Tukey's post-hoc test, $p < 0.05$). The trend underscores the pivotal role of intra- and inter-chain interactions within chitosan and its derivatives. The presence of thiol and disulfide groups likely contributes to enhanced matrix cohesion via covalent cross-linking, making the films more resistant to both salivary and mechanical stresses in the buccal environment [49]. These findings support the hypothesis that CS functionalization can be strategically exploited to tailor the mechanical integrity and residence time of buccal films.

A parallel pattern emerged in the dissolution profiles measured via the Modified Petri Dish method. As shown in Fig. 7B, the fastest release from ODF-1 aligns with

its rapid breakup, whereas the inclusion of PEO/HPMC in MAF-2 created a more sustained release. The CS-based films further extended drug liberation, with CS–SH and CS–MNA likely contributing to a more controlled release profile. The observed sustained release may result from a combination of slowed molecular diffusion and potential matrix restructuring or gradual surface disintegration. Such tunable release is particularly valuable: immediate-release films like ODF-1 are ideal for rapid analgesic onset, while sustained-release formulations (MAF-3–5) can provide prolonged local anaesthesia, reducing dosing frequency and improving patient comfort. For this reason, the mucoadhesive properties and mucosal drug-release behaviour of MAF-2–5 were further investigated.

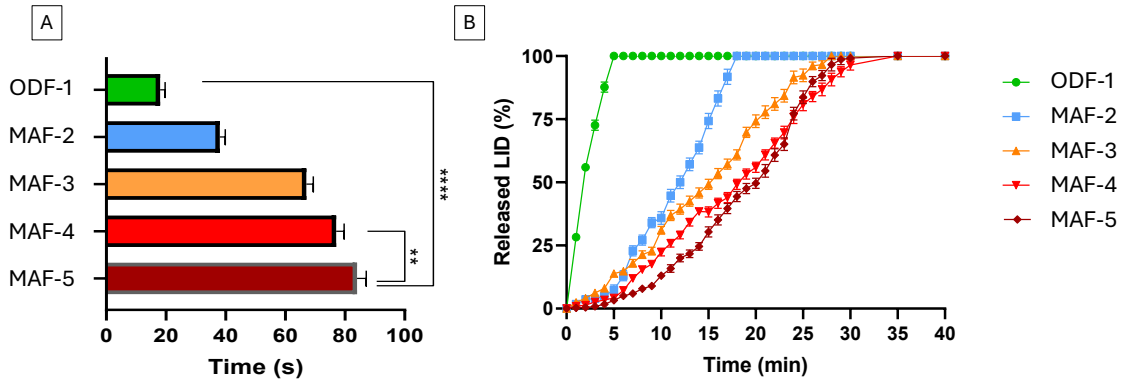

Fig. 7 - Total disintegration time (A) and dissolution profile (B) of the films.

3.4 Mucoadhesive properties

The test was performed to provide a complementary characterization of the films' mucoadhesive properties. As shown in Table 5, significant differences in film mucoadhesive properties were observable. As expected, films containing mucoadhesive polymers showed an enhancement of the force needed to provide their complete detachment from mucin compacts (MAF-3–5 vs ODF-1 and MAF–2; $p < 0.01$). On the contrary, other formulative parameters seem not to impact on the mucoadhesive properties (ODF-1 vs MAF-2; $p = 0.70$).

The presence of CS resulted in a 1.5-fold increase in detachment force (DF) compared to the equivalent non-mucoadhesive film (MAF-2 vs. MAF-3). Moreover,

the thiolation of CS (MAF-4) led to a further and statistically significant enhancement in mucoadhesion compared to both MAF-2 and MAF-3 ($p < 0.001$), in agreement with previous findings reported for other pharmaceutical dosage forms [50]. Notably, although the introduction of S-protection (MAF-5) preserved a significant degree of mucoadhesion, its performance was lower than that of the unprotected thiolated counterpart (MAF-4, $p = 0.03$), yet still superior to the non-thiolated formulation (MAF-3, $p = 0.04$). This difference can be rationalized by considering the total amount of thiol groups present in the two formulations, as reported in Table 3. In fact, when normalizing for the difference in total thiol content (MAF-4 contains approximately 1.15 times more thiol groups than MAF-5), the mucoadhesion results appear to be fully comparable. However, considering the amount of reduced –SH groups, which is four times lower in MAF-5 compared to MAF-4 (Table 3), the higher mucoadhesive performance of MAF-5 can be attributed to the enhanced reactivity of the MNA-protected thiol groups.

Table 5 - Results of mucoadhesive tests performed on LID-loaded films, expressed as mean ± S.D. (n=4).

Form. ID	DF_{max} (N/mm^2)	AUC (mJ)
ODF-1	38.84 ± 5.14	0.568 ± 0.294
MAF-2	34.70 ± 7.81	0.522 ± 0.442
MAF-3	54.26 ± 1.34	1.308 ± 0.098
MAF-4	79.21 ± 0.69	1.570 ± 0.219
MAF-5	66.63 ± 1.22	1.464 ± 0.248

3.5 *Ex-vivo* mucoadhesion and dissolution test

The wash-off mucoadhesion and release data (Fig. 8) reveal a clear correspondence between polymer composition, mucoadhesive strength, and LID release kinetics. ODF-1 exhibited the lowest mucoadhesion, detaching rapidly yet still delivering 100% of its LID payload within 5 minutes. This behaviour aligns perfectly with its design as an immediate-release system, where prolonged mucosal residence is unnecessary and rapid onset of action is paramount. MAF-2, built on a PEO/HPMC

matrix, showed both enhanced mucoadhesive resistance to wash-off and a prolonged release profile, with complete drug release achieved within 10 minutes. The introduction of unmodified CS in MAF-3 further increased mucosal retention, extending full LID liberation to approximately 20 minutes. This improvement reflects CS's ionic and hydrogen-bonding interactions with mucin, which slow film erosion under continuous flow. Interestingly, MAF-4 and MAF-5, which incorporate CS–SH, and CS–MNA, respectively, showed progressively slower disintegration. These formulations resisted wash-off longest and delivered LID over 35 minutes (MAF-4) to 40 minutes (MAF-5). This trend highlights the pivotal role of the added network cohesion provided by thiol and disulfide cross-links, which strengthen the polymer matrix against salivary and mechanical stresses. Notably, the S-protected CS–MNA derivative not only preserves free thiols from premature oxidation but also engages in reversible disulfide exchange with mucin cysteines, further extending mucosal adhesion in situ [51].

These wash-off results are fully consistent with the dissolution profiles: films with greater matrix tenacity under external solvent and mechanical stress invariably showed slower, more sustained LID release [52]. By tuning from purely hydrophilic carriers to mucoadhesive and thiomer-enhanced matrices, we have thus demonstrated a versatile MAF platform capable of both immediate and prolonged buccal analgesia.

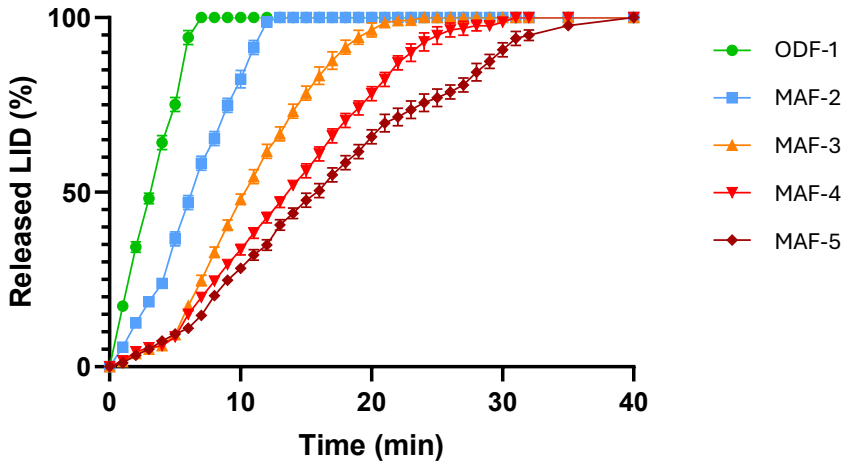

Fig. 8 - LID release profile from the formulations set on the animal mucosa.

3.6 *In vitro* permeation and retention studies

As a consequence of the short interaction period of ODF-1 with the oral mucosa given its low mucoadhesive power the permeation and retention test was performed only on MAF-2–5. As reported in Fig 9 and Table 6, LID penetrated significantly through the oesophageal mucosa. About 0.1-0.6 mg/cm^2 of LID permeated the oesophageal mucosa in about 8 hours, whereas about 0.3-0.8 mg/mg (corresponding to 0.4-1.0 mg/cm^2 of mucosa) was retained in it. Such findings were in line with published results by using different types of mucoadhesive films [52], [53]. However, it is noteworthy noting that, based on obtained results, the presence of CS-SH has a role in penetration of LID into the epithelium. MAF-4 and MAF-5 resulted in significantly lower permeation fluxes in comparison to both MAF-2 and MAF-3 ($p < 0.05$; Fig. 2; Table 3). This behaviour may be explained by specific interactions between LID and the thiol or disulfide groups present in CS–SH and CS–MNA. In fact, the formation of microdomains or dense crosslinked networks in the presence of thiolated chitosans could hinder drug mobility within the matrix, slowing release and permeation kinetics [54]. However, the protection of thiolate groups in MAF-5 seems to partially mitigate negative effects on LID penetration. Indeed, although the permeation flux of MAF-5 was comparable to that of MAF-4 (Table 6), the presence of CS-MNA in MAF-5 promoted a higher accumulation of LID within the epidermis. The reduced transdermal flux likely results in a lower risk of systemic absorption, thereby minimizing the potential for systemic toxicity. At the same time, the MNA moiety acts as a self-catalyst for the interaction with cysteine residues in mucin, leading to a mucopenetrating effect that facilitates the passage of LID through the mucosal layer covering the tissue [55]. This outcome is particularly relevant for enhancing the topical analgesic effect of the formulation while avoiding the risks associated with systemic drug exposure.

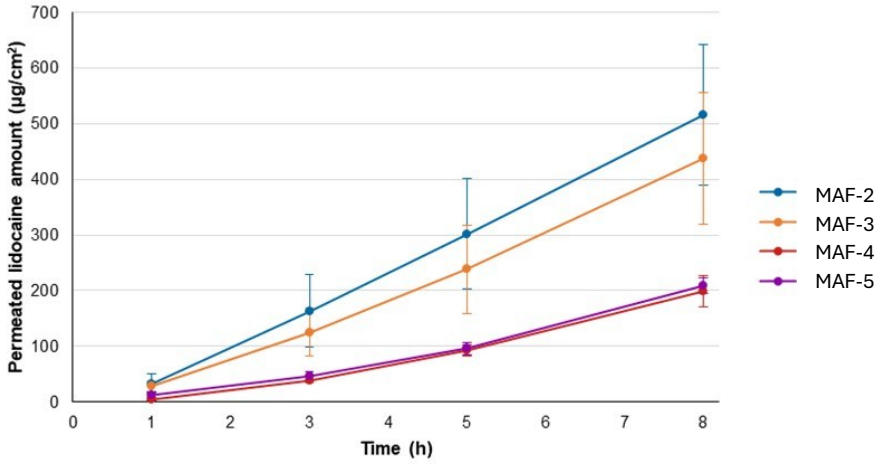

Fig. 9 - Results of permeation studies performed on mucoadhesive films through porcine oesophageal mucosa, expressed as mean ± S.E.M. (n=3).

Table 6 - Results of retention studies performed on mucoadhesive films through porcine oesophageal mucosa, expressed as mean ± St. Dev. (n=3).

Form. ID	J (µg/cm²h)	$Q_{8h,\ perm}$ (µg/cm²)	$Q_{8h,\ ret}$ (µg/g)	Q_{ret}/J
MAF-2	70.42 ± 22.84	515.44 ± 219.79	676 ± 241	9.60
MAF-3	62.71 ± 26.26	437.15 ± 205.50	745 ± 235	11.88
MAF-4	33.95 ± 10.51	198.79 ± 49.68	397 ± 101	11.69
MAF-5	32.70 ± 4.44	207.96 ± 24.34	788 ± 265	24.10

3.7 Stability studies

The printed formulations were stored in a Climacell 222 – ECO line climatic chamber (MMM Group, Germany) at 25 °C and 60 % relative humidity for 12 months and monitored by HPLC analysis. The results demonstrated that there was no drug loss over time, and HPLC analysis showed no evidence of the formation of degradants, demonstrating the stability of the drug in the printed formulations during storage (Table 7).

Tensile properties were also re-evaluated, and no changes were observed, indicating that the polymeric matrices used to produce the MAF remained mechanically stable after one year of storage.

Finally, an Ellman's assay was repeated on MAF-4 and MAF-5 to assess the status of thiol groups in the stored samples. The results shown in Table 7 indicate that the

total amount of thiol groups remained unchanged after one year; however, MAF-4 exhibited a markedly lower content of reduced –SH groups compared to freshly printed samples, suggesting oxidation occurred during storage. In contrast, MAF-5, in which thiol groups were protected by the MNA moiety, showed no significant variation from the freshly printed sample.

These findings demonstrate the superior stability of MAF-5, implying that its mucoadhesive and release properties are likely to remain unaltered even after 12 months of storage.

Table 7 - Amount of reduced thiols (–SH), oxidized thiols (–S–S–), and total thiols (Σ–SH), as well as the percentage of LID content in MAF-4 and MAF-5 after 12 months of storage (t_{12}), compared to the values obtained immediately after printing (t_0).

Form. ID	-SH t_{12} (-SH t_0)	-S-S- t_{12} (-S-S- t_0)	Σ-SH t_{12} (Σ-SH t_0)	Measured LID t_{12} (Measured LID t_0)
		mmol/g		% w/w
MAF-4	0.03 ± 0.01 (0.16 ± 0.03)	0.43 ± 0.05 (0.31 ± 0.03)	0.46 ± 0.09 (0.47 ± 0.05)	2.86 ± 0.09 (2.87 ± 0.11)
MAF-5	0.04 ± 0.01 (0.04 ± 0.01)	0.37 ± 0.05 (0.37 ± 0.04)	0.41 ± 0.07 (0.41 ± 0.05)	2.90 ± 0.07 (2.92 ± 0.12)

4. CONCLUSIONS

The present study established a versatile DPE 3D-printing platform for the production of LID-loaded MAF with tailored release kinetics. Extensive physicochemical characterization confirmed that extrusion at 170 °C amorphized LID into a stable glassy state, eliminating its crystalline melting peak, without API degradation or excipient compromise. Immediate-release formulations based on Kollidon VA 64 (ODF-1) disintegrated and released their full LID payload within minutes, delivering rapid onset of analgesia without requiring prolonged mucosal contact. By contrast, the strategic incorporation of hydrophilic carriers and mucoadhesive CS derivatives enabled sustained release profiles (10 to 40 minutes), supporting prolonged mucosal anesthesia. This effect may be therapeutically beneficial in scenarios where maintaining local analgesia over an extended period is

desired, such as in recurrent aphthous ulcers, mucositis, or paediatric dental interventions. CS–SH and its S-protected derivative (CS–MNA) endowed the matrix with reversible disulfide cross-links and covalent mucin interactions, achieving the greatest wash-off resistance and the most controlled release kinetics. Moreover, the use of protected thiolated CS also maximizes the extent of LID that is retained in the mucosa after the penetration. Indeed, despite a similar permeation flux, MAF-5 was better than MAF-4 in sustaining LID retention on the mucosal layer (Table 3). This evidence makes films containing protected thiolated chitosan (MAF-5) promising candidates for developing locally-applied formulations intended for use in local anaesthesia, as they are able to maximize the drug concentration at the therapeutic site, reducing the risk of systemic concentration and, therefore, potential side effects.

Taken together, these findings illustrate that by simply modulating powder blend composition—from purely hydrophilic carriers to thiolated and S-protected one, DPE 3DP allows the production of MAF ranging from immediate to sustained release in a single, reproducible manufacturing process. This versatility offers significant promise for personalized paediatric therapies, accommodating both acute pain relief and extended analgesia while leveraging the precision of 3D printing.

5. REFERENCES

[1] E. A. Hall, H. E. Sauer, M. S. Davis, and D. L. Anghelescu, "Lidocaine Infusions for Pain Management in Pediatrics," *Pediatric Drugs*, vol. 23, no. 4, pp. 349–359, Jul. 2021, doi: 10.1007/s40272-021-00454-2.

[2] J. B. Gunter, "Benefit and Risks of Local Anesthetics in Infants and Children," *Pediatric Drugs*, vol. 4, no. 10, pp. 649–672, 2002, doi: 10.2165/00128072-200204100-00003.

[3] J. M. Goddard and R. L. Reaney, "Lidocaine 5%–medicated plaster (Versatis) for localised neuropathic pain: results of a multicentre evaluation of use in children and adolescents," *Br J Pain*, vol. 12, no. 3, pp. 189–193, Aug. 2018, doi: 10.1177/2049463718756431.

[4] G. Bebawy, M. S. Sokar, and O. Y. Abdallah, "Buccal lidocaine mucoadhesive patches for pediatrics' teething pain: overcoming possible hazards of oral gels," *Pharm Dev Technol*, vol. 29, no. 8, pp. 805–813, Sep. 2024, doi: 10.1080/10837450.2024.2393729.

[5] M. Preis and J. Breitkreutz, "Pediatric Drug Development and Dosage Form Design," *AAPS PharmSciTech*, vol. 18, no. 2, pp. 239–240, Feb. 2017, doi: 10.1208/s12249-016-0705-x.

[6] W. Malkawi, E. AlRafayah, M. AlHazabreh, S. AbuLaila, and A. Al-Ghananeem, "Formulation Challenges and Strategies to Develop Pediatric Dosage Forms," *Children*, vol. 9, no. 4, p. 488, Apr. 2022, doi: 10.3390/children9040488.

[7] A. D. Galande, N. A. Khurana, and S. Mutalik, "Pediatric dosage forms—challenges and recent developments: A critical review," *J Appl Pharm Sci*, pp. 155–166, 2020, doi: 10.7324/JAPS.2020.10718.

[8] M. He, L. Zhu, N. Yang, H. Li, and Q. Yang, "Recent advances of oral film as platform for drug delivery," *Int J Pharm*, vol. 604, p. 120759, Jul. 2021, doi: 10.1016/j.ijpharm.2021.120759.

[9] M. Orlu, S. R. Ranmal, Y. Sheng, C. Tuleu, and P. Seddon, "Acceptability of orodispersible films for delivery of medicines to infants and preschool children," *Drug Deliv*, vol. 24, no. 1, pp. 1243–1248, Jan. 2017, doi: 10.1080/10717544.2017.1370512.

[10] M. Gupta, D. Gowda, T. Kumar, and J. Rosenholm, "A Comprehensive Review of Patented Technologies to Fabricate Orodispersible Films: Proof of Patent Analysis (2000–2020)," *Pharmaceutics*, vol. 14, no. 4, p. 820, Apr. 2022, doi: 10.3390/pharmaceutics14040820.

[11] H.-R. Park, S. H. Seok, K.-M. Hwang, J.-Y. Kim, C.-W. Park, and E.-S. Park, "Formulation of sustained-release orodispersible film containing drug–resin complexes of donepezil hydrochloride," *J Pharm Investig*, vol. 52, no. 2, pp. 259–272, Mar. 2022, doi: 10.1007/s40005-022-00560-4.

[12] T. Cerveto *et al.*, "The promising role of semi-solid extrusion technology in custom drug formulation for pediatric medicine," *Int J Bioprint*, vol. 0, no. 0, p. 4063, Aug. 2024, doi: 10.36922/ijb.4063.

[13] M. Fanous, S. Gold, S. Muller, S. Hirsch, J. Ogorka, and G. Imanidis, "Simplification of fused deposition modeling 3D-printing paradigm: Feasibility of 1-step direct powder printing for immediate release dosage form production," *Int J Pharm*, vol. 578, p. 119124, Mar. 2020, doi: 10.1016/j.ijpharm.2020.119124.

[14] A. Goyanes, N. Allahham, S. J. Trenfield, E. Stoyanov, S. Gaisford, and A. W. Basit, "Direct powder extrusion 3D printing: Fabrication of drug products using a novel single-step process," *Int J Pharm*, vol. 567, p. 118471, 2019, doi: https://doi.org/10.1016/j.ijpharm.2019.118471.

[15] M. Pistone *et al.*, "Direct cyclodextrin-based powder extrusion 3D printing for one-step production of the BCS class II model drug niclosamide," *Drug Deliv Transl Res*, vol. 12, no. 8, pp. 1895–1910, 2022, doi: 10.1007/s13346-022-01124-7.

[16] S. Maddineni, S. K. Battu, J. Morott, S. Majumdar, S. N. Murthy, and M. A. Repka, "Influence of Process and Formulation Parameters on Dissolution and Stability Characteristics of Kollidon® VA 64 Hot-Melt Extrudates," *AAPS PharmSciTech*, vol. 16, no. 2, pp. 444–454, Apr. 2015, doi: 10.1208/s12249-014-0226-4.

[17] G. F. Racaniello *et al.*, "3D printed mucoadhesive orodispersible films manufactured by direct powder extrusion for personalized clobetasol propionate based paediatric therapies," *Int J Pharm*, vol. 643, p. 123214, Aug. 2023, doi: 10.1016/j.ijpharm.2023.123214.

[18] A. Bernkop-Schnürch and S. Steininger, "Synthesis and characterisation of mucoadhesive thiolated polymers," *Int J Pharm*, vol. 194, no. 2, pp. 239–247, Jan. 2000, doi: 10.1016/S0378-5173(99)00387-7.

[19] G. Leonaviciute, S. Bonengel, A. Mahmood, M. Ahmad Idrees, and A. Bernkop-Schnürch, "S-protected thiolated hydroxyethyl cellulose (HEC): Novel mucoadhesive excipient with improved stability," *Carbohydr Polym*, vol. 144, pp. 514–521, Jun. 2016, doi: 10.1016/j.carbpol.2016.02.075.

[20] G. F. Racaniello *et al.*, "Spray-dried mucoadhesive microparticles based on S-protected thiolated hydroxypropyl-β-cyclodextrin for budesonide nasal delivery," *Int J Pharm*, vol. 603, p. 120728, 2021, doi: https://doi.org/10.1016/j.ijpharm.2021.120728.

[21] F. Ricci *et al.*, "Thermoresponsive mucoadhesive hydrogel based on Pluronic F127/thiolated glycol chitosan for intravesical administration of celecoxib/gemcitabine," *J Drug Deliv Sci Technol*, vol. 86, p. 104687, Sep. 2023, doi: 10.1016/j.jddst.2023.104687.

[22] G. Balenzano *et al.*, "S-protected thiolated surfactants enhancing surface properties of lipid-based nanocarriers," *J Drug Deliv Sci Technol*, vol. 95, p. 105540, May 2024, doi: 10.1016/j.jddst.2024.105540.

[23] M. Perrone *et al.*, "S-preactivated thiolated glycol chitosan useful to combine mucoadhesion and drug delivery," *European Journal of Pharmaceutics and Biopharmaceutics*, vol. 132, pp. 103–111, Nov. 2018, doi: 10.1016/j.ejpb.2018.09.015.

[24] P. Bhusal *et al.*, "Development, Validation and Application of a Stability Indicating HPLC Method to Quantify Lidocaine from Polyethylene-co-Vinyl Acetate (EVA) Matrices and Biological Fluids," *J Chromatogr Sci*, vol. 55, no. 8, pp. 832–838, Sep. 2017, doi: 10.1093/chromsci/bmx043.

[25] G. M. Khalid, F. Selmin, U. M. Musazzi, C. G. M. Gennari, P. Minghetti, and F. Cilurzo, "Trends in the Characterization Methods of Orodispersible Films," *Curr Drug Deliv*, vol. 18, no. 7, pp. 935–946, Aug. 2021, doi: 10.2174/1567201818999201210212557.

[26] A. Casiraghi, C. G. Gennari, U. M. Musazzi, M. A. Ortenzi, S. Bordignon, and P. Minghetti, "Mucoadhesive Budesonide Formulation for the Treatment of Eosinophilic Esophagitis.," *Pharmaceutics*, vol. 12, no. 3, Mar. 2020, doi: 10.3390/pharmaceutics12030211.

[27] U. M. Musazzi, C. G. M. Gennari, S. Franzè, P. Minghetti, and F. Cilurzo, "Printing of cutaneous patches loaded with propranolol for the treatment of infantile haemangiomas," *J Drug Deliv Sci Technol*, vol. 66, Dec. 2021, doi: 10.1016/j.jddst.2021.102767.

[28] Y. Takeuchi *et al.*, "Characterization of mannitol granules and powder: A comparative study using two flowability testers," *Int J Pharm*, vol. 547, no. 1–2, pp. 106–113, Aug. 2018, doi: 10.1016/j.ijpharm.2018.05.061.

[29] D. Tank, K. Karan, B. Y. Gajera, and R. H. Dave, "Investigate the effect of solvents on wet granulation of microcrystalline cellulose using hydroxypropyl methylcellulose as a binder and evaluation of rheological and thermal characteristics of granules," *Saudi Pharmaceutical Journal*, vol. 26, no. 4, pp. 593–602, May 2018, doi: 10.1016/j.jsps.2018.02.007.

[30] G. Mora-Castaño *et al.*, "Optimising 3D printed medications for rare diseases: In-line mass uniformity testing in direct powder extrusion 3D printing," *Int J Pharm*, vol. 668, p. 124964, Jan. 2025, doi: 10.1016/j.ijpharm.2024.124964.

[31] G. Mora-Castaño, M. Millán-Jiménez, V. Linares, and I. Caraballo, "Assessment of the Extrusion Process and Printability of Suspension-Type Drug-Loaded AffinisolTM Filaments for 3D Printing," *Pharmaceutics*, vol. 14, no. 4, p. 871, Apr. 2022, doi: 10.3390/pharmaceutics14040871.

[32] C. Bendicho-Lavilla *et al.*, "Ensuring the quality of 3D printed medicines: Integrating a balance into a pharmaceutical printer for in-line uniformity of mass testing," *J Drug Deliv Sci Technol*, vol. 92, p. 105337, Feb. 2024, doi: 10.1016/j.jddst.2024.105337.

[33] J. Fu and S. Q. Turn, "Oxidation mechanism of sulfur-containing compounds and antioxidant depletion dynamics: Insights into interactions," *Fuel*, vol. 381, p. 133341, Feb. 2025, doi: 10.1016/j.fuel.2024.133341.

[34] M. Kemp, Y.-M. Go, and D. P. Jones, "Nonequilibrium thermodynamics of thiol/disulfide redox systems: A perspective on redox systems biology," *Free Radic Biol Med*, vol. 44, no. 6, pp. 921–937, Mar. 2008, doi: 10.1016/j.freeradbiomed.2007.11.008.

[35] M. S. Gupta and T. P. Kumar, "Characterization of Orodispersible Films: An Overview of Methods and Introduction to a New Disintegration Test Apparatus Using LDR - LED Sensors," *J Pharm Sci*, vol. 109, no. 10, pp. 2925–2942, Oct. 2020, doi: 10.1016/j.xphs.2020.06.012.

[36] M. B. Pimparade *et al.*, "Development and evaluation of an oral fast disintegrating anti-allergic film using hot-melt extrusion technology," *European Journal of Pharmaceutics and Biopharmaceutics*, vol. 119, pp. 81–90, Oct. 2017, doi: 10.1016/j.ejpb.2017.06.004.

[37] R. Wibel *et al.*, "In Vitro Investigation of Thiolated Chitosan Derivatives as Mucoadhesive Coating Materials for Solid Lipid Nanoparticles," *Biomacromolecules*, vol. 22, no. 9, pp. 3980–3991, Sep. 2021, doi: 10.1021/acs.biomac.1c00776.

[38] J. Iqbal, G. Shahnaz, S. Dünnhaupt, C. Müller, F. Hintzen, and A. Bernkop-Schnürch, "Preactivated thiomers as mucoadhesive polymers for drug delivery," *Biomaterials*, vol. 33, no. 5, pp. 1528–1535, Feb. 2012, doi: 10.1016/j.biomaterials.2011.10.021.

[39] Y. Wei, M. P. Nedley, S. B. Bhaduri, X. Bredzinski, and S. H. S. Boddu, "Masking the Bitter Taste of Injectable Lidocaine HCl Formulation for Dental Procedures," *AAPS PharmSciTech*, vol. 16, no. 2, pp. 455–465, Apr. 2015, doi: 10.1208/s12249-014-0239-z.

[40] A. B. Anane-Adjei *et al.*, "Amorphous solid dispersions: Utilization and challenges in preclinical drug development within AstraZeneca," *Int J Pharm*, vol. 614, p. 121387, Feb. 2022, doi: 10.1016/j.ijpharm.2021.121387.

[41] J. A. Baird, B. Van Eerdenbrugh, and L. S. Taylor, "A Classification System to Assess the Crystallization Tendency of Organic Molecules from Undercooled Melts," *J Pharm Sci*, vol. 99, no. 9, pp. 3787–3806, Sep. 2010, doi: 10.1002/jps.22197.

[42] S. E. Bakhtiari, Z. Zhu, O. V. Magdysyuk, S. Brocchini, and G. R. Williams, "Amorphous solid dispersions of lidocaine and lidocaine HCl produced by ball milling with well-defined RAFT-synthesised methacrylic acid polymers," *Int J Pharm*, vol. 644, p. 123291, Sep. 2023, doi: 10.1016/j.ijpharm.2023.123291.

[43] A. Mathers, F. Hassouna, M. Klajmon, and M. Fulem, "Comparative Study of DSC-Based Protocols for API–Polymer Solubility Determination," *Mol Pharm*, vol. 18, no. 4, pp. 1742–1757, Apr. 2021, doi: 10.1021/acs.molpharmaceut.0c01232.

[44] D. Medarević, J. Djuriš, P. Barmpalexis, K. Kachrimanis, and S. Ibrić, "Analytical and Computational Methods for the Estimation of Drug-Polymer Solubility and Miscibility in Solid

Dispersions Development," *Pharmaceutics*, vol. 11, no. 8, p. 372, Aug. 2019, doi: 10.3390/pharmaceutics11080372.

[45] U. Gala, M. C. Chuong, R. Varanasi, and H. Chauhan, "Characterization and Comparison of Lidocaine-Tetracaine and Lidocaine-Camphor Eutectic Mixtures Based on Their Crystallization and Hydrogen-Bonding Abilities," *AAPS PharmSciTech*, vol. 16, no. 3, pp. 528–536, Jun. 2015, doi: 10.1208/s12249-014-0242-4.

[46] C. Peniche-Covas, W. Argüelles-Monal, and J. San Román, "A kinetic study of the thermal degradation of chitosan and a mercaptan derivative of chitosan," *Polym Degrad Stab*, vol. 39, no. 1, pp. 21–28, Jan. 1993, doi: 10.1016/0141-3910(93)90120-8.

[47] M. T. Soe, T. Pongjanyakul, E. Limpongsa, and N. Jaipakdee, "Modified glutinous rice starch-chitosan composite films for buccal delivery of hydrophilic drug," *Carbohydr Polym*, vol. 245, p. 116556, Oct. 2020, doi: 10.1016/J.CARBPOL.2020.116556.

[48] A. Hu *et al.*, "The Properties of HPMC:PEO Extended Release Hydrophilic Matrices and their Response to Ionic Environments," *Pharm Res*, vol. 34, no. 5, pp. 941–956, May 2017, doi: 10.1007/s11095-016-2031-0.

[49] M. Rinaudo, "Chitin and chitosan: Properties and applications," *Prog Polym Sci*, vol. 31, no. 7, pp. 603–632, Jul. 2006, doi: 10.1016/j.progpolymsci.2006.06.001.

[50] C. Federer, M. Kurpiers, and A. Bernkop-Schnürch, "Thiolated Chitosans: A Multi-talented Class of Polymers for Various Applications," *Biomacromolecules*, vol. 22, no. 1, pp. 24–56, Jan. 2021, doi: 10.1021/acs.biomac.0c00663.

[51] G. Balenzano *et al.*, "S-protected thiolated surfactants enhancing surface properties of lipid-based nanocarriers," *J Drug Deliv Sci Technol*, vol. 95, p. 105540, May 2024, doi: 10.1016/J.JDDST.2024.105540.

[52] C. Padula, L. Pozzetti, V. Traversone, S. Nicoli, and P. Santi, "In Vitro Evaluation of Mucoadhesive Films for Gingival Administration of Lidocaine," *AAPS PharmSciTech*, vol. 14, no. 4, pp. 1279–1283, Dec. 2013, doi: 10.1208/s12249-013-0020-8.

[53] R. O. do Couto *et al.*, "Combining amino amide salts in mucoadhesive films enhances needle-free buccal anesthesia in adults," *Journal of Controlled Release*, vol. 266, pp. 205–215, Nov. 2017, doi: 10.1016/J.JCONREL.2017.09.039.

[54] T. M. Ways, W. Lau, and V. Khutoryanskiy, "Chitosan and Its Derivatives for Application in Mucoadhesive Drug Delivery Systems," *Polymers (Basel)*, vol. 10, no. 3, p. 267, Mar. 2018, doi: 10.3390/polym10030267.

[55] S. Dünnhaupt *et al.*, "S-Protected Thiolated Chitosan for Oral Delivery of Hydrophilic Macromolecules: Evaluation of Permeation Enhancing and Efflux Pump Inhibitory Properties," *Mol Pharm*, vol. 9, no. 5, pp. 1331–1341, May 2012, doi: 10.1021/mp200598j.

CHAPTER 3: β-GALACTOSIDASE ORODISPERSIBLE DOSAGE FORMS FOR THE TREATMENT OF LACTOSE INTOLERANCE

1. INTRODUCTION

Lactose intolerance is associated with the manifestation of abdominal pain, bloating and diarrhoea after the ingestion of foods that contain lactose. It can be due to congenital lactase deficiency, which is a rare paediatric disease, or an abnormal reduction of the lactase activity, which peaks at the time of birth and progressively decreases till adulthood [1]. In the most serious cases, lactose malabsorption not only limits food consumption due to the manifestation of symptoms, but also affects the bioavailability of drugs administered by oral dosage forms containing lactose as an excipient. As an example, the presence of lactose in levothyroxine tablets requires a significant increase of the dose in patients affected by lactose intolerance [2]. Beside reducing or eliminating the consumption of dairy products, possible treatments also include the use of food supplements containing probiotic strains such as Lactobacilli spp., Bifidobacteria encoding the glycoside hydrolase β-galactosidase (β-gal), or, more frequently, β-gal itself [3], [4]. Exogenically supplemented β-gal formulations are usually available as capsules or tablets, which are not adequate for patients with dysphagia, travellers, and people with fear of choking. Orodispersible dosage forms (ODx) are among the first choices to solve these issues since they rapidly dissolve/disintegrate in saliva, producing a fine suspension or solution of the drug, without requiring fluid intake or chewing. The disintegration occurs within 3 min, depending on the excipients selected and adopted production strategy [5]. The first developed ODx were oral lyophilizates (OL) which disintegrate within a few seconds, thanks to the high solubility of excipients and the porosity of matrices [6]. Orodispersible films (ODF) are plasticized polymeric sheets [7] which combine the prompt release of the payload

(i.e. small molecules, nanocrystals or microparticles) with the elimination of the fear of choking [5].

Although they represent a valid alternative to OL, ODF have not yet been exploited to administer biomolecules because of the relatively high temperature required in the main production techniques (i.e., solvent casting, hot-melt extrusion and 3D printing). Moreover, the compatibility between proteins and film forming polymers and the limited formulation space are among the common challenges to address to avoid protein denaturation [8]. Among polysaccharides generally used to design ODF, maltodextrins (MDX) are an amorphous film-forming material obtained by the depolymerization of starch, which was demonstrated suitable to microencapsulate sensitive biomolecules, especially probiotics [9].

Based on these considerations, the main purpose of this study was to develop ODF based on MDX for the release of β-gal. The importance of this investigation lies in offering a novel formulation able to address current challenges associated with lactose intolerance. First, ODF meet patient's special needs, keeping in mind not only the paediatric, but also the increased age of population and the occurrence of psychiatric and neurodegenerative diseases. In addition, β-gal loaded ODF can be proposed to hydrolyse lactose released from immediate-release dosage forms before intake.

Preliminarily, to assess the feasibility of obtaining ODF loaded with β-gal, two different preparation methods were tested: the conventional solvent casting method and hot-melt ram-extrusion (HMRE) 3D printing [10] to allow the scale down of the production, adapting it to a pharmacy setting .

The enzymatic activity of different amounts of β-gal loaded into ODF was investigated after preparation and subsequent storage, and the best formulations were selected to hydrolyse lactose released from a placebo capsule in a glass of commercially available spring water, or contained in a complex matrix (i.e., milk). All results were compared to the performance of β-gal loaded in an OL formulated with a similar quali-quantitative composition to better evaluate the possible impact

of stirring and heating on the stability of the protein and more in general the ODF performance.

2. MATERIALS AND METHODS

2.1 Materials

β-galactosidase from Aspergillus oryzae (β-gal, ACEF, Italy); maltodextrin DE6 (MDX 6), DE12 (MDX 12), DE19 (MDX 19) and DE38 (MDX 38; Roquette, France); trehalose, (VWR International, Italy); glycerol and sorbitol (Farmalabor, Italy); propylene glycol monocaprylate type II (CAPRYOL®90, Gattefosse, France). All the solvents were of analytical grade, unless otherwise specified.

Table 1 - Composition of the mixtures used for the preparation of ODx (%, w/w).

Form.	β-gal	MDX		Gly	Capryol90	Trehalose	Sorbitol	TiO_2	Water
		IT6	IT19						
ODF-3DP	1.00	77.20	-	19.80	-	-	-	0.10	1.90
ODF-1	2.23	56.20	-	15.53	2.22	-	-	-	23.77
ODF-2	6.17	53.96	-	14.91	2.13	-	-	-	22.83
ODF-3	11.78	50.74	-	14.02	2.00	-	-	-	21.46
ODF-4	24.49	43.43	-	12.00	1.71	-	-	-	18.37
OL-1	1.20	-	40.00	-	-	-	-	-	58.80
OL-2	2.40	-	40.00	-	-	-	-	-	57.60
OL-3	3.60	-	40.00	-	-	-	-	-	56.40
OL-4	1.80	-	20.00	-	-	-	10.00	-	69.10
OL-5	1.80	-	20.00	-	-	10.00	-	-	68.20
OL-6	2.70	-	20.00	-	-	10.00	-	-	67.30
OL-7	4.00	-	20.00	-	-	10.00	-	-	66.00

2.2 Orodispersible films (ODF) preparation by solvent casting

ODF with a β-gal content ranging from 50 to 650 UI/cm^2 were prepared by the solvent-casting technique using a Mathis LTE apparatus [11]. The formula contained MDX 6 plasticized by glycerol; Capryol®90 was added to allow the wetting of a siliconized foil upon spreading of the slurry (ODF-1-4, Table 1). The impact of process parameters (e.g., drying temperature and time) on enzyme activity was also preliminarily evaluated and set to 70 °C, 20 min and 1500 rpm (Table 2).

2.3 Orodispersible films (ODF) preparation by hot-melt ram-extrusion 3D printing

ODF were also prepared by HMRE 3D printing, a technique in which the API and the excipients are mixed in a mortar to obtain a paste which is then transferred into an extrusion chamber, heated until it melts, and extruded through a nozzle onto a plate according to a pattern defined by the user. A custom-made printer was used. Again, maltodextrin DE 6 was used as film-forming polymer and plasticized with glycerol and water, and titanium dioxide (TiO_2) was added as an anti-adherent and opacifier. A mixture with 1% w/w β-gal (ODF-3DP, Table 1) and a placebo mixture with the same excipient composition were prepared. ODF 2x3 cm were printed as a single layer with an external perimeter and rectilinear infill, with a 45° fill angle. Extrusion temperature was set to 70 °C, and the distance between the nozzle and the plate was 500 μm.

The technological features of ODF were assessed by determining the loss on drying (LOD) (thermobalance, Gilbertini, Italy), film thickness (MI 1000 μm, ChemInstruments, USA), and stickiness following the same experimental protocols already described by Musazzi and coworkers [12]. In particular, ODF stickiness was measured by the thumb tack test and expressed by the following score system: A (not sticky), B (sticky), and C (very sticky).

2.4 Oral lyophilizate (OL) preparation

2.4.1 Thermal characterization of the MDX slurries

To tailor the process and formulation parameters, the glass transition temperature of a maximally cryo-concentrated solution (Tg′) of MDX 12, MDX 19, MDX 38, or MDX/cryoprotectant (i.e., trehalose and sorbitol) solutions with or without β-gal (Table 1) were investigated using a DSC Star System (Mettler Toledo, CH). Aliquots of each solution of about 20 mg were accurately weighed and transferred to an aluminium pan, then closed with crucible lid and sealed with a press. Samples were cooled from 25 °C to −40 °C at a rate of 1.5 °C min−1 and maintained for 10 min, then thawed from −40 °C to 20 °C at a rate of 5 °C/min under a nitrogen gas flow of 80 mL/min.

2.4.2 Freeze-drying process

For the preparation of OL, blisters composed of an aluminium sheet comprising 80 cavities with a maximum volume of 1.5 mL each were used. One sheet was cut into pieces with 10 cavities each to allow the placement procedure on the central plate of a Martin Christ freeze-dryer Epsilon 2–6 (Martin Christ, D). Slurries made of MDX 19, β-gal and with/without cryoprotectants (i.e., trehalose and sorbitol) were frozen at the rate of 1 K/min to −40 °C and held for 5 h.

Then, the chamber pressure was set to 0.180 mBar to initiate the main drying at −10 °C for 23 h. In the secondary drying, the shelf temperature was increased to 30 °C at the rate of 0.1 K/min and held for 5 h.

After freeze-drying, samples were removed from the blisters and transferred into vials. To protect them from the environmental moisture, the vials were stoppered under vacuum. OL were stored at 25 ± 1 °C until use and characterized in terms of visual appearance, uniformity of mass, enzymatic content, and residual activity.

2.5 Disintegration time

The disintegration test on OL and ODF-1-4 (6 cm^2) was carried out in purified water using the apparatus and specifications described in the Ph. Eur. monograph on "Disintegration of tablets and capsules" for orodispersible tablets.

2.6 β-gal content

The quantification of β-gal in the OL and ODF-1-4 was carried out by using a bicinchoninic acid protein assay (BCA) kit under manufacturer's instructions (Thermo Scientific, USA). Briefly, ODx were dissolved in citrate buffer at pH = 5 so that all samples had the same excipients concentration. Then, 25 µL of samples were mixed with 200 µL of working solution in 96-well polystyrene microtiter plates and incubated for 30 min at 37 ± 1 °C. Subsequently, the absorbance was measured at 562 nm using a Tecan Spark microplate reader (Tecan, CH) and values were correlated with protein concentration by referring to a calibration curve of unformulated β-gal solution (0.25–1.00 mg/mL).

2.7 Enzymatic activity assay

The β-gal activity was determined by a spectrophotometric assay as follows: 96-well microtiter plates were filled with a mixture of i) various concentrations of β-gal from ODF-1-4 and OL and ii) ortho-nitrophenyl β-d-galactopyranoside (ONP-G) substrate (1.5 mg/mL) in 50 mM citrate buffer at pH = 5 (total volume, 0.1 mL). The mixtures were subsequently incubated for 10 min at room temperature and, then, the reaction was stopped by adding 0.1 mL of 1 M Na_2CO_3 to reach pH = 9. The substrate cleavage was correlated with enzyme activity by measuring the absorbance of ortho-nitrophenol (ONP) at 410 nm after 0 and 10 min of incubation, as well as after Na_2CO_3 addition using Tecan Spark microplate reader (Tecan, CH). The enzyme units in each sample were calculated by referring to those of the unformulated β-gal used as standard (theoretical specific activity of β-gal: 100 UI/mg).

2.8 *In vitro* lactose hydrolysis

2.8.1 Hydrolysis of lactose contained in placebo capsules

To simulate the ability of β-gal released from ODF1-4 or OL-7 to hydrolyse lactose used as excipient in a medicinal product, a hard-capsule containing 500 mg lactose was compounded and put in a glass containing 50 mL of commercially available spring water (measured pH = 6.40; fixed residue = 14 mg/L) and mixed with a teaspoon until disintegration. After 10 min, an OL or an ODF with a surface area of 6 cm^2 was added. At predetermined times (i.e., 5 and 10 min), aliquots of 200 µL were withdrawn and mixed with 100 µL of 0.1 M NaOH to stop the hydrolysis. The experiment was performed in triplicate for each formulation.

2.8.2 Simulated digestion of lactose contained in milk

To simulate the performance of β-gal contained in ODx after the ingestion of 150 mL of UHT-milk, a set of experiments was carried out using simulated gastric fluid media (Table 3).

Table 2 - Composition and physicochemical properties of fed gastric medium simulating two phenotypes (Fe–V1 and Fe–V2) and fasted gastric medium Fa-V0 [13].

Component	**Composition**		
	Fe-V1	**Fe-V2**	**Fa-V0**
Acetic acid (mM)	-	17.12	-
Sodium acetate (mM)	-	29.75	-
Ortho-phosphoric acid (mM)	-	-	-
Sodium dihydrogen phosphate (mM)	-	-	-
Milk/buffer	1:0	1:1	-
Hydrochloric acid/sodium hydroxide	qs pH=6.4	qs pH=5	-
Sodium taurocholate (µM)	-	-	80
Lecithin (µM)	-	-	20
Pepsin (mg/mL)	-	-	0.1
Sodium chloride (mM)	148	237.02	34.2
Hydrochloric acid	-	-	qs pH=1.6
Deionized water	-	-	qs ad 1 L

pH	6.4	5.0	1.6
Osmolality (mOsm kg^{-1})	559	400	120.7
Buffer capacity (mmol L^{-1} ΔpH^{-1})	21.33	21.33	-

Briefly, about 6 cm^2 ODF-4 or OL-7 were dispersed in 180 mL (simulating the condition of patients with grade 1 antrum who took 150 mL of UHT-milk; Fe–V1) or 300 mL (simulating the condition of patients with grade 2 antrum who took 150 mL of UHT-milk, Fe–V2) of the digestion medium. Independently of the vessel volume, each vessel contained approximately 6.5 g of lactose. A series of experiments was performed dissolving 6.5 g of lactose in Fa-V0 to control for the effect of milk composition on β-gal hydrolysis activity. For both experimental series, the USP dissolution apparatus was set to 37 ± 1 °C with paddle stirring at 50 rpm. At predetermined times, an aliquot of 2 mL was withdrawn, and the enzymatic reaction was stopped by adding 0.1 M NaOH.

2.8.3 HPLC determination of undigested lactose

The remaining lactose was quantified using an isocratic HPLC (HP1100 series, Agilent, USA), equipped with a quaternary pump, an auto-sampler, a thermostated column compartment at 35.0 ± 0.1 °C, and a RI detector. An aliquot of 10 µL was eluted through a HILIC column (Luna® Omega SUGAR, 3 µm, 100 Å 150 × 4.6 mm, Phenomenex, Italy) using a mixture of Milli Q® water/acetonitrile (25:75, % v/v) at the flow rate of 1 mL/min. Calibration curve was in the 1–25 mg/mL range (R^2 > 0.99).

2.9 Stability assay

Both ODF-4 and OL-7 were stored for 3 months at 25 °C/60% RH to evaluate the enzyme stability. At the end of study, formulation specimens were tested in terms of disintegration time, β-gal content, and enzymatic activity. Experiments were performed in triplicate for each formulation.

3. RESULTS AND DISCUSSION

3.1 Orodispersible films (ODF) preparation

The films containing β-gal 1% (w/w) exhibited a light brown colour, which contrasted with the white colour of the placebo films and the starting materials, suggesting that degradation of the enzyme had occurred during the printing process. Consequently, this technique was excluded from further studies on heat-sensitive proteins.

In the case of solvent casting, the drying variables were preliminarily optimized to avoid stickiness of ODF (Table 2): air temperature and speed were the main parameters worthy of consideration as potentially affecting handling and the enzymatic activity.

Table 3 - Set up of process parameters to obtain homogeneous and non-sticky laminates for ODF. The experiments were carried out using the formulation ODF-2, containing 8% w/w of β-gal. ODF stickiness was expressed by the following score system: A (not sticky), B (sticky), and C (very sticky).

Run	Thickness (μm)	Air		Drying time (min)	Stickiness	LOD (%, w/w)	β-gal	
		Temperature (°C)	Speed (rpm)				mg/ODF	UI/ODF (%)
1	300	60	1200	30	C	n.d.(*)	n.d.(*)	n.d.(*)
2	300	70	1200	20	C	n.d.(*)	n.d.(*)	n.d.(*)
3	300	70	1200	25	B	7.8±2.3	8.09±0.85	743±73 (90.52)
4	300	70	1500	20	A	6.0±1.2	8.23±1.45	821±73 (99.71)
5	300	70	1500	45	A	5.2±0.8	8.14±2.57	623±42 (75.80)

* Not determined due to the stickiness of the ODF.

The solvent evaporation carried out at 70 °C for 20 min led to ODF that were homogeneously opaque in appearance, easy to handle and able to disintegrate within 30 s. Independently of the enzyme content (3%–30% w/w), the drying parameters did not significantly affect either the protein content, or the enzymatic activity (Table 4). ODF with enzymatic activity ranging between 300 and 4000 UI were easily obtained considering an ODF size not more than 6 cm^2. It is worth noting that a good recovery of β-gal activity was obtained despite the drying step, which is a possible cause of protein denaturation. Indeed, the possible loss of the protein's

hydration shells upon drying can lead to a change in the three-dimensional structures. In ODF, 7% moisture content, generally present after drying to allow the proper handling of films, and glycerol may be responsible of the hydrogen bonds between the protein and hydroxyl groups of water and/or plasticizer, conserving the protein's three-dimensional structure. Moreover, it can be assumed that, in agreement with the vitrification theory, the molecular mobility of a protein is strongly reduced when incorporated in the amorphous matrix made of MDX.

Table 4 - β-gal content and enzymatic activity in the ODx formulations at preparation and after 3 months at 25 °C/60% RH.

Form. ID	At preparation			After 3 months		
	β-GAL content, mg/ODx[(A)]	β-GAL activity		β-GAL content, mg/ODx[(A)]	β-GAL activity	
		UI/ODx	%[(B)]		UI/ODx	%[(B)]
ODF-1	5.16±0.14	303±29	86.35	5.22±0.21	298±30	83.95
ODF-2	12.34±1.45	821±73	97.80	11.8±0.16	830±50	103.44
ODF-3	35.43±1.91	2364±545	98.12	34.8±0.60	2360±157	99.73
ODF-4	57.72±3.02	3910±75	99.62	56.82±0.93	4025±108	104.17
OL-7	56.94±2.04	3890±29	100.79	57.03±1.34	3922±62	101.28

[(A)] ODF having area equal to 6 cm^2.

[(B)] Compared to a theoretical β-GAL activity estimated by considering the specific activity equal to 67.9 ± 1.2 UI/mg.

Furthermore, no significant deviations from expected values of β-gal content and activity were observed either at preparation or after 3 months of storage at room temperature (Table 4).

3.3 Oral lyophilizates (OL) preparation

A preliminary study was carried out to tune up the composition of slurries to be freeze-dried. Since T_g' of MDX was strongly dependent on the molecular weight, MDX 38 presenting a T_g' value of −23 °C was discarded. Despite the similar values of T_g' between MDX 12 and MDX 19 (T_g' MDX 12 = −10.7 °C and T_g' MDX 19 = −13.3 °C), MDX 19 was preferred due to the faster disintegration time.

At the highest amount of β-gal loaded, lyophilized cakes presented bubbles and an inhomogeneous structure (formulations OL-1-3, Table 1). This result may be due to the significant decrease of T_g' values in presence of increasing amount of β-gal (Fig. 1). Hence, the concentration of MDX 19 was decreased from 40% to 20% and sugar, i.e. trehalose or sorbitol, was added (formulations OL-4-6, Table 1). In all cases, the visual appearance improved without compromising the enzymatic activity. However, only the composition MDX 19/trehalose in the ratio 2:1 w/w allowed to preserve about 97% of β-gal activity after 3 months of storage at 25 °C; while in presence of MDX or MDX 19/sorbitol, a 50% reduction of activity was measured. The combination of MDX 19/trehalose was loaded with up to 12% β-gal and the final OL, weighing about 340 mg, presented a final enzyme content of about 4000 UI/OL (formulation OL-7, Table 1).

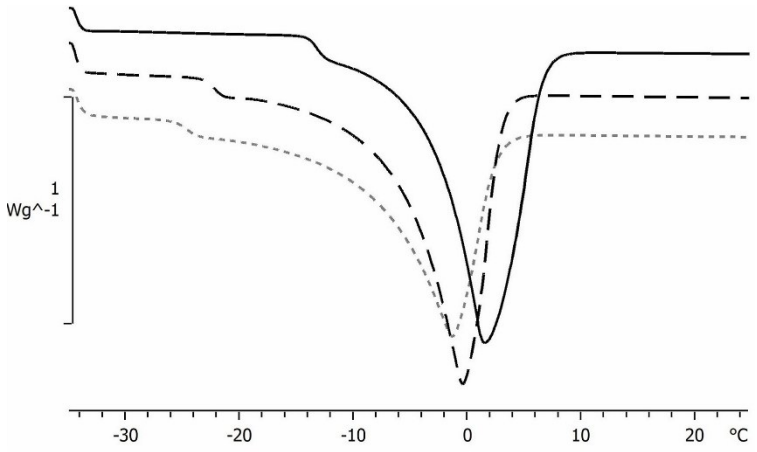

Fig. 1 - Thermograms of 20% MDX 19 solution (solid line) containing 1.5 % (dashed line) and 9% (dotted line) β-gal.

3.4 Hydrolysis of lactose contained in a medicinal product in water

The experiment was conducted to evaluate the performances of ODF and OL-7 when used to hydrolyse lactose contained in an oral immediate release dosage form. The idea is that a capsule or tablet would disintegrate in a glass of water. Subsequently, an ODx would be added, allowing the patient to consume a dispersion or solution in which the lactose has already been hydrolysed.

Fig. 2 evidenced that lactose hydrolysis occurred very fast for almost all tested formulations. As expected, the efficiency in lactose hydrolysis is concentration and time dependent. In the case of ODF-1, the amount of loaded β-gal was too low for the intended use. ODx at higher content of β-gal hydrolysed more 40% of lactose in the first 5 min, and more than 55% within 10 min. Only in the case of ODF-4, the concentration of non-hydrolysed lactose after 15 min was lower than the LOQ (data not shown). Similarly to ODF-4, OL-7 containing 3900 UI of β-gal completely degraded the lactose after 15 min. Thus, based on the performance in water, ODF-4 and OL-7 can be proposed to eliminate lactose contained in a tablet or capsule before intake. Indeed, considering the lactose amount generally present in a single tablet or capsule, it is reasonable to suppose that a polytherapy subject would intake maximum 500 mg of this excipient per oral administration. Hence, this approach can be a valuable alternative if lactose-free oral dosage forms are not available on the market or cannot be compounded in a pharmacy setting.

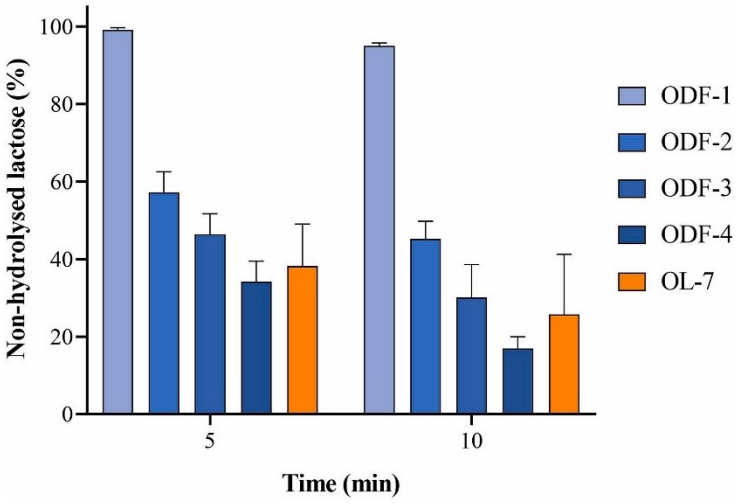

Fig. 2 - Remaining percentage of non-hydrolysed lactose 5 and 10 min after ODx disintegration. A capsule containing 500 mg lactose was previously disintegrated in the same glass of water.

3.5 *In vitro* lactose hydrolysis to simulate the digestion of milk

The *in vitro* lactose hydrolysis in presence of β-gal released from ODF-4 and OL-7 was evaluated in simulated fed gastric medium, simulating the condition in which 150 mL of UHT-milk was taken by a subject. Considering that it is well-known that

volume of pre-existing gastric fluids may vary based on the physiological and anatomical features of patients, two digestion media were prepared: fed state simulated gastric fluids, namely Fe–V1 and Fe–V2. Fe–V1 is referred to a subject with a pre-existing gastric volume of 20 mL (grade 1 antrum) who drinks a glass of milk; Fe–V2 simulates the milk intake in patients with larger gastric volumes (≈150 mL; grade 2 antrum). Experiments using fasted gastric medium (Fa-V0) as control condition were also performed to determine the impact of fed medium on the enzyme performance [13].

The hydrolysis rate constants (K) in the three conditions are summarized in Fig. 3. When ODx were added to Fa-V0, all the K values are maximal (Fig. 3); 3900 UI loaded in ODx seem sufficient to hydrolyse lactose in less than 15 min.

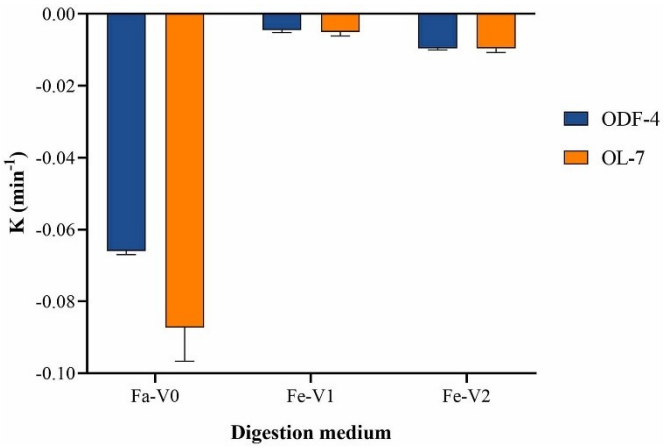

Fig. 3 - Hydrolysis rate constants (K) of lactose in presence of ODF-4 and OL-7 in Fa-V0 at pH = 1.2, Fe–V1 at pH = 5.4 and Fe–V2 at pH = 6.8.

A slightly better performance was observed for OL-7 ($p = 0.017$, Student's T-Test), but this difference is not relevant. When dissolved in biorelevant media simulating the food intake (i.e., Fe–V1 at pH = 6.4 and Fe–V2 at pH = 5.0), the hydrolysis kinetics slowed down, minimizing the differences between ODF-4 and OL-7 in terms of enzyme performances ($p > 0.05$, Student's T-Test). A marked dependence of hydrolysis rate on digestion medium was also observed. After 30 min the amount of hydrolysed lactose was 15% and 22% in the case of Fe–V1 and Fe–V2, respectively. This trend was confirmed over time: at 90 min, almost the whole quantity of lactose present in Fe–V2 was hydrolysed, whereas about half the initial amount of lactose was still present in Fe–V1. These results suggest that both pH and concentration of

milk components (e.g., micronutrients) can impact on the enzyme's performance (Fig. 3). These findings were in line with literature data [14], above all the effect related to the pH value. Indeed, it is reported that the optimal pH for β-gal from A. oryzae ranges between 5.0 and 6.2 without requiring ionic activators or inhibitors [15]. This range includes the pH values of both media (Fe–V1, pH = 6.4; Fe–V2, pH = 5.0).

Considering that Fe–V1 and Fe–V2 mainly differ in nutrients' composition, a strong dependence of the β-gal activity on concentration of milk components can be foreseen; this confirms the importance of testing ODx performance in media simulating the physiological microenvironment of biomolecules. Although an *in vitro/in vivo* correlation is desirable, these results could be exploited also for a clinical point of view since they provide the evidence that the physiology of the stomach may strongly impact on the β-gal efficiency even if in a fasted state. In general, patients are advised to take β-gal used as dietary supplements between 0 and 30 min before the food consumption [15]. However, these indications do not consider the disintegration time of a dosage form containing β-gal and the physiologic volume of gastric fluids in fasted state. Such parameters are not critical for immediate-release dosage forms (e.g., tablets and capsules), that generally disintegrate between 15 and 30 min, but they can affect the performance of β-gal released from ODx in few minutes. In this context, for light meals (e.g., 150 mL of milk), a different fluid volume in the gastric antrum (patient at grade 0 = 0 ± 2 mL; patients at grade 1 = 16 ± 36 mL; patients at grade 2 = 180 ± 83 mL [16]) may result in a different dilution of bolus after food intake. Based on obtained results on ODx, the lactose hydrolysis rate seemed faster when the buffering effect of bolus was less significant, namely in patients having physiologically appreciable gastric fluid in fasted conditions (corresponding to grade 1 and 2 antrum [16]). On the contrary, the buffer capacity and the fat content of bolus (i.e., milk) have a strong impact in patients with very limited volume of gastric fluid, resulting in a slow degradation of lactose. This implies that patients at grade 0 and 1 would be exposed to a higher risk of side effects due to the remaining amount of not-degraded lactose with respect to patients at grade 2, after administration of the same dose of β-gal. To have similar

efficiency of the enzyme in Fe–V1 and Fe–V2 in 30 min, two dosage forms should be taken.

4. CONCLUSIONS

This proof-of-concept confirms the suitability of ODF to load active substances with different characteristics, including enzymes, which can pose some issues in the definition of the production process due to their sensitivity to various stresses (i.e., thermal and shear stress). Based on the preliminary studies, it was possible to design ODF enabling to extend the patient's choice of dosage forms and their applications in the treatment of lactose intolerance. In another words, these dosage forms allow the tune-up of the amount of β-gal as a function of the lactose content in oral dosage forms or foods, and the physiological features of the patient. The first feature is relevant to fulfil the special needs of patients, when alternatives are not commercially available. Hence, ODF can be proposed to hydrolyse lactose released from an immediate-release dosage form directly in a glass of water, which can help to improve the patient's adherence to treatment, above all in case of chronic diseases or polytherapy. Finally, this study on the ability of β-gal to hydrolyse lactose in different biorelevant conditions reveals the dependence of the degradation kinetic not only on the fed or fasted conditions, but also on phenotype of the subject affected by lactose intolerance. This aspect is important in terms of patient-centric formulations because the proposed ODF can satisfy different phenotypes of subjects.

5. REFERENCES

[1] B. Misselwitz, M. Butter, K. Verbeke, and M. R. Fox, "Update on lactose malabsorption and intolerance: pathogenesis, diagnosis and clinical management," *Gut*, vol. 68, no. 11, pp. 2080–2091, Nov. 2019, doi: 10.1136/gutjnl-2019-318404.

[2] M. Cellini *et al.*, "Systematic Appraisal of Lactose Intolerance as Cause of Increased Need for Oral Thyroxine," *The Journal of Clinical Endocrinology & Metabolism*, vol. 99, no. 8, pp. E1454–E1458, Aug. 2014, doi: 10.1210/jc.2014-1217.

[3] R. Baijal and R. K. Tandon, "Effect of lactase on symptoms and hydrogen breath levels in lactose intolerance: A crossover placebo-controlled study," *JGH Open*, vol. 5, no. 1, pp. 143–148, Jan. 2021, doi: 10.1002/jgh3.12463.

[4] R. Gingold-Belfer *et al.*, "Use of a Novel Probiotic Formulation to Alleviate Lactose Intolerance Symptoms—a Pilot Study," *Probiotics & Antimicro. Prot.*, vol. 12, no. 1, pp. 112–118, Mar. 2020, doi: 10.1007/s12602-018-9507-7.

[5] F. Cilurzo, U. M. Musazzi, S. Franzé, F. Selmin, and P. Minghetti, "Orodispersible dosage forms: biopharmaceutical improvements and regulatory requirements," *Drug Discovery Today*, vol. 23, no. 2, pp. 251–259, Feb. 2018, doi: 10.1016/J.DRUDIS.2017.10.003.

[6] C. R. S. Siow, P. Wan Sia Heng, and L. W. Chan, "Application of freeze-drying in the development of oral drug delivery systems," *Expert Opinion on Drug Delivery*, vol. 13, no. 11, pp. 1595–1608, Nov. 2016, doi: 10.1080/17425247.2016.1198767.

[7] V. Garsuch and J. Breitkreutz, "Comparative investigations on different polymers for the preparation of fast-dissolving oral films," *Journal of Pharmacy and Pharmacology*, vol. 62, no. 4, pp. 539–545, Apr. 2010, doi: 10.1211/jpp.62.04.0018.

[8] S. Bashir, R. Fitaihi, and H. E. Abdelhakim, "Advances in formulation and manufacturing strategies for the delivery of therapeutic proteins and peptides in orally disintegrating dosage forms," *European Journal of Pharmaceutical Sciences*, vol. 182, p. 106374, Mar. 2023, doi: 10.1016/j.ejps.2023.106374.

[9] P. Jayaprakash, C. Gaiani, J.-M. Edorh, E. Beaupeux, A. Maudhuit, and S. Desobry, "Impact of matrices composition and processes on β-galactosidase encapsulation," *Journal of Food Engineering*, vol. 353, p. 111547, Sept. 2023, doi: 10.1016/j.jfoodeng.2023.111547.

[10] U. M. Musazzi *et al.*, "Personalized orodispersible films by hot melt ram extrusion 3D printing," *International Journal of Pharmaceutics*, vol. 551, no. 1–2, pp. 52–59, Nov. 2018, doi: 10.1016/J.IJPHARM.2018.09.013.

[11] G. M. Khalid, F. Selmin, U. M. Musazzi, C. G. M. Gennari, P. Minghetti, and F. Cilurzo, "Trends in the Characterization Methods of Orodispersible Films," *CDD*, vol. 18, no. 7, pp. 935–946, Aug. 2021, doi: 10.2174/1567201818999201210212557.

[12] U. M. Musazzi *et al.*, "Poly(methyl methacrylate) salt as film forming material to design orodispersible films," *European Journal of Pharmaceutical Sciences*, vol. 115, pp. 37–42, Mar. 2018, doi: 10.1016/J.EJPS.2018.01.019.

[13] E. Jantratid, N. Janssen, C. Reppas, and J. B. Dressman, "Dissolution Media Simulating Conditions in the Proximal Human Gastrointestinal Tract: An Update," *Pharm Res*, vol. 25, no. 7, pp. 1663–1676, July 2008, doi: 10.1007/s11095-008-9569-4.

[14] S. Gargova, I. Pishtijski, and I. Stoilova, "Purification and Properties of β-Galactosidase from Aspergillus Oryzae," *Biotechnology & Biotechnological Equipment*, vol. 9, no. 4, pp. 47–51, Jan. 1995, doi: 10.1080/13102818.1995.10818861.

[15] M. Corgneau *et al.*, "Recent advances on lactose intolerance: Tolerance thresholds and currently available answers," *Critical Reviews in Food Science and Nutrition*, vol. 57, no. 15, pp. 3344–3356, Oct. 2017, doi: 10.1080/10408398.2015.1123671.

[16] A. Perlas, L. Davis, M. Khan, N. Mitsakakis, and V. W. S. Chan, "Gastric Sonography in the Fasted Surgical Patient: A Prospective Descriptive Study," *Anesthesia & Analgesia*, vol. 113, no. 1, pp. 93–97, July 2011, doi: 10.1213/ANE.0b013e31821b98c0.

CHAPTER 4: DESIGN AND CONSTRUCTION OF A SEMI-SOLID EXTRUSION 3D PRINTER FOR THE EXTEMPORANEOUS PREPARATION OF HIGHLY CUSTOMIZABLE ORODISPERSIBLE FILMS

1. INTRODUCTION

Orodispersible films (ODF) are defined as single- or multilayer sheets designed for administration to the buccal cavity, upon which they disperse rapidly releasing the loaded drug in the saliva [1]. Since they don't have to be swallowed as solid objects, they are suitable for dysphagic patients, children, and the elderly, and even among the general population they are associated with high patient acceptability [2]. From a manufacturing perspective, ODF are easy to dose, since different drug strengths can easily be produced from the same starting material simply by changing the size of the film. All these characteristics combined make ODF a potentially ideal dosage form in the field of personalized therapy. However, this potential depends on the availability of manufacturing techniques suitable for the production of small, personalized batches in the compounding laboratories of community or hospital pharmacies in terms of the size, cost, and complexity of the equipment required.

One such technique is 3D printing, which consists in the fabrication of solid objects from a 3D digital model in a layer-by-layer fashion, usually by means of a printer that can fit on a desk. Among the many known 3D printing technologies, extrusion-based techniques, namely fused deposition modeling (FDM), direct powder extrusion (DPE), and semi-solid extrusion (SSE), are currently the most studied in the pharmaceutical field due to their flexibility, versatility, and compatibility with a wide range of polymers [3]. The common working principle of these techniques is that the starting material is extruded through a nozzle and deposited onto a print bed to form the printed object. The starting material is either a filament (FDM), a powder blend (DPE), or a gel or viscous liquid (SSE). The main difference between the three is that,

while in the case of FDM and DPE heating is required to fuse the filament or powder blend before it can be extruded, SSE can normally be conducted at room temperature, which makes it compatible with API and excipients that are vulnerable to thermal stress. SSE does however require a drying step to promote the evaporation of the solvent from the semisolid material before the finished solid object is obtained, but the temperatures that are used in this stage are significantly lower than those required to fuse the polymers used in FDM and DPE. Another advantage of SSE is that the relatively low pressure required for the extrusion of semisolids allows for the use of disposable syringes, which makes it so that none of the mechanical parts of the printer come into contact with the medicated material under normal operating conditions, almost eliminating the risk of cross-contamination. For these reasons, SSE may be regarded as the most suitable method for the compounding of medicines.

Data that demonstrates the feasibility of producing tailored dosage forms carrying precise doses of API using this technique already exist [4], confirming its potential as a tool for point-of-care manufacturing of personalized therapies. However, the exploitation of this potential is hindered by the scarcity or inadequacy of commercially available printers. Indeed, benchtop printers specifically designed for the extemporaneous production of pharmaceutical dosage forms do exist on the market [5], [6], [7], [8], but the cost of these machines makes them incompatible with most community and hospital pharmacies. The use of bioprinters has also been reported [9], [10] but, in this case, too, cost is an issue. In response to this, general-purpose low-cost printers are constantly being developed to expand the accessibility of this technology [11]. However, like bioprinters, these are not specifically designed for pharmaceutical manufacturing and would therefore have to be adapted.

In this chapter, the design, construction, and testing of a new SSE 3D printer prototype for the one-step extemporaneous preparation of tailored ODF is described. Both commercially available components and 3D-printed parts were used, and the result was a printer that can easily fit on a laboratory benchtop. A built-in oven was included to automate the final drying stage, limiting the necessity for user intervention.

To test the versatility of the prototype and its suitability for the production of tailored ODF, three case studies are presented: the preparation of ODF loaded with the enzyme β-galactosidase, the preparation of ODF loaded with CBD oil, and the preparation of ODF loaded with lipid microparticles for the taste masking of diclofenac.

2. MATERIALS

All the structural and electronic components used were either purchased from local shops or from the internet. The parts that had to be custom-built were designed in Fusion (Autodesk) and 3D-printed in-house with a Form 3B+ stereolithography printer (FormLabs) using a general-purpose resin.

3. DESIGN AND CONSTRUCTION

3.1 Outer structure

2040 and 2020 aluminum profiles were used to build the frame of the printer (Fig. 1) due to their robustness, relatively low weight, and ease of cutting. Adjustable rubber feet were added for leveling. The final size was 40x40x30 cm.

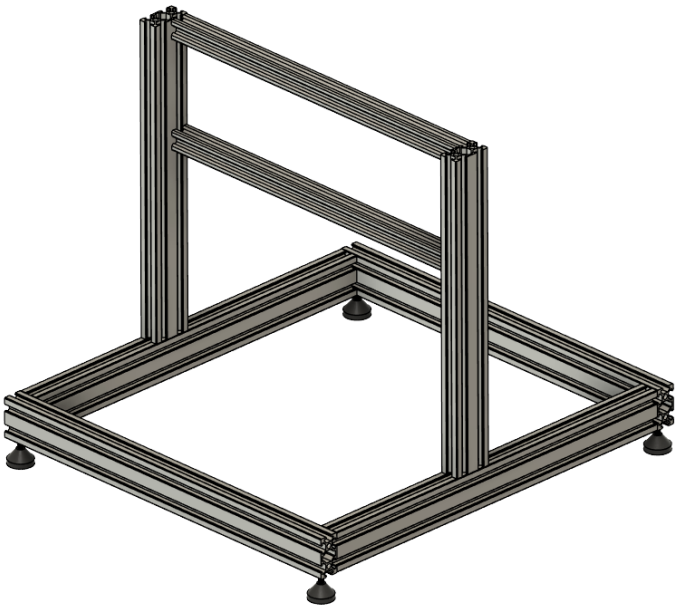

Fig. 1 - Frame of the printer.

3.2 XY axes

For the X and Y axes, GT2 timing belts were used with 10 mm guide rods to allow for high print speeds. The X axis consists of a carriage that moves the extruder from left to right along a 230 mm path, while the Y axis is responsible for the front-to-back movements of a 230x110 mm print bed along a 330 mm path. Both axes are driven by NEMA17 stepper motors and equipped with mechanical endstops.

3.3 Z axis

The Z axis sets the vertical distance between the extruder and the print bed. Since this is one of the critical parameters affecting the integrity and surface uniformity of the printed films, a NEMA17-driven lead screw system was used for high accuracy movements, and a Hall effect proximity sensor (3DTouch, Geeetech) was mounted instead of mechanical endstops. This sensor (Fig. 2) was chosen due to its suitability for achieving accurate bilinear bed leveling, an operation in which a set number of points are sampled on the print bed in a grid by lowering the Z axis until the sensor's extended tip touches the bed surface, at which point it retracts, triggering the Hall effect. The position of the Z axis relative to its zero in each sampled point is used to

create a 3D model of the bed, which makes it possible to compensate for bed curvature and tilt during a print run by automatically adjusting Z height, allowing for the production of films with uniform thickness. The design of the Z carriage allows the height of the probe to be adjusted when switching between different syringe types so that the vertical distance between the tip of the syringe and the tip of the probe is kept between 2.3 and 4.3 mm, a necessary condition according to the probe's specifications. The maximum height of the Z axis is 20 mm.

3.4 Syringe pump extruder (E0 axis)

The extruder (Fig. 2) was adapted from a DIY open-source syringe pump [12]: a NEMA17 stepper motor was coupled with a T8 lead screw to move a carriage up and down, pushing the plunger of a syringe and resulting in the extrusion of its content. Again, a lead screw was selected over timing belts because of the low operating speed of the axis as well as the high accuracy required, as extrusion accuracy translates to weight uniformity of the printed films, which, in turn, translates to accurate dosing of the API. The carriage can move along a 15 cm path and is stabilized by two 8 mm lateral guide rods with LM8UU linear bearings. The extruder is compatible with syringes up to 20 mL.

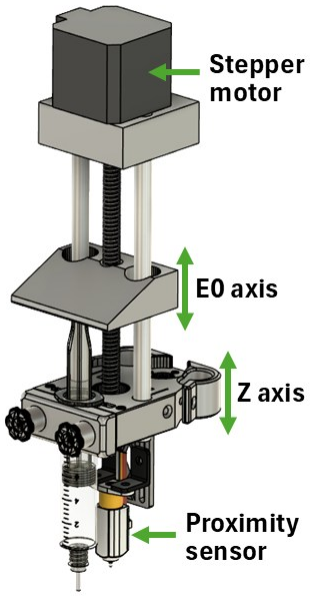

Fig. 2 - Extruder with 3DTouch proximity sensor.

3.5 Drying oven (E1 axis)

When a print run is done, the print bed enters the in-built oven, where the films undergo the final stage in the process: solvent evaporation. The oven consists of five insulated walls and a door, which can be raised and lowered by a pinion and rack system with lateral guide rods operated through a NEMA17 stepper motor. A 150W electric heater with a fan on top was positioned on the roof of the oven to blow hot air over the films, and an NTC100K thermistor was placed on the inside of the chamber. Once the drying stage begins, the target temperature set by the user in the gcode file is reached and maintained thanks to a PID control loop that uses the thermistor's readings as feedback. Because the high current requirements of the heater made it so that it could not be driven directly by the controller board, an external high-current MOSFET module was added.

3.6 Control system

The printer's controller board is a BTT SKR2 (BIGTREETECH), with an ARM Cortex-M4 MCU running at 168MHz. It was equipped with TMC2209 drivers to control each stepper motor and a fan to cool the board when powered up. To facilitate communication with the printer, a touchscreen (BTT TFT35 E3 V3.0.1, BIGTREETECH) was added and a case was 3D printed. The whole system is powered by a 12V / 30A switching power supply. The board and its connections to the components of the printer are shown in Fig. 3.

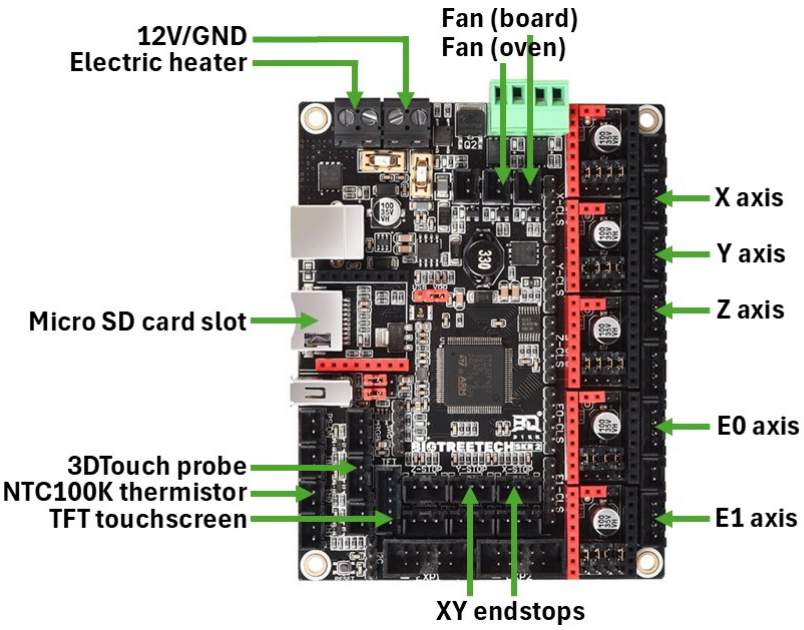

Fig. 3 - Controller board and its connections.

The open-source firmware Marlin 2.0.9 was edited and compiled in Visual Studio Code (Microsoft) and loaded onto the board via a micro SD card.

A picture of the finished printer is shown in Fig. 4.

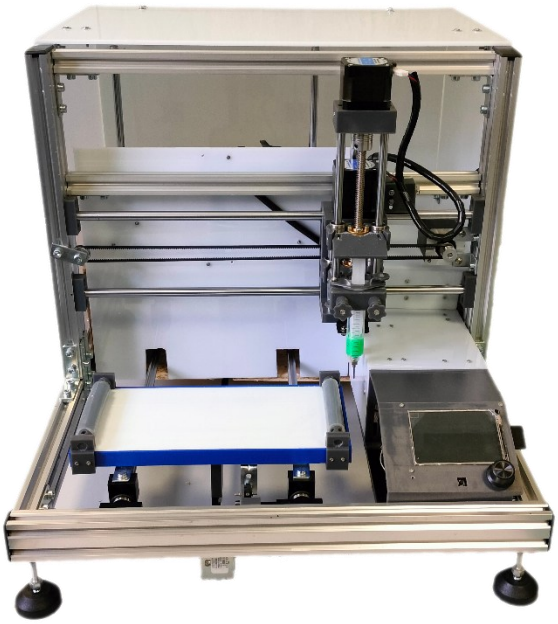

Fig. 4 - The finished SSE 3D printer

4. DESCRIPTION OF A TYPICAL PRINT RUN AND PRELIMINARY STEPS

4.1 Generating a 3D model

First, a 3D model of an ODF with the desired shape and size is designed using CAD software, such as Fusion (Autodesk). This model can be multiplied by the number of ODF that the user wishes to print on a single run, which can fill a space up to 230x110 mm, i.e. the size of the print bed. The model is then exported as an STL file.

4.2 Generating the gcode file

A gcode file that the printer can then convert into machine instructions is obtained by uploading the 3D model to a slicing software, such as Slic3r. The gcode is generated according to the slicing parameters set by the user, e.g. layer height, infill pattern, and infill density. To complete the process, the file is then modified manually using a text editor to add printer-specific functions and finally transferred to an SD card, which can be inserted into a slot in the touchscreen module. A screenshot of a typical gcode is reported in Fig. 5 as an example.

```
G28 ; home all axes
G29 ; perform auto bed leveling 3x2

; Filament gcode

M221 S35        ; set extrusion rate to 35% of default value (defined in firmware)
G21             ; set units to millimeters
G90             ; use absolute coordinates for XYZ
M82             ; use absolute distances for E0 and E1
G92 E0          ; set current E0 position as 0

; Syringe primning

G1 Z20 F500     ; lift nozzle to avoid bumping into obstacles
G28 X0          ; home X --> position extruder above Eppendorf tube (waste)
G1 E3 F500      ; push plunger 3 mm at 500 mm/min
G4 S10          ; wait 10s

; Print instructions

G92 E0                          ; set current E0 position as 0
G1 X98.220 Y60.625 F4998.000    ; move X to begin print
G1 Z0.400 F800                  ; lower syringe to 0.4 mm from print bed
G1 E0.00000 F2400.00000
G1 F690                         ; set speed for XY movements (mm/min)
G1 X98.220 Y79.745 E0.06518     ; start printing external perimeter of object
G1 X69.100 Y79.745 E0.14922
G1 X69.100 Y60.625 E0.20440
G1 X98.100 Y60.625 E0.28809
G1 X97.802 Y62.133 F4998.000
G1 F690
G1 X96.712 Y61.043 E0.29229     ; start filling in object
G1 X95.662 Y61.043 E0.29515
G1 X97.802 Y63.183 E0.30339
```

```
G1 X193.059 Y31.370 E2.29681
G1 X194.609 Y32.921 E2.30258

; Drying instructions

G92 E0          ; set current E0 position as 0
G1 E-1 F1000    ; retract E0 axis by 1 mm to relieve pressure from plunger
G1 Z20 F1000    ; raise Z to move extruder out of the way before moving print bed into oven
G28 X0          ; home X to move extruder out of the way before moving print bed into oven
T1              ; switch from E0 to E1
G92 E0          ; set current E1 position as 0
G1 E-21         ; raise E1 by 21 mm to open oven door
G1 Y300 F4000   ; move print bed into oven
G1 E0           ; lower E1 to close oven door
M84             ; disable motors
M106 S255       ; activate oven fan
M141 S60        ; set chamber temp to 60°C without waiting until target is reached before moving to next instruction
G4 S1500        ; wait 1500 s = 25 min
M141 S0         ; stop heating
M17 Y E         ; enable motors Y and E1
G1 E-21         ; raise E1 by 21 mm to open oven door
G4 S180         ; wait 2 min for printed objects to cool down to room temperature
G28 Y0          ; home Y axis to move the printe bed out of the oven
G1 E0           ; lower E1 to close oven door
M84             ; disable motors
```

Fig. 5 - Screenshot of a typical gcode file, shown as an example.

4.3 Setting up the printer

A disposable syringe filled with a viscous liquid (starting material) and equipped with a needle is placed in the extruder, and the E0 carriage is lowered until contact with the plunger is made. A release liner is placed on the print bed.

The vertical distance between the tip of the needle and the proximity sensor's trigger point, known as probe Z offset, has to be reset every time a new syringe is placed in the extruder. To do this, the Z axis is lowered until the needle tip touches the release liner. The value of the Z coordinate corresponding to this position, which is displayed in the touchscreen, is used to calculate the new offset as follows:

$$New\ offset = Old\ offset - current\ Z\ value$$

By setting the resulting value as the new offset, the position of the Z axis that corresponds to the needle tip touching the release liner becomes the new 0 coordinate, and, as a result, a layer height set to 0.4 mm, such as in the gcode presented as an example, will actually correspond to a distance of 0.4 mm between the needle tip and the release liner.

4.4 Execution of a print job

The print can now be started by selecting the desired gcode file from the micro SD card using the touchscreen. Once this is done, the first operations that are performed

are (1) homing of the XYZ axes to find the 0 coordinates that will be used as reference for all the following positioning instructions and (2) automatic bed leveling. The syringe is then primed by extruding a minimal fraction of its content (approximately 250 µl) into an Eppendorf tube to achieve a smooth flow of the slurry before starting a print. This step was introduced after observing that the first printed film was always lighter than the rest due to the initial inertia of the viscous slurry. The material collected in the tube can be recovered for later use.

After priming the syringe, the actual print starts: the ODF are produced by depositing the slurry on the release liner according to the pattern defined in the gcode, after which they are dried at the temperature and time defined in the gcode.

5. TESTING THE VERSATILITY OF THE PRINTER FOR THE PREPARATION OF ODF

Proof-of-concept data have already been published concerning the suitability of this technique for the preparation of ODF, and studies on how formulation and process parameters affect the quality of printed pharmaceutical products are also available [13]. However, the vast majority of the literature on this topic only focuses on the incorporation of small-molecule API into ODF. To investigate the versatility of this technique further, we attempted to load complex API as well as drug delivery systems. Specifically, films containing the enzyme β-galactosidase, olive oil for the vehiculation of lipophilic molecules, and solid lipid microparticles for the taste masking of bitter drugs were prepared using the newly built printer.

All films described in the following sections were obtained from aqueous slurries containing maltodextrin (DE 6) as film-forming polymer and glycerol as plasticizer with a viscosity between 15000 and 25000 (measured using an IKA ROTAVISC me-vi viscometer set at 10 RPM with a VOL-SP-11.0 spindle at room temperature), which preliminary data indicated as the optimal range both in terms of extrudability and spreadability on the release liner after extrusion.

All films were printed as single layers using the following slicing parameters: layer height 0.4 mm, fill pattern rectilinear, fill density 90%, fill angle 45°, filament diameter 5 mm, extrusion multiplier 0.1, print movements speed 690 mm/min, travel movements speed 5000 mm/min. In all cases, 10 mL disposable syringes with ½" G24 needles were used.

Case study 1: β-galactosidase ODF

Introduction. β-galactosidase (β-gal) is an enzyme used in the treatment of lactose intolerance that can be potentially administered as ODF as demonstrated in Chapter 3. Thus, the stability of β-gal loaded in printed ODF was compared with that prepared by the conventional solvent casting method.

Methods. A maltodextrin-based slurry (composition reported in Table 1) was prepared and mixed with β-gal in a 30:70 weight ratio between β-gal and the dry excipients. The slurry was then used to print 6 cm^2 ODF that were dried at 60 °C for 25 min.

Table 1 - Composition of the slurry before the addition of β-gal.

Excipient type	Excipient	%w/w (slurry)	%w/w (dry)
Film-forming polymer	Maltodextrin DE6	57.5	76.0
Plasticizer	Glycerol	15.9	21.0
Surfactant	Capryol® 90	2.3	3.0
Solvent	Water	24.3	-

The obtained β-gal ODF were tested in terms of disintegration time, protein content uniformity and enzymatic activity according to the methods reported in Chapter 3. In particular, protein content and enzymatic activity were measured again after 1 month of storage at room temperature.

Results. The resulting films exhibited a good mass uniformity, no stickiness, satisfactory mechanical properties, and a disintegration time lower than 30 s.

Results (Table 2) showed that the process did not negatively impact either protein content or enzymatic activity. Moreover, after 1 month of storage both protein content and enzymatic activity were found to be above 90% of their nominal values. These results align well with previous data obtained on films with the same composition prepared by solvent casting (Chapter 3).

Table 2 - Protein content and enzymatic activity of β-gal in the ODF after preparation and after 1 month of storage at room temperature.

At preparation			**After 1 month**		
β-GAL content, mg/ODF	**β-GAL activity**		**β-GAL content, mg/ODF**	**β-GAL activity**	
	UI/ODF	%		UI/ODF	%
51.76 ± 0.45	4141 ± 12	100.9	50.16 ± 2.00	3849 ± 18	93.8

Conclusions. β-gal ODF with quality close to ODF obtained by solvent casting and compliant with Ph.Eur. were successfully prepared. It can therefore be concluded that, unlike other extrusion-based techniques such as HMRE (Chapter 3), SSE 3D printing is indeed suitable for the preparation of films loaded with highly heat-sensitive molecules, such as biomolecules.

Case study 2: CBD oil ODF

CBD is used as an anti-epileptic in the paediatric treatment of Dravet syndrome, Lennox-Gastaut syndrome. It is currently available in the form of a 100 mg/mL oil solution to be administered with a graduated syringe. The recommended dose of CBD ranges from 2.5 to 10 mg/kg twice a day, to be divided into two daily administrations [14]. The availability of ODF containing CBD would allow for improved dosing accuracy and simplify administration, thereby reducing the risk of administration errors. In this light, the feasibility of printing CBD-oil-loaded ODF was investigated by using SSE.

Methods. Composition and preparation method. CBD in olive oil (50% w/w) was emulsified in a pre-made maltodextrin-based slurry (composition reported in Table 3) using a homogenizer (T18D, IKA, Germany). Based on preliminary analyses, homogenization was optimized by setting speed, time and temperature at: 15000 rpm, 25°C, 20 min. The obtained emulsified slurry mixture was then transferred into a 10-mL syringe and printed to obtain 6 cm^2 ODF. The drying step was conducted at 60°C for 25 min.

Table 3 - Composition of the formulations prepared.

Form. ID	Maltodextrin DE6	Glycerol	Span® 80	Tween® 80	Water	CBD oil
			(% w/w)			
E1	43.29	11.90	3.17	1.06	31.84	8.72
E2	39.31	10.85	2.87	0.97	28.98	17.02
E3	33.95	9.35	2.99	0.00	31.00	22.69
E4	31.31	8.63	2.90	0.00	28.59	28.56

Water content. The residual water was determined by using a Karl-Fisher titration apparatus (Mettler Toledo, Switzerland) adapting the method described by Khalid and coworkers [15]. Briefly, an ODF sample was accurately weighed and transferred into an empty glass vial; then, 1.5 mL anhydrous methanol was added and sealed with a rubber closure. The vial was sonicated for 30 min; afterward, 0.5 mL of the prepared sample suspension was injected into the titration chamber. The water content was calculated according to Equation (1):

$$Water\ content\ (\%) = \frac{Ms - Mm}{M_0} \times 100 \qquad Equation\ 1$$

where Ms is the mass of water in the sample introduced into the titration chamber, Mm is the mass of water in the anhydrous methanol, and M_0 is the initial mass of the ODF.

HPLC analysis. The CBD content in each film was determined by HPLC-UV (HP1100 series, Agilent, USA) at 215 nm using a Luna® 5 μm C8(2) 100 Å, with a flow rate of 1.0 mL/min. The mobile phase was acetonitrile 70%/pH 3 acidified water 30%, and

injection volume was set at 20 µL. Briefly, an ODF was dispersed in 100 mL methanol and sonicated for 30 min at 25°C. The obtained suspension was then filtered through a 0.45-µm PVDF filter before HPLC analysis.

Results. The resulting ODF exhibited good mass uniformity (135 ± 4 mg), no stickiness, and a disintegration time under 30 s. The water content was lower than 3.5 ± 0.2 % in all tested formulations, suggesting that the loading of the oil contributed to the flexibility of the films. Indeed, it was observed that moisture content lower than 7% usually led to fragile maltodextrin films (unpublished data). As shown in Table 4, all the obtained ODF were uniform in terms of drug content. (< 10% of theoretical assay).

Table 4 – CBD content in tested ODF; mean ± St.Dev. (n=3).

Form.	**CBD content (% w/w)**		**CBD dose (mg)/ODF**	
ID	Theoretical	Experimental	6 cm^2	9 cm^2
E1	6.40	6.36 ± 0.22	9	13
E2	11.98	12.02 ± 0.24	16	24
E3	16.45	16.14 ± 0.90	22	33
E4	20.00	21.47 ± 1.36	30	43

Conclusions. ODF loaded with up to 10 mg/cm^2 of CBD olive oil solutions were successfully prepared, proving the feasibility of 3D printing emulsions with this technique to vehiculate lipophilic API, such as CBD, or vitamins. In the case of CBD, the application of SSE to print oil-containing ODF can permit titrating easily the CBD dose according to patient's needs and weight.

Case study 3: diclofenac-loaded solid lipid microparticles ODF

Diclofenac is a NSAID characterized by a bitter taste, which makes it incompatible with orodispersible dosage forms. Indeed, even if several attempts have been made to mask its bitterness by adding to the ODF composition several taste-masking agents, the final compliance of patients remains unsatisfied. A possible alternative to obtain an effective taste masking resides in the encapsulation in solid lipid

microparticles (LM) [16], [17]. In this case study, the feasibility of printing ODF loaded with diclofenac-LM was studied.

Methods. Composition and preparation. The solid lipids used were Compritol® HD5 (mono, di-and triglycerides and PEG-8 mono-and di- esters of (C22) behenic acid) and Precirol® ATO5 (esters of palmitic (C_{16}) and stearic (C_{18}) acids, predominantly diester), and Crodamol® GTCC (fully-saturated medium-chain triglycerides) was added to improve the affinity of diclofenac Na for the LM. LM were prepared using the melt emulsification method: the lipid components were melted at 72 °C, diclofenac sodium was added and homogenously dispersed, and the melt (composition reported in Table 5) was emulsified in a 17:25 w/w ratio with a pre-heated aqueous phase containing the surfactant Tween®80 as a stabilizer (0.1% w/v) and citric acid (0.4% w/w) to reduce the affinity of diclofenac for the aqueous phase. The emulsion was allowed to cool at room temperature, resulting in the formation of the LM. Maltodextrin DE6 (MDX) and glycerol were then added to form a slurry (ODF-1–3, Table 6) from which 6 cm^2 ODF were printed and dried at 40 °C for 30 min. The expected amount of diclofenac Na in each ODF is 15 mg. ODF containing the same concentration of free diclofenac were also printed and used as control in the dissolution studies (ODF-0, Table 6).

Table 5 - Composition of the LM. The LM were emulsified in an aqueous phase (citric acid 0.4% w/w, Tween®80 0.1% w/w).

Form. ID	Compritol® HD5	Precirol® ATO5	Compritol® 888ATO	Crodamol®	Diclofenac Na
			(% w/w)		
LM1	61	-	-	13	26
LM2	-	61	-	13	26
LM3	-	-	61	13	26

Table 6 - Composition of the ODF printed and dried.

Form. ID	MDX	Glycerol	LM1	LM2	LM3	Diclofenac Na	Span® 80
				(% w/w)			
ODF-0	67.5	18.6	-	-	-	10	3.9

ODF-1	46.8	13.8	39.7	-	-	-	-
ODF-2	46.8	13.8	-	39.7	-	-	-
ODF-3	46.8	13.8	-	-	39.7	-	-

Particle size analysis. Granulometric analysis was performed using a Mastersizer 3000 equipped with a Hydro cell (Malvern Panalytical Ltd, UK) to assess the particle size distribution of the LM before and after their incorporation into ODF.

Dissolution test. The dissolution tests were conducted at 37 ± 1 °C using a Ph.Eur. dissolution apparatus (SR8 PLUS Dissolution Test Station, Hanson Research, USA) with paddle stirring at 50 rpm. ODF were placed in vessels containing Simulated Salivary Fluid (Na_2HPO_4 2.4 g/L, KH_2PO_4 0.2 g/L, NaCl 8 g/L, pH 6.8 ± 0.1) for 30 min. At defined intervals (2, 4, 6, 8, 10, 15, 20, 25, 30 min), 2 mL of medium was withdrawn from each vessel and transferred to a vial using a syringe equipped with a needle and a cannula filter. The test was performed in duplicate for each formulation.

HPLC analysis. Diclofenac content and the dissolved amounts were analysed by HPLC-UV (HP1100 series, Agilent, USA) at 270 nm using a C18 stationary phase (5 µm, 100 Å, 150 x 4.6 mm) and acetonitrile 60% / phosphate buffer 30 mM pH=3 40% as mobile phase, with a flow rate of 1.0 mL/min. The percentage of diclofenac dissolved was calculated for each time point and plotted as a function of time.

Results. The resulting films exhibited good weight uniformity, no stickiness, satisfactory mechanical properties, and a disintegration time under 30 s. All three LM formulations had a similar size distribution after preparation (d50 ≈ 30 µm; span ≈ 2.0) and in all cases the microparticles remained intact after the printing and drying process (Fig. 6).

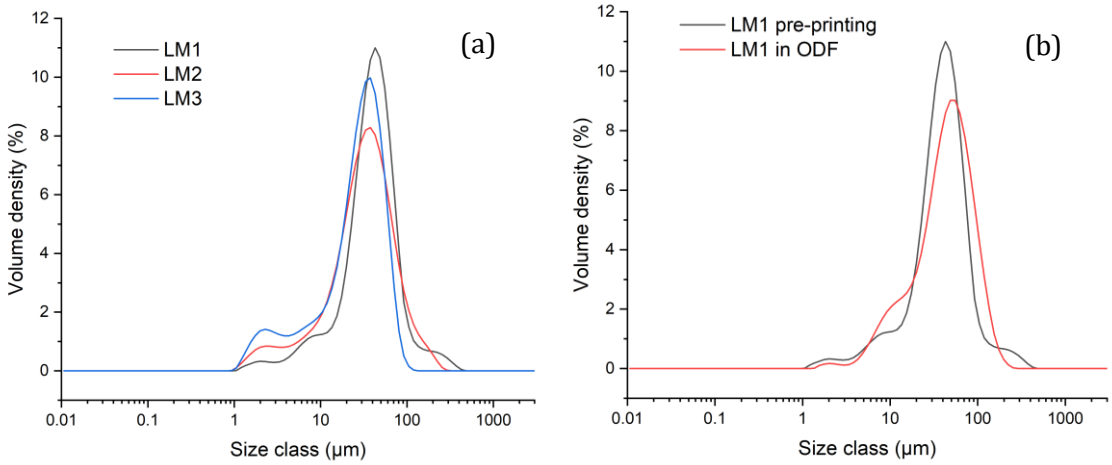

Fig. 6 – (a) size distribution of LM after preparation; (b) size distribution of LM1 before and after incorporation into ODF.

The results of the dissolution studies are reported in Fig. 7. All the formulations released 100% of the loaded drug in under 15 min, and can therefore be classified as immediate release. However, the amount of diclofenac released from the LM-loaded ODF after 5 min of contact with the medium was lower than that released from the control ODF containing free diclofenac, indicating that a taste masking effect of diclofenac was potentially achieved.

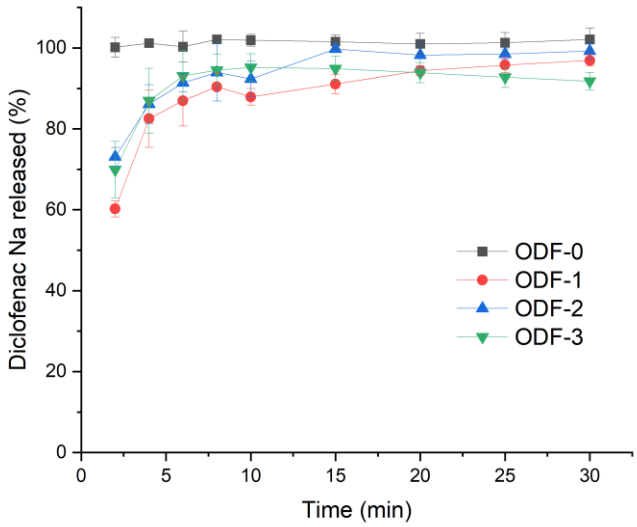

Fig. 7 - Dissolution profiles of the LM-loaded ODF (ODF-1–3) and the control ODF containing free diclofenac (ODF-0).

Conclusions: solid lipid microparticles loaded with diclofenac sodium were prepared and successfully incorporated into ODF without negatively impacting size

distribution. Moreover, dissolution tests performed in simulated saliva showed a slower release of diclofenac from the LM-loaded ODF compared to the control ODF carrying free diclofenac, which could potentially translate to a taste masking effect of diclofenac. This data proves the suitability of SSE 3D printing for the preparation of ODF loaded with LM for the taste masking of bitter drugs.

6. CONCLUSIONS

A desktop semi-solid extrusion 3D printer with an in-built drying oven for the preparation of orodispersible films was designed and constructed from scratch starting from commercially available components and 3D printed parts.

The printing and drying process is very simple. Indeed, the steps in the process can be summarized as follows: (1) generating a gcode file; (2) setting up the printer; (3) printing and drying.

Before starting a print, a 3D model of the desired ODF is imported to a slicing software, where it is translated into print instructions in the form of gcode according to the print parameters set by the user. The resulting gcode file is copied onto a micro SD card, which is then inserted into a slot in the printer. The printer is set up by placing a pre-filled syringe in the extruder module of the printer and attaching a release liner to the print bed. The user can now select the gcode file from the touchscreen and start a print job. Before the actual print begins, some preliminary operations are carried out, namely homing of the XYZ axes, automatic bed leveling, and priming of the syringe. Once this is done, the print can start: the slurry is deposited onto the release liner according to the pattern defined in the gcode. Finally, the print bed enters the oven for the final drying stage. The total duration of the process is usually between 25 – 35 min, depending on the ODF number, ODF geometry, and print parameters such as fill density and speed of print movements (set in the slicing software) and the drying time, which is the longest step of the process (up to 20 min).

The versatility of both the printer and the SSE technique was put to the test by attempting to produce ODF loaded with complex API or drug delivery systems that would not be compatible with other extrusion-based printing techniques, namely an enzyme, an oil, and lipid microparticles. In all cases, preliminary data showed that the films possessed satisfactory physical properties, and the loaded entity was not altered by the process. This, coupled with the size and production cost of the printer and its ease of use, makes this printer potentially suitable for the extemporaneous compounding of highly customizable ODF in a community or hospital pharmacy.

7. REFERENCES

[1] "Orodispersible Films, monograph 3195. Ph. Eur. Suppl. 11.8. Strasbourg, France: Council of Europe; 2025."

[2] M. Scarpa *et al.*, "Orodispersible films: Towards drug delivery in special populations," *International Journal of Pharmaceutics*, vol. 523, no. 1, pp. 327–335, May 2017, doi: 10.1016/j.ijpharm.2017.03.018.

[3] M. A. Azad, D. Olawuni, G. Kimbell, A. Z. M. Badruddoza, Md. S. Hossain, and T. Sultana, "Polymers for Extrusion-Based 3D Printing of Pharmaceuticals: A Holistic Materials–Process Perspective," *Pharmaceutics*, vol. 12, no. 2, p. 124, Feb. 2020, doi: 10.3390/pharmaceutics12020124.

[4] J. T. Y. Cheng, E. C. K. Tan, and L. Kang, "Pharmacy 3D printing," *Biofabrication*, vol. 17, no. 1, Oct. 2024, doi: 10.1088/1758-5090/ad837a.

[5] "Pharmaceutical 3D Printing | FABRX Ltd. - Personalized Medicine." [Online]. Available: https://fabrx.co.uk/

[6] "Customized Medication with On-Demand 3D Printing," MB Therapeutics. [Online]. Available: https://mb-therapeutics.com/en/pharmacies-3/

[7] "DiHeSys | Digital-Health-Systems | 3D & 2D Printed Drugs | Deutschland." [Online]. Available: https://www.digital-health-systems.com/en

[8] "Craft Health | 3D Printed Personalized Medicines and Supplements |Home." [Online]. Available: https://www.crafthealth.me

[9] T.-T. Yan *et al.*, "Semi-solid extrusion 3D printing ODFs: an individual drug delivery system for small scale pharmacy," *Drug Dev Ind Pharm*, vol. 46, no. 4, pp. 531–538, Apr. 2020, doi: 10.1080/03639045.2020.1734018.

[10] J. Hu, R. Fitaihi, S. Abukhamees, and H. E. Abdelhakim, "Formulation and Characterisation of Carbamazepine Orodispersible 3D-Printed Mini-Tablets for Paediatric Use," *Pharmaceutics*, vol. 15, no. 1, p. 250, Jan. 2023, doi: 10.3390/pharmaceutics15010250.

[11] J. D. Weiss *et al.*, "A Low-Cost, Open-Source 3D Printer for Multimaterial and High-Throughput Direct Ink Writing of Soft and Living Materials," *Advanced Materials*, vol. 37, no. 10, p. 2414971, 2025, doi: 10.1002/adma.202414971.

[12] A. S. Samokhin, "Syringe Pump Created using 3D Printing Technology and Arduino Platform," *J Anal Chem*, vol. 75, no. 3, pp. 416–421, Mar. 2020, doi: 10.1134/S1061934820030156.

[13] I. Seoane-Viaño, P. Januskaite, C. Alvarez-Lorenzo, A. W. Basit, and A. Goyanes, "Semi-solid extrusion 3D printing in drug delivery and biomedicine: Personalised solutions for healthcare challenges," *Journal of Controlled Release*, vol. 332, pp. 367–389, Apr. 2021, doi: 10.1016/j.jconrel.2021.02.027.

CHAPTER 5: CUSTOMIZABLE EXTENDED-RELEASE ORODISPERSIBLE FILMS CONTAINING TRIHEXYPHENIDYL

1. INTRODUCTION

Trihexyphenidyl HCl (THP) is an anticholinergic drug indicated as an adjunct in the symptomatic treatment of all types of Parkinsonism (idiopathic, post-encephalitic, arteriosclerotic, drug-induced) to alleviate tremors, spasms, stiffness, and poor muscle control. It was first approved by the FDA in 1949 in the form of immediate-release tablets and an elixir, to be taken two to four times per day with a daily dose normally ranging from 6 to 20 mg [1]. To reduce the frequency of administration and possibly the side effects related to oscillating plasma levels of the drug, in 1962 5-mg extended-release capsules were approved [2]. In a clinical trial, two thirds of patients expressed a preference for these over the immediate-release tablets due to the convenience of once-daily administration, the smoother and more sustained beneficial effect, and the lower frequency of side effects [3]. The main limitation of conventional extended-release dosage forms, however, is that the drug strength is fixed, but the dose of THP required to achieve a therapeutic effect with limited side effects depends on the patient's response and has to be calibrated at the start of treatment [1], making the conventional one-size-fits-all approach unsuitable for this drug. This may be part of the reason why the extended-release capsules were eventually discontinued. The availability of a customizable dosage form that allows for flexible dosing would therefore be beneficial.

Orodispersible films (ODF) are an innovative patient-centric dosage form defined as sheets of suitable materials intended to be placed in the buccal cavity, where they dissolve or disperse rapidly upon contact with saliva, forming a suspension or solution of the loaded drug that can then be swallowed. One of their main advantages over conventional solid oral dosage forms is that they are easy to dose, since different drug strengths can be obtained simply by changing the size of the

ODF. This is why they are widely studied for personalized therapy. Another advantage is their ease of administration, as no water is required and no solid objects have to be swallowed. This feature is what makes them suitable for special populations with swallowing difficulties such as children, elders, or dysphagic patients, which is particularly relevant in the context of managing Parkinson's disease seeing as 80% of patients develop dysphagia over its course [4]. ODF could therefore be a suitable option to vehiculate individualized doses of THP, however they cannot control drug release on their own. Therefore, to obtain extended-release ODF, a delivery system that can prolong the release of THP and is compatible with being incorporated into an ODF formulation has to be devised.

Clays are biocompatible inorganic materials that have been investigated as carriers for controlled drug release due their ability to interact with substances through various mechanisms, the most studied being cation exchange with basic molecules [5], [6], [7]. Exploiting this mechanism, a drug/clay hybrid can be prepared by mixing the clay with a cationic drug in solution, such as a protonated base. After administration, the drug would gradually be displaced from the anionic sites in the clay by the counterions present in biological fluids, resulting in a prolonged release [7].

The aim of this study was to obtain orodispersible films loaded with a prolonged-release clay-based trihexyphenidyl formulation for the individualized treatment of Parkinson's disease. Four different clays were tested to assess the feasibility of obtaining a controlled-release drug/clay complex using a high drug:clay ratio: halloysite (Hal), the sepiolite Pangel® S9 (PS9), the hectorite Pangel® HT11 (HT11), and the smectite Veegum® HS (VHS). The drug/clay hybrids were prepared by mixing THP and the clays in water, and then characterized and compared with the corresponding physical mixtures. Finally, they were incorporated into a maltodextrin-based slurry from which ODF were obtained by semi-solid extrusion 3D printing, and the release profile of THP from the ODF was studied.

2. MATERIALS AND METHODS

2.1 Materials

Trihexyphenidyl hydrochloride was kindly donated by TEOFARMA SpA (Italy); clays were provided by the University of Granada; maltodextrin DE6 was purchased from Roquette (France); glycerol was purchased from Farmalabor (Italy); sorbitan monooleate (Span®80) was purchased from Croda International PLC (UK). All the solvents used were of analytical grade, unless otherwise specified.

2.2 Preparation of the drug/clay hybrid

Each clay and THP were transferred in a 3:1 w/w ratio into 15 ml Falcon tubes with 4 ml of MilliQ® water and shaken for 6, 12 or 24 h in an oscillating water bath at 25 °C. Then, the tubes were centrifuged for 45 min at 6000 rpm (Z306, Hermle, Germany) and the supernatant was removed. The solid was rinsed twice by adding 5 ml of water, shaking for 5 min, centrifuging and removing the supernatant. The rinsed solid was dried in an oven at 60 °C overnight. The supernatants were filtered through 0.45-µm PVDF syringe filters and used to indirectly quantify the amount of THP retained by the clay according to the HPLC method reported in section 2.5.

A physical mixture with the same drug/clay ratio was also prepared by mixing weighed amounts of THP and the clays in an agate mortar.

The resulting powders were stored in an Eppendorf tube until use.

2.3 Solid state characterization

2.3.1 Thermal analysis

THP, the clays, the physical mixtures, and the drug/clay hybrids were analyzed by thermogravimetric analysis (TGA) and differential scanning calorimetry (DSC) (TGA/DSC 3+, Mettler Toledo, Switzerland). Both analyses were carried out under air atmosphere at 10 K/min from 28 to 950°C and from 26 to 400°C, respectively. TGA data (n=3) was used to calculate the loading efficiency of THP using the following equation (Equation 1):

$$Loading\ efficiency(\%) = \frac{Residual\ weight(hybrid)(\%) - Residual\ weight(clay)(\%)}{Weight\ of\ THP\ loaded(\%)=25\%} * 100$$

Equation 1

2.3.2 Powder X-ray diffraction

Powder X-ray diffraction (PXRD) was conducted on THP, the physical mixtures, and the drug/clay hybrids using a Philips® XPert diffractometer with Cu Kα radiation. The diffraction data were analyzed using the XPOWDER® software [8].

2.4 Preparation and characterization of the ODF by semi-solid extrusion 3D printing

2.4.1 Preparation of the semi-solid mixture

Maltodextrin DE6 was used as film-forming polymer, with glycerol as plasticizer. According to ratio reported in Table 1, maltodextrin DE6 (MDX), glycerol (Gly), and water were placed in a heated vessel set to 80 °C and stirred for 20 min. The solution was then allowed to cool to room temperature under continuous stirring, and the surfactant Span®80 was added to reduce the interfacial tension between the aqueous mixture and the siliconized foil on which it would be printed. Based on the results of the dissolution studies discussed in paragraph 3.2, the THP/VHS hybrid was selected as the most promising and added to the mixture in a concentration of 23 and 42% (w/w) (ODF-1-2, Table 1). This corresponds to ODF with 5 - 10 mg of THP, which, according to the literature, is the therapeutic strength for an extended-release THP formulation [3]. A placebo ODF was also printed to be used as control (ODF-P, Table 1)

Table 1 – Composition of slurry for printing ODF containing THP/clay.

Form. ID	MDX	Gly	THP/clay	Span® 80	Water
			(% w/w)		
ODF-P	43.8	12.1	-	4.0	40.1
ODF-1	37.2	10.3	15.0	3.4	34.1
ODF-2	30.7	8.5	30.0	2.8	28.1

2.4.2 Design of the 3D model and definition of print and drying parameters

A 20 x 30 x 0.4 mm parallelepiped was designed in Fusion (Autodesk), corresponding to a 6 cm^2 ODF. The model was then sliced using Slic3r to obtain a G-code file. Slicing parameters were set so that ODF would be printed as a single layer with a thickness of 400 µm, with one external perimeter and 90%-density 45° rectilinear infill. Speed for print moves was set to 690 mm/min. Drying commands were added manually to the G-code so that, at the end of a print run, the print bed would move into the printer's in-built oven and the films would be dried at 60 °C for 20 min.

2.4.3 Semi-solid extrusion 3D printing and drying

The in-house custom-built SSE 3D printer described in Chapter 4 was used. 10-ml disposable syringes equipped with ½" G16 needles were filled with the mixture and placed in the syringe pump module of the printer, a siliconized release liner was taped to the print bed, and the print was started. After drying, the films were stored in heat-sealed packages at room temperature until use.

2.4.4 Physical characterization

The technological features of ODF were assessed by determining film stickiness and disintegration time. In particular, ODF stickiness was measured by the thumb tack test described by Musazzi and coworkers [9] and expressed by the following score system: A (not sticky), B (sticky), and C (very sticky). Disintegration time was determined according to the specifications of the monograph 'Disintegration of tablets and capsules' reported in the European Pharmacopoeia (Ph. Eur.).

2.4.5 Tensile properties

Tests were conducted according to ASTM International Test Method for Thin Plastic Sheeting (D 882-02) using an Instron 5965 texture analyzer (Instron, UK), equipped with a 50 N load cell. The samples were 50×13mm film strips.

Each test strip was longitudinally placed in the tensile grips on the texture analyzer. Initial grip separation and the crosshead speed were 12.5 mm/min. The test was considered concluded at the film break. The following parameters were determined:

- Tensile strength (TS) was calculated by dividing the maximum load by the original cross-sectional area of the specimen.
- Percent elongation at break (E%) was calculated according to the following equation (Equation 2):

$$E\% = \frac{L - L_0}{L_0}\ x\ 100 \qquad \textit{Equation 2}$$

where L_0 is the initial gage length of the sample and L is the length at the rupture.

- Elastic modulus or Young's modulus (Y) was calculated as the slope of the linear portion of the stress–strain curve.

2.5 Dissolution studies

The dissolution tests were conducted at 37 ± 1 °C using a Ph.Eur. dissolution apparatus (SR8 PLUS Dissolution Test Station, Hanson Research, USA) with paddle stirring at 50 rpm. To simulate the passage through the GI tract, the THP/clay hybrids or drug-loaded ODF were placed in vessels containing Simulated Gastric Fluid (HCl 0.1 N, pH 1.2 ± 0.1; SGF) for 2 hours, after which a concentrated solution of Na_2HPO_4 was added to raise the pH to 6.8 ± 0.1, turning the medium into Simulated Intestinal Fluid (SIF). At defined intervals (15, 45, 60, 90, 120, 135, 150, 180, 240, 300, 360 min), 2 ml of medium was withdrawn from each vessel and transferred to a vial using a syringe equipped with a needle and a cannula filter. The content of each vial was analyzed by HPLC-UV (HP1100 series, Agilent, USA) at 210 nm using a C18 stationary phase (5 µm, 100 Å, 150 x 4.6 mm) and acetonitrile 50% / acetate buffer 50 mM pH=4.5 50% as mobile phase, with a flow rate of 1.0 ml/min.

3. RESULTS

The percentages of THP retained by each clay after being dispersed in water for different times (i.e., 6, 12, 24 h) are reported in Table 2.

Table 2- Percentage of THP retained by each clay after shaking in water for 6, 24, or 48 h.

Time	Encapsulation efficiency (%)			
(h)	PS9	Hal	VHS	HT11
6	38.7 ± 1.0	20.7 ± 0.8	73.9 ± 0.8	96.8 ± 0.9
12	42.9 ± 0.9	21.4 ± 1.0	76.4 ± 0.9	97.5 ± 0.8
24	49.0 ± 1.1	17.7 ± 0.9	77.5 ± 0.8	97.8 ± 0.8

These data suggest a different affinity of the drug for the different clays with the following rank order: Hal< PS9< VHS<HT11. Since in the case of Hal, VHS, and HT11 a stirring time of 24 or 48 h in water did not result in a significant increase in the amount of THP retained compared to 6 h, this stirring time was selected to prepare the samples used for further characterization of the hybrids. In the case of PS9, a longer stirring time improved THP retention significantly, so 48 h was selected as the optimal stirring time.

3.1 Solid state characterization

TGA and DSC curves of the studied samples are shown in Fig. 1 and 2, respectively. TGA data showed a weight loss event that was seen in all hybrids at about 260 °C corresponding to the degradation of THP. This event was proportional to the retained amount and therefore was used to confirm the THP content (Table 2) determined by HPLC-UV. The only exception was Hall, in which case a higher variability was observed.

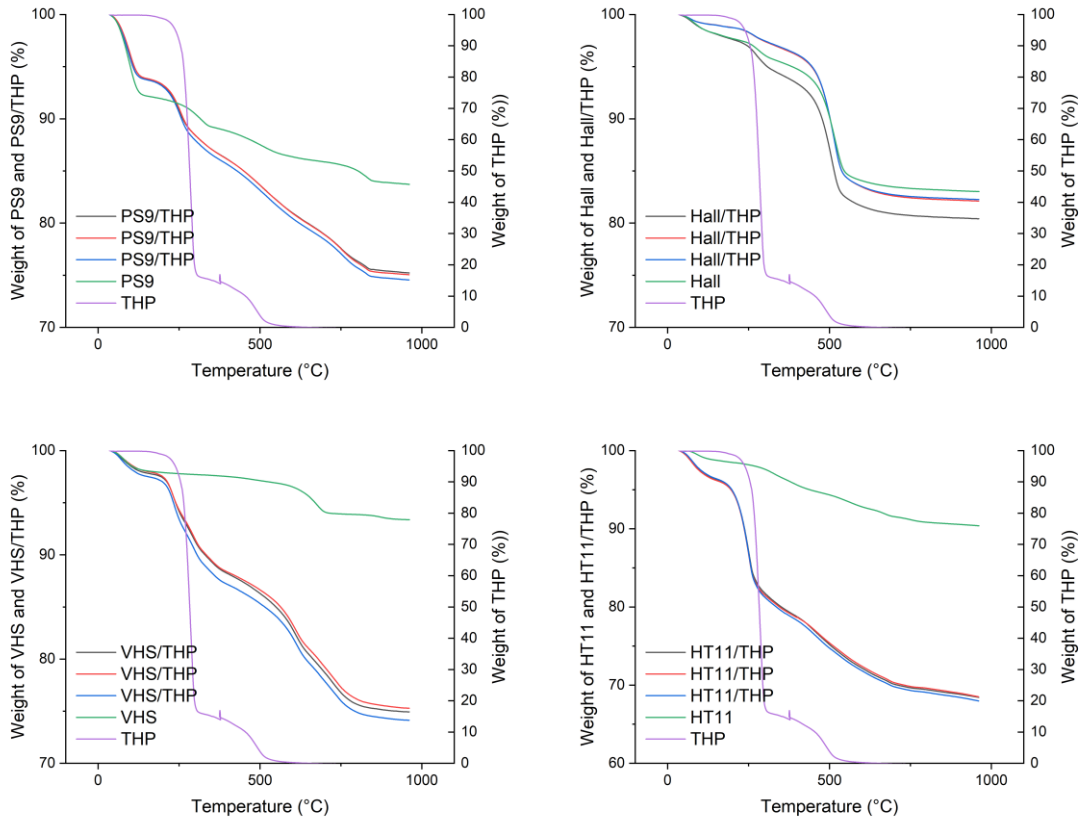

Fig. 1 - TGA thermograms of THP, the pure clays, and the hybrids (n=3).

Table 3 - Percentage of THP present in each complex relative to the loaded amount (25%), calculated from TGA data.

	PS9	**Hal**	**VHS**	**HT11**
		(% w/w)		
THP content in drug/clay hybrid (%)	10.5± 0.4	1,7±1,1	20.0± 0,5	24.5± 0.2
Calculated encapsulation efficiency (%)	41.9 ± 1.5	6.7 ± 4.1	79.8 ± 2.1	97.8 ± 0.9

DSC analysis (Fig. 2) revealed that THP undergoes melting around 255 °C followed by decomposition. In the case of the PS9 and Halloysite, an endothermic peak corresponding to THP melting overlapping with the evaporation of bound water from the clay followed by exothermic decomposition of the drug is present in the physical mixture, but wasn't detected in the hybrid, probably due to the low amount of THP present. In the case of VHS, THP melting and decomposition is clearly visible in the thermogram of the physical mixture, while in the hybrid no THP melting was detected before decomposition, indicating successful interaction between the clay

and the drug. Interestingly, in the case of HT11, the clear melting peak seen in the other physical mixtures was not present, even though an endothermic event between 200 and 240 °C was observed. Since TGA data shows that in this sample weight loss started at 200 °C, it is impossible to state that melting takes place, indicating that THP probably interacts with HT11 even in the solid state. Melting of THP was also not detected in the hybrid, although a new endothermic peak not associated with weight loss appeared at 115 °C. This corresponds to the melting temperature of the free-base form of THP, which may have formed during the drug/clay interaction in water and then precipitated onto the clay's surface during drying.

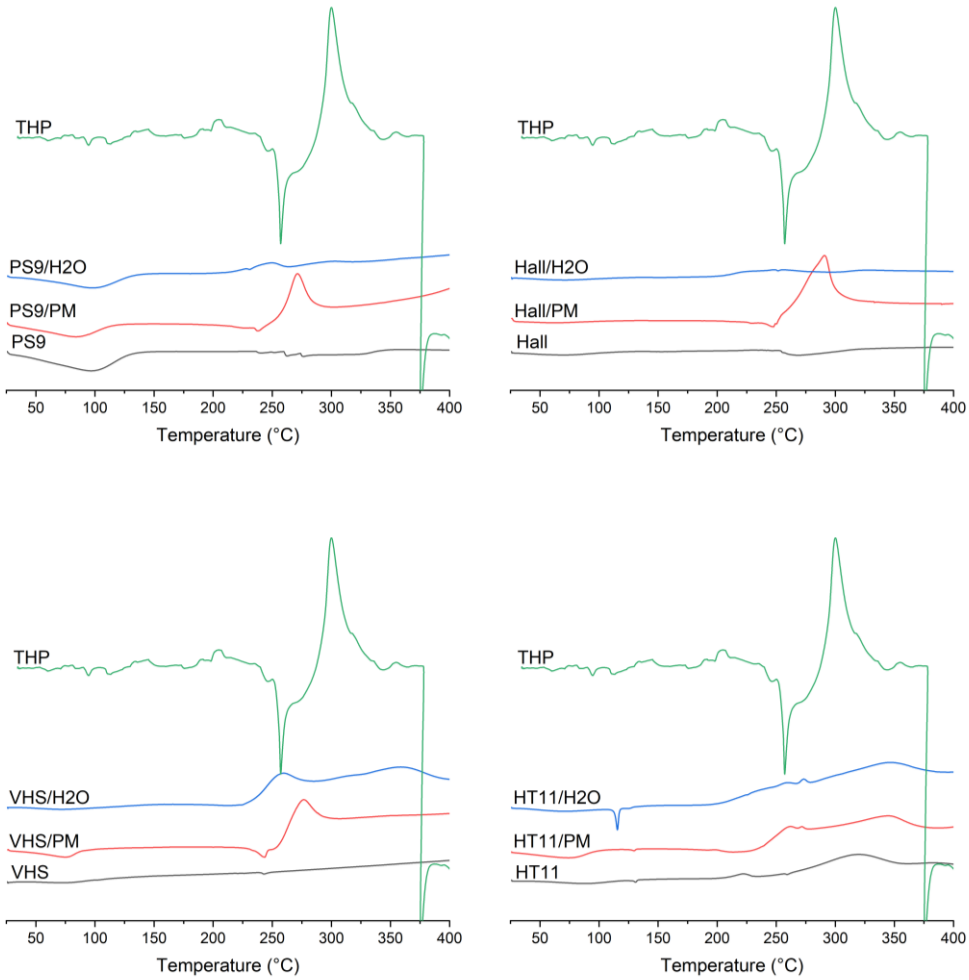

Fig. 2 - DSC thermograms of THP, the hybrids, the physical mixtures and the pure clays (↓endo).

These data are in agreement with PXRD, which is a fundamental technique for determining the crystalline structure and interlayer spacing of nanoclays. By analyzing the diffraction patterns, researchers can identify the specific clay mineral type, assess the degree of crystallinity, and monitor surface modification and intercalation [10]. PXRD patterns are reported in Fig. 3. THP showed a crystalline pattern whose main reflections are visible in all of the physical mixtures. They are also partially visible in the hybrids, except in the case of VHS, where they completely disappear. This result aligns well with the disappearance of the melting peak of THP in the hybrid's DSC thermogram, indicating that THP has indeed interacted with VHS and is no longer present in the crystalline state.

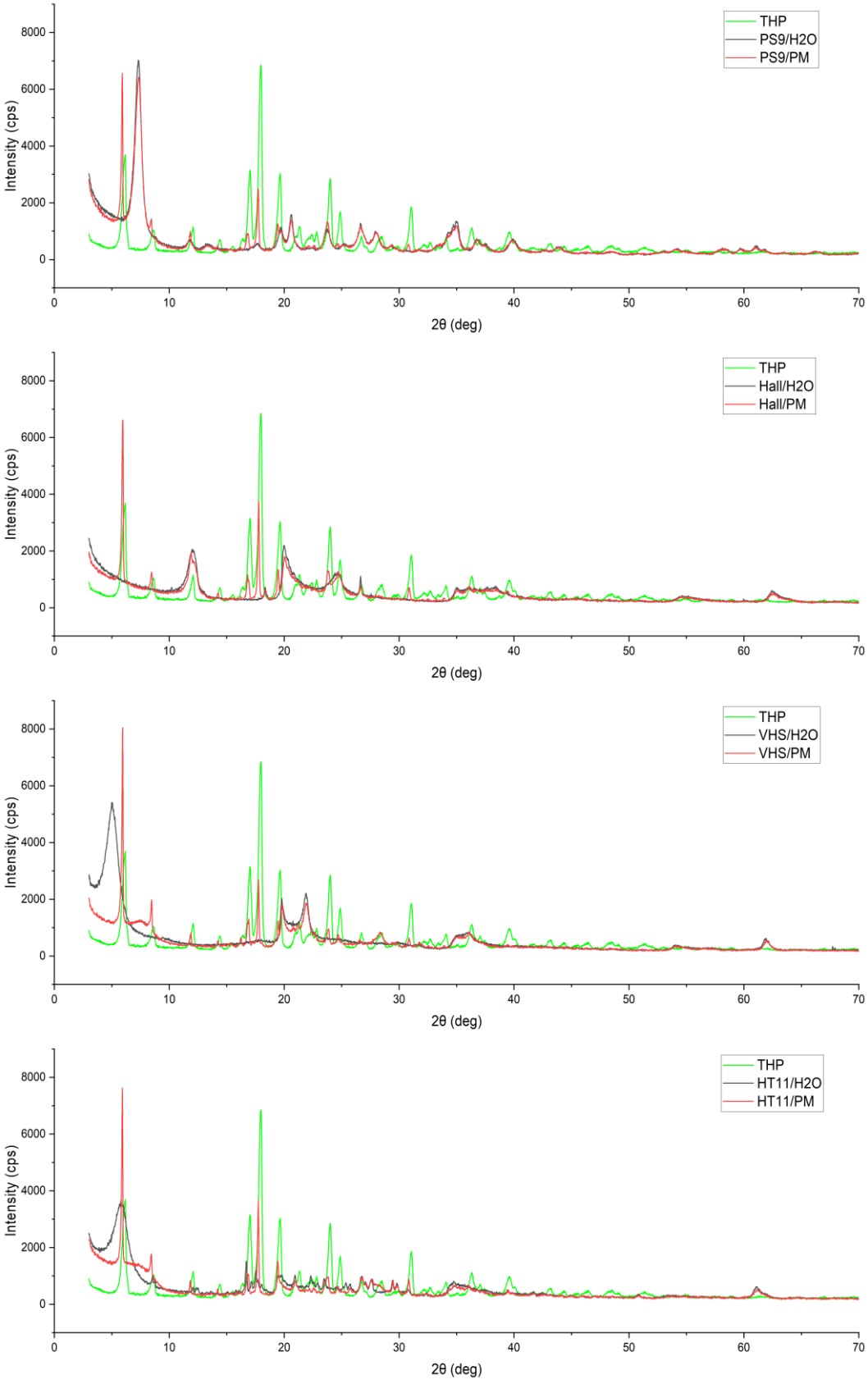

Fig. 3 - XRPD diffractograms of the physical mixtures, the hybrids, and THP.

3.2 Dissolution studies on the THP/clay hybrids

As depicted in Fig. 4, HT11 and VHS, which had shown the highest affinity for the drug, were also able to control its release more effectively than PS9 and Hal. In particular, the intercalation of THP in VHS prolonged the release of THP significantly compared to the corresponding physical mixture. The higher burst effect recorded for the HT11 preparation can be attributed to the dissolution of the free-base THP fraction that had not interacted with the clay. However, neither HT11 nor VHS released 100% of the loaded drug, which is a known drawback of these clays. Nonetheless, VHS was considered suitable for assuring a prolonged release of THP since the drug, after a burst effect of about 25% of the loaded amount, was gradually released over a six-hour period independently of the pH change. Therefore, the THP/VHS hybrid was selected for the preparation of ODF.

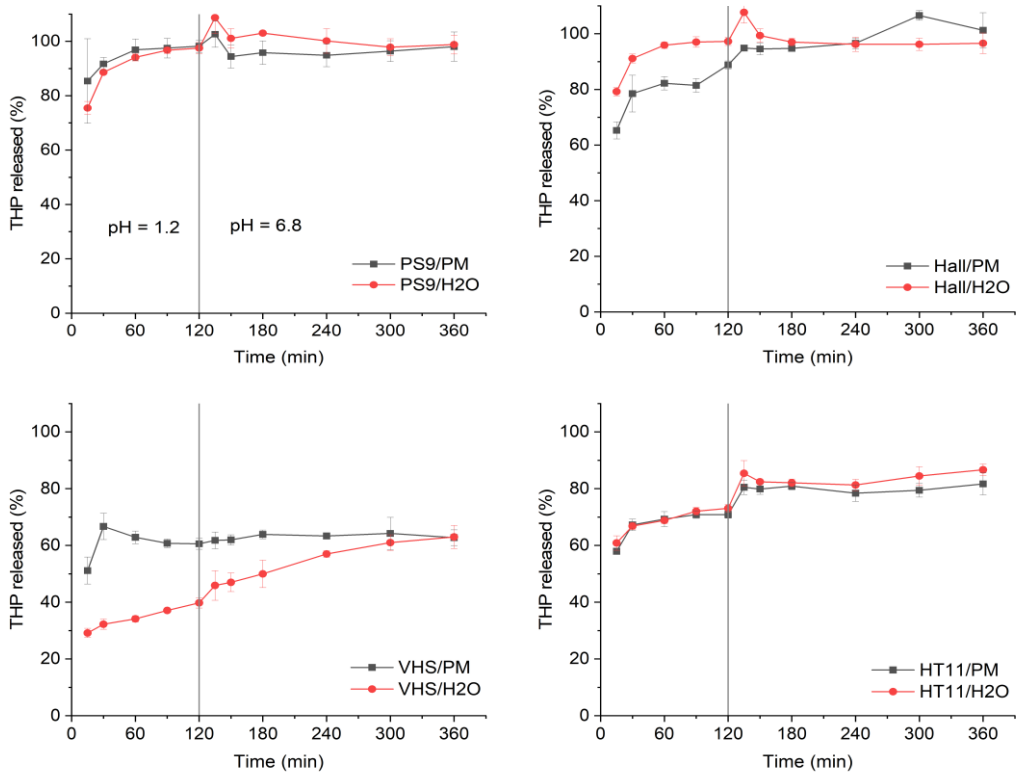

Fig. 4 - Release profiles of the THP/clay hybrids and the THP/clay physical mixtures (n=3).

3.3 Characterization of the THP-loaded ODF

The addition of the THP/VHS hybrid to the formulation increased significantly the viscosity of the printed mixture: only the formulation with 23% w/w of clay (ODF-1, Table1), corresponding to a THP content of about 1.25 mg/cm^2, was sufficiently printable to obtain homogeneous films, whereas a higher content (ODF-2, Table 1) resulted in a mixture that was too stiff for printing. The printed ODF-1 had a uniform appearance and acceptable stickiness, and the disintegration time complied with the Ph. Eur. requirements for orodispersible dosage forms. The addition of clay impacted on the ODF mechanical properties. As shown in Table 4, a significant increase in toughness (see TS values; p = 0.0002) and a reduction in film plasticity (see E% values; p = 0.0359) were observed.

Table 4 – Stickiness and Tensile properties of ODF loaded with VHS versus placebo; mean ± St.Dev. (n=3).

Form. ID	Stickiness	TS (MPa)	Y (MPa)	E% (%)
ODF-P	A (no sticky)	0.49 ± 0.05	12.08 ± 3.29	27.09 ± 11.41
ODF-1	A (no sticky)	2.51 ± 0.27	106.71 ± 8.56	6.56 ± 0.81

This data agrees with previously published results obtained by preparing ODF made of MDX with other substances acting as filler [11]. Regarding the drug release, the profile was superimposable to that shown in Fig.4, demonstrating that the incorporation of the THP/VHS hybrid into ODF did not interfere with the ability of VHS to control the release of THP.

4. CONCLUSIONS

The experimental data presented herein demonstrate, for the first time, that drug/clay hybrids can be effectively loaded into orodispersible films, enabling the development of prolonged-release solid dosage forms suitable for the pharmacological treatment of dysphagic populations. Moreover, the integration of printing technologies, such as the SSE 3D printer developed in this thesis, offers the possibility to customize the shape and surface area of the films. This personalization

allows for precise tailoring of the administered dose to meet the specific therapeutic needs of individual patients.

In the current study, the VHS/THP hybrid formulation enabled a controlled drug release over a 6-hour period. This extended-release profile may reduce the frequency of administration and mitigate side effects associated with fluctuating plasma drug levels, thereby improving treatment adherence in patients with Parkinson's disease.

5. REFERENCES

[1] U.S. Food and Drug Administration, "New Drug Application Approval Notice 6-773/36." June 25, 2003. [Online]. Available: https://www.accessdata.fda.gov/drugsatfda_docs/nda/2003/006773_S036_ARTANE.pdf

[2] U.S. Food and Drug Administration, "New Drug Application Approval Notice 012947." Apr. 18, 1962. [Online]. Available: https://www.accessdata.fda.gov/scripts/cder/daf/index.cfm?event=overview.process&ApplNo=012947

[3] R. S. Schwab and L. J. Doshay, "Slow-release trihexyphenidyl in Parkinson's disease," *JAMA*, vol. 180, no. 2, pp. 159–161, Apr. 1962, doi: 10.1001/JAMA.1962.03050150000018A.

[4] I. Suttrup and T. Warnecke, "Dysphagia in Parkinson's Disease," *Dysphagia*, vol. 31, no. 1, pp. 24–32, Feb. 2016, doi: 10.1007/S00455-015-9671-9.

[5] Y. Chen, A. Zhou, B. Liu, and J. Liang, "Tramadol hydrochloride/montmorillonite composite: Preparation and controlled drug release," *Applied Clay Science*, vol. 49, no. 3, pp. 108–112, July 2010, doi: 10.1016/J.CLAY.2010.04.011.

[6] J. K. Park, Y. B. Choy, J.-M. Oh, J. Y. Kim, S.-J. Hwang, and J.-H. Choy, "Controlled release of donepezil intercalated in smectite clays," *International Journal of Pharmaceutics*, vol. 359, no. 1, pp. 198–204, July 2008, doi: 10.1016/j.ijpharm.2008.04.012.

[7] C. Aguzzi, P. Cerezo, C. Viseras, and C. Caramella, "Use of clays as drug delivery systems: Possibilities and limitations," *Applied Clay Science*, vol. 36, no. 1–3, pp. 22–36, Apr. 2007, doi: 10.1016/J.CLAY.2006.06.015.

[8] Martin JD, "Xpowder. A software package for powder X-ray diffraction analysis." 2004. [Online]. Available: https://www.xpowder.com/wp-content/uploads/QuickUserGuideForXPowderX.pdf

[9] U. M. Musazzi *et al.*, "Poly(methyl methacrylate) salt as film forming material to design orodispersible films," *European Journal of Pharmaceutical Sciences*, vol. 115, pp. 37–42, Mar. 2018, doi: 10.1016/J.EJPS.2018.01.019.

[10] Moore DM and Reynolds RC, *X-Ray Diffraction and the Identification and Analysis of Clay Minerals*. Oxford University Press, 1989.

[11] I. Franceschini, F. Selmin, S. Pagani, P. Minghetti, and F. Cilurzo, "Nanofiller for the mechanical reinforcement of maltodextrins orodispersible films," *Carbohydrate Polymers*, vol. 136, pp. 676–681, Jan. 2016, doi: 10.1016/j.carbpol.2015.09.077.

FINAL REMARKS

The aim of this thesis was to demonstrate the feasibility of using 3D printing technologies to prepare personalized mucoadhesive and orodispersible films in community or hospital pharmacies on demand. In order for a technique to be considered suitable for this purpose, it should allow for accurate and flexible dosing, it should be compatible with a wide range of excipients and API to meet the individual needs or preferences of patients, and the equipment required should be low-cost and compact. With this in mind, among the many 3D printing techniques that have been proposed for pharmaceutical manufacturing, direct powder extrusion and semi-solid extrusion 3D printing were selected as potentially ideal due to their versatility and compatibility with a wide range of materials, as well as the fact that the only equipment required is a benchtop printer and the overall process is simple, relatively quick, and requires little user intervention.

First, the possibility of using DPE to produce MAF for the local treatment of buccal pathologies was tested using a commercially available printer specifically designed for pharmaceutical manufacturing (Chapter 1 and 2). MAF loaded with clobetasol propionate and MAF loaded with lidocaine hydrochloride were prepared using polyethylene oxide blended with chitosan or chitosan derivatives. The resulting films were acceptable in terms of weight uniformity, drug content, mechanical properties, and mucoadhesive performance, proving that MAF with satisfactory qualities can indeed be produced on a small scale with this simple technique.

Then, to expand the range of compatible API, a milder technique known as hot melt ram extrusion 3D printing, whose operating temperatures are lower than those of DPE, was briefly explored. The enzyme β-galactosidase, chosen as a model of thermolabile molecules, was loaded into maltodextrin-based ODF prepared both by HMRE and by the traditional solvent casting technique, a process in which a slurry is spread onto a release liner at room temperature and then dried to obtain a laminate from which individual films can be cut (Chapter 3). While HMRE caused thermal degradation of the enzyme, positive results were obtained from the films produced by solvent casting, with no loss of enzymatic activity detected.

The focus was therefore shifted to scaling down this technique and eliminating the need for manually cutting the laminate to obtain films with the desired size, making it suitable for compounding. This can be achieved by SSE 3D printing, where individual films of the desired size can be printed from a slurry and solidified by drying. However, unlike in the case of DPE, a SSE printer optimized for the manufacturing of pharmaceutical dosage forms wasn't available on the market, so a new printer with an in-built oven was designed and built from scratch (Chapter 4). This printer was successfully used to produce ODF carrying a wide variety of payloads, including β-galactosidase (Chapter 4), CBD oil (Chapter 5), taste-masking solid lipid microparticles loaded with diclofenac sodium (Chapter 6), and sustained-release clay nanoparticles loaded with trihexyphenidyl hydrochloride (Chapter 7).

In conclusion, personalized MAF and ODF can be prepared by using 3D printers appositely designed for a pharmacy setting. A comparison of the techniques examined in this thesis is reported in Table 1.

Table 1 - Comparison of the techniques explored in this thesis

	HMRE	DPE	SSE
	Dosage forms		
Printable dosage forms	Orodispersible films Mucoadhesive films Minitablets Lozenges	Orodispersible films Mucoadhesive films Tablets Minitablets Lozenges	Orodispersible films • Orodispersible films containing emulsions • Orodispersible films containing lipid microparticles Mucoadhesive films Lozenges Pastilles
	Ease of use		
Preparation of the starting material	**++** Mixing of powders and wetting	**+++** Mixing of powders	**+** Dispersion of the components in water
Cleaning operations	**++** Washing of removable syringe	**+** Washing of extrusion chamber	**+++** (Disposable syringe)
	Compatibility with thermolabile substances		
Maximum process temperature (and exposure time)	**+/-**	**-**	**+**
	60-90°C (approx. 15 min)	Circa 170°C (up to 1 min)	45-60°C (up to 20 min)

Moreover, knowledge on the versatility of ODF, which are generally thought of as limited to the immediate release of small molecules, has been expanded. Indeed, using SSE printing, the feasibility of loading complex molecules such as enzymes has been demonstrated, as well as the feasibility of incorporating oils, microparticles to achieve taste masking of bitter drugs, and nanoparticles to prolong the release of the loaded drug.

Finally, the work described in this thesis has also led to the construction of a new SSE printer suitable for the extemporaneous compounding of ODF.